



# Advanced Strategies for Stabilizing Single-Atom Catalysts for Energy Storage and Conversion

Wenxian Li<sup>1,2,3</sup> · Zehao Guo<sup>1</sup> · Jack Yang<sup>2</sup> · Ying Li<sup>1,3</sup> · Xueliang Sun<sup>4</sup> · Haiyong He<sup>5</sup> · Sean Li<sup>2</sup> · Jiuju Zhang<sup>3</sup>

Received: 29 November 2021 / Revised: 15 February 2022 / Accepted: 10 May 2022 / Published online: 5 September 2022  
© The Author(s) 2022

## Abstract

Well-defined atomically dispersed metal catalysts (or single-atom catalysts) have been widely studied to fundamentally understand their catalytic mechanisms, improve the catalytic efficiency, increase the abundance of active components, enhance the catalyst utilization, and develop cost-effective catalysts to effectively reduce the usage of noble metals. Such single-atom catalysts have relatively higher selectivity and catalytic activity with maximum atom utilization due to their unique characteristics of high metal dispersion and a low-coordination environment. However, freestanding single atoms are thermodynamically unstable, such that during synthesis and catalytic reactions, they inevitably tend to agglomerate to reduce the system energy associated with their large surface areas. Therefore, developing innovative strategies to stabilize single-atom catalysts, including mass-separated soft landing, one-pot pyrolysis, co-precipitation, impregnation, atomic layer deposition, and organometallic complexation, is critically needed. Many types of supporting materials, including polymers, have been commonly used to stabilize single atoms in these fabrication techniques. Herein, we review the stabilization strategies of single-atom catalyst, including different synthesis methods, specific metals and carriers, specific catalytic reactions, and their advantages and disadvantages. In particular, this review focuses on the application of polymers in the synthesis and stabilization of single-atom catalysts, including their functions as carriers for metal single atoms, synthetic templates, encapsulation agents, and protection agents during the fabrication process. The technical challenges that are currently faced by single-atom catalysts are summarized, and perspectives related to future research directions including catalytic mechanisms, enhancement of the catalyst loading content, and large-scale implementation are proposed to realize their practical applications.

**Keywords** Single-atom catalyst · Stabilization strategy · Coordination environment · Polymer · Encapsulation agent · Protection agent

## 1 Introduction

The decline in available fossil fuels and the environmental pollution problems associated with their consumption have been considered as major challenges to the sustainable development of human society [1, 2]. To mitigate

these issues, many strategies have been explored, such as exploring clean and sustainable energy sources including solar, sea-wave, geothermal, wind, and hydropower energy to replace fossil fuels [3–5] and then developing corresponding electrochemical energy technologies, such as batteries, supercapacitors, and brine electrolysis, to store

✉ Wenxian Li  
shuliwx@t.shu.edu.cn

✉ Jiuju Zhang  
jiuju.zhang@i.shu.edu.cn

<sup>1</sup> Institute of Materials, Shanghai University, Shanghai 200072, China

<sup>2</sup> UNSW Materials and Manufacturing Futures Institute, School of Materials Science and Engineering, The University of New South Wales, Sydney, NSW 2052, Australia

<sup>3</sup> College of Sciences, Institute for Sustainable Energy, Shanghai University, Shanghai 200444, China

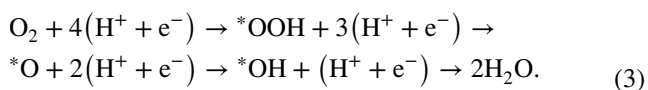
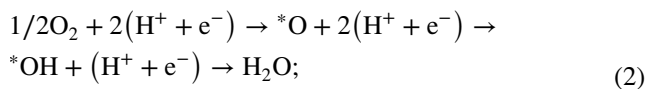
<sup>4</sup> Department of Mechanical and Materials Engineering, University of Western Ontario, London, ON N6A 5B9, Canada

<sup>5</sup> Ningbo Institute of Materials Technology and Engineering, Chinese Academy of Sciences, Ningbo 315201, Zhejiang, China

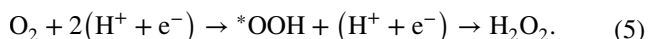
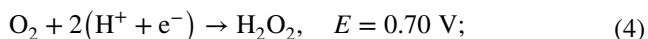
the intermittent electrical energy generated from these sustainable sources [6–11]. Although electrochemical energy technologies have been proved to be efficient and practical, further improvement in their energy and power densities and lifetime is still in high demand for many applications such as electric vehicles [12]. To improve the performance of electrochemical energy devices, the pressing need is to develop high-performance electrode and electrolyte materials [13].

An electrode is always composed of an outstanding electrocatalytically stable and active electrocatalyst supported on an electrically conductive current collector. For example, in a low-temperature fuel cell or a metal–air battery, the cathode is normally coated with carbon-supported platinum (Pt) to catalyze the oxygen reduction reaction (ORR) [14–18]. This Pt-based electrocatalyst can accelerate the reduction from oxygen (O<sub>2</sub>) to water (H<sub>2</sub>O) (4-electron reduction pathway) and/or from oxygen to hydrogen peroxide (2-electron reduction pathway) in aqueous solutions [19–21]. The elemental steps of the ORR are usually presented in the following equations (where species with \* denotes that this species is adsorbed to a catalyst active site) [22, 23].

Four-electron pathway:



Two-electron pathway:



Different electrocatalysts have been employed in electrochemical energy devices to catalyze the ORR, carbon dioxide reduction reaction (CO<sub>2</sub>RR), nitrogen reduction reaction (NRR), oxygen evolution reaction (OER), hydrogen oxidation reaction (HOR), and hydrogen evolution reaction (HER) [24–36]. The catalytic activity and stability of an electrocatalyst are strongly dependent on its morphology, structure, composition, conductivity, particle size, and specific surface area [37–39]. Among these properties, one of the most important factors that affect the catalytic activity and stability is the particle size. Particle size reduction can induce a high surface free energy and high specific surface area, thereby lowering the catalytic reaction barrier and giving rise to a high utilization rate of the catalysts in the reaction [40]. Different types of nanocatalysts, such as metals, metal

oxides, carbides, nitrides, and other compounds [41–49], have been explored and developed intensively through both experimental and theoretical approaches and subsequently used as nanoscale catalysts with high surface free energy to catalyze the targeted chemical reactions. The combination of different types of materials can form heterogeneous catalysts to enhance the interaction between the reactants and nanoparticles, enhance charge separation, and improve and even guide charge transfer [50–61].

Atomically dispersed metal catalysts, representing the lower limit of particle size, have attracted intensive attention for further improving the catalytic efficiency, increasing the abundance of active components, and effectively reducing the consumption of noble metals. There is also a need for further fundamental understanding of their catalytic mechanisms [62]. For example, single atoms of Pt can be dispersed on a FeO<sub>x</sub> support to form Pt/FeO<sub>x</sub> single-atom catalysts [63, 64]. The as-prepared Pt/FeO<sub>x</sub> single-atom catalyst (Pt loading of 0.17 wt.%, wt.% means weight percentage) shows a turnover frequency (TOF) of 0.311 s<sup>-1</sup> with a catalytic CO conversion rate of 20% at 80 °C [65]. Lin et al. [66] synthesized a series of single-atom catalysts with different Ir loadings (Ir/FeO<sub>x</sub>) by a co-precipitation method. With decreasing Ir loading, more positive charging of Ir species led to the same result as that of Pt single atoms supported on FeO<sub>x</sub> reported by Qiao et al. [65]. Electron transport from Pt atoms to the FeO<sub>x</sub> surface through vacant d orbitals of Pt atoms stabilizes Pt single atoms and generates positively charged Pt atoms. Wang et al. [67] synthesized Pt catalysts with single atoms or clusters immobilized on CeO<sub>2</sub> by an impregnation method for the CO<sub>2</sub>RR. The obtained activity of the metal single-atom catalyst was tenfold higher than that of its nanoparticle or cluster counterpart under the same conditions. This result indicates that the isolated Pt atom arrangement induces the weak binding of CO to restrict its further hydrogenation and minimize CO poisoning of the catalyst surface, achieving 100% CO selectivity and excellent catalytic stability. The authors also found that the Pt single-atom catalyst accelerated the CO<sub>2</sub>RR reaction at a relatively low temperature of 150 °C.

The instability of single atoms makes them easily coalesce into clusters or even nanoparticles to reduce their surface free energy, which can compromise their advantages of high catalytic activity in their single-atom forms [68–71]. Han et al. [72] observed the beam-induced surface migration of Ir atoms supported on MgO using fast-scan aberration-corrected (AC) scanning transmission electron microscopy (STEM) with the aid of a high-angle annular dark-field (HAADF) Z-contrast imaging function. The results indicated that the isolated atoms were mobile at elevated temperatures, leading to their agglomeration into nanoparticles. Therefore, the development of stabilization strategies is important to keep the metal atoms in their dispersed states to maintain

their high activity for catalytic reactions. Stabilizing precursors, such as mononuclear metal complexes, on carrier surfaces at the atomic level is extremely challenging. This is because the posttreatment process induces the aggregation of the atoms once the stabilizing ligands are removed from the highly dispersed mononuclear metal complexes. The most direct and convenient way to prevent this issue from happening is to reduce the loading of the metal single atoms and choose carriers with high specific areas. Another approach is to employ nitrogen (N), phosphorus (P), and sulfur (S) atoms to construct a proper coordination environment to adsorb and anchor the monometallic complexes on the carrier surface. This strategy focuses on the maintenance of the strong interaction between metal species and coordination sites on the carriers during synthesis. Another approach is to apply metal nanoparticle precursors, but such strategies are limited by the strong metal–metal bonds. A suitable energy source is required to cleave the metal–metal bonds to form atomically dispersed metal species anchored on carriers without the occurrence of aggregation. To overcome such a problem, it is necessary to engineer the coordination sites to capture the atomically dispersed metal species by establishing strong interactions between metal atoms and carriers. These strategies include mass-separated soft landing, one-pot pyrolysis, co-precipitation, impregnation, step reduction, atomic layer deposition (ALD), and organometallic complexation, as shown in Fig. 1a [73–80].

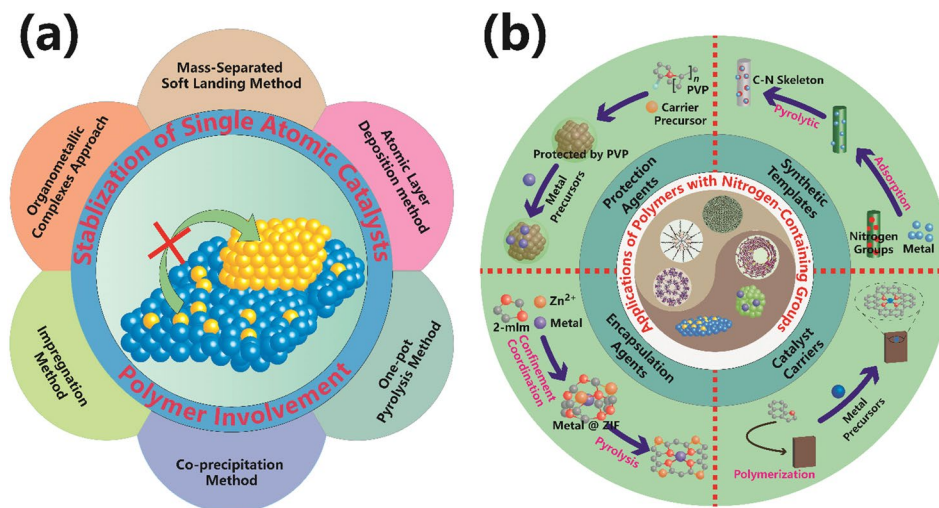
Regarding the synthesis of single-atom catalysts, many organic materials, particularly polymers, have been used as synthetic templates, catalyst carriers, protection agents, and encapsulation agents in numerous fabrication methods, as illustrated in Fig. 1b. Many polymers are suitable for anchoring additional active sites due to their well-defined porosity, high surface area, flexible tunability, and many unique functional groups [81–88]. For example, Chen et al. [89] took advantage of the Kirkendall effect to construct a

functionalized hollow structure using metal–organic framework (MOF) materials. The electronic modulation of the active center can be achieved via long-range interactions with phosphorus and sulfur and close-range coordination with nitrogen. Wang et al. [90] utilized  $Zr_6O_4(OH)_4(BDC)_6$  (UiO-66, in which BDC is 1,4-benzenedicarboxylate) with abundant dangling uncoordinated  $-NH_2$  groups as the carrier to stabilize single Ru sites using these abundant N sites.

Polymers with molecular-scale cages have also been used in synthesis to limit the size of the catalytically active component and protect the active component from migrating and agglomerating during subsequent material preparation steps. Wang et al. [91] prepared single-atom Fe by trapping single ferrocene molecules within cage cavities as precursors, and Fe atoms were buried within nitrogen-doped carbon (Fe–N–C) after high-temperature pyrolysis. The cage configuration prevented both the loss of caged molecules and the migration and agglomeration of Fe atoms during pyrolysis, resulting in abundant  $FeN_x$  sites that showed satisfactory ORR performance. Chen et al. [92] also separated and encapsulated the metal precursor  $Fe(acac)_3$  using zeolitic imidazolate frameworks (ZIFs) as molecular-scale cages. The isolated single iron atoms were coordinated with four neighboring nitrogen atoms due to reduction of  $Fe(acac)_3$  by carbonization of the organic linker. Similarly, Ji et al. [93] separated precursors using ZIFs. In the synthesis,  $Ru_3(CO)_{12}$  and precursors of ZIF-8 were mixed to encapsulate  $Ru_3(CO)_{12}$  in ZIF-8 during ZIF-8 crystallization.  $Ru_3$  clusters were obtained after heat treatment. These clusters are uniformly stabilized through coordination with nitrogen species.

In addition, polymers can be used as surfactants to regulate the crystallization of the target catalyst. For example, He et al. [94] developed a surfactant-assisted MOF approach. An atomically dispersed Co-doped carbon was fabricated with a core–shell structure. The confinement effect mitigated

**Fig. 1** **a** Summary of the stabilization techniques of single-atom catalysts. **b** The function of polymers with nitrogen-containing groups for single-atom catalyst stabilization



the collapse of the internal microporous structures of ZIF-8 by suppressing the agglomeration of Co atomic sites during thermal activation. This unique confinement effect is attributed to the cohesive interactions of Co-doped ZIF-8 nanocrystals and selected surfactants. The hydrophilic groups in the surfactants coordinate with  $Zn^{2+}$  and  $Co^{2+}$  sites on the Co-ZIF-8 polyhedron surface. Because of the coordination effect, the crystal growth rate was slowed, and the crystal size, as well as the morphology of Co-ZIF-8 crystals, was controlled [95, 96].

Polymers containing nitrogen groups are favorable candidates for dispersing active single atoms without aggregation and influencing the charge distribution to improve the performance of catalysts. Heteroatoms with lone electron pairs, such as N, are usually abundant in polymers or their derivatives. These heteroatoms can anchor single metal atoms via strong coordination interactions. The lone electron pair coordination environment can enlarge the average adsorption distance between the single metal precursors and polymer matrix, effectively preventing agglomeration behavior during pyrolysis and favorably forming single-atom catalysts. In this regard, polymers with nitrogen-containing groups are widely used to prepare single-atom catalysts [97].

The research progress in metal single-atom catalysis has been summarized by several review papers, focusing on insights into the development of single-atom catalysts [98–102]. The main arguments focus on synthetic procedures, characterizations, reaction mechanisms, precise control of catalyst surface metal atomic structures, structure–performance relationships, applications, and challenges. In this review, the stabilization strategies for single-atom catalysts are reviewed in terms of synthesis methods along with a detailed analysis of their advantages and disadvantages. In particular, the application of polymers in the fabrication and stabilization of single-atom catalysts is discussed based on their functions as synthetic templates, carriers for metal single atoms, encapsulation agents, and protection agents during fabrication or catalysis. The employment of polymers with nitrogen-containing groups is emphasized regarding their specific functions in the capture of single atoms during fabrication and improving the conductivity of carbon-based carriers [103]. Finally, this review points out current challenges and potential applications in the field of monatomic catalysts, and future research directions are provided for the development of single-atom catalysts.

## 2 Single-Atom Catalysts

Single-atom catalysts, in which only isolated single-atom active centers are dispersed on support materials, are a new category of heterogeneous catalysts [78, 79, 104]. Single-atom catalysts have the properties of homogeneous catalysts,

i.e., single active centers, but with easy separation characteristics. Therefore, single-atom catalysis represents a special type that bridges both heterogeneous and homogeneous catalysis [105, 106]. In general, single-atom catalysts are different from other forms of nanocatalysts (such as metal clusters) based on their novel metal–carrier interaction due to the absence of metal–metal interactions in the system, an unsaturated coordination environment, a high surface free energy, and quantum size effects [104]. Owing to the strong coupling between carriers and metal atoms, they have higher inherent catalytic selectivity and activity than conventional catalysts for the OER, ORR, and other reactions [107–110]. In this aspect, research on single-atom catalysts has progressed from monometallic single-atom catalysts [111–116] (Pt [117–130], Rh [131–135], Au [136–140], Fe [141–144], Cu [145–147], Ni [148–150], Pd [151–153], Ir [154–156], Co [157, 158], Ru [159, 160], Zn [161, 162], Mn [163], V [164]) to bimetallic single-atom catalysts [165, 166], double-atom catalysts (Sn–Zn [167], Co–Fe [168]), bimetallic alloy catalysts [169] (Au–Pd alloy [170], Cu–Pd alloy [171]), and nonmetallic single-atom catalysts (Si [172]). The involvement of secondary metal atoms can affect the steric and electronic environments of the primary metal atoms, which can separate the latter atoms and enhance the catalytic performance by synergistic action [172].

Although single-atom catalysts have great potential in practical applications in the ORR, OER, HER, and  $CO_2RR$ , their developments are challenged by low single-atom loading, poor chemical/thermal stability, and the limitations of catalytic reactions, which require further development of novel fabrication methods, characterization techniques, and stabilization strategies. Normally, (1) the metal–metal interaction is stronger than the metal–carrier interaction in single metal catalyst, and individual atoms can move and combine easily with each other to form metal clusters and nanoparticles under practical reaction conditions [173]; (2) single atoms can also drive self-agglomeration and cluster formation because of the high surface free energy in the fabrication environments and during catalytic cycling, both of which can lead to catalyst deactivation. Therefore, the stabilization of single atoms represents the key task to achieve highly dispersed single-atom catalysts.

The core factor in stabilizing single-atom catalyst active species is to establish strong interactions between the single atoms and their carriers [174–176]. Such a strong interaction plays a dominant role: preventing isolated metal atoms from aggregating and producing single-atom metal catalysts with stability and good dispersity [80]. As identified, the interaction comes from the redistribution of electrons between the single atom and the carrier, which has a vital impact on the electronic structure and catalytic ability of the atom. Several stabilization techniques have been developed to enhance this

interaction, thereby fabricating single-atom catalysts effectively and conveniently [177].

In most synthetic methods, polymers play important roles as carrier precursors, microstructure templates, inhibitors to limit the size of metallic particles, and protective agents for single-atom catalysts [178]. As recognized, the use of polymers as carriers is the most common approach because the structures and morphologies based on polymers can be adjusted through chemical or physical methods to achieve a high porosity, provide a high surface area, and impart chemical stability. Another critical function of polymer carriers is to anchor single atoms on their surface through coordination with metal atoms via their abundant functional groups. Lyu et al. [179] synthesized a single-atom catalyst (Fe–N–C) in which Fe single atoms were loaded on nitrogen-doped carbon through a Schiff base condensation reaction, as shown in Fig. 2a. This catalyst features a nitrogen-doped graphitic carbon matrix with a well-defined spherical morphology. The ultrahigh surface area of this matrix is  $1796\text{ m}^2\text{ g}^{-1}$ , which is decorated with single Fe atoms coordinated with nitrogen. The images of Cs-corrected HAADF-STEM (Fig. 2b, c) show nanospheres with a hollow structure decorated with scattered large bright spots, which represent homogeneously distributed Fe single atoms. Figure 2d presents the high-resolution image, which demonstrates that the spherical shell

is graphite-type carbon, indicating that the carbon sphere is covered with few-layer graphene. In this case, the Fe-coordinated bis(imino)-pyridine ligand acts as both a carrier during synthesis and a precursor of nitrogen-doped carbon.

### 3 Stabilization of Single-Atom Catalysts

As identified, single-atom catalysts face the challenges of large-scale production and low stability in reactions [180–185]. Appropriate synthetic strategies are crucial for the stabilization of isolated single metal atoms to fabricate high-quality single-atom catalysts [186–188]. During synthesis, the defects or vacancies of the carrier precursors can anchor, reduce, and confine metal atoms. Regarding the increase in metal atom loading, two factors have been identified theoretically to avoid single-atom agglomeration: one is to increase the carrier surface area, and the other is to improve the bonding strength of the metal atoms on the carrier surfaces. Based on these principles, several preparation methods for single-atom catalysts, such as mass-separated soft landing, one-pot pyrolysis, co-precipitation, impregnation, step reduction, ALD, and organometallic complexation, have been developed [189–191].

#### 3.1 Mass-Separated Soft-Landing Method

In the mass-separated soft-landing method, metal atoms are vaporized by a high-frequency laser evaporation source, and then, a mass spectrometer is used to control the vapor deposition to obtain metal particles of different sizes and loadings on the carrier surface [181]. As shown in Fig. 3a, a pure metal solid is heated to above its vaporization temperature by a heat source, and the vaporized metal atoms are transported and aggregated through the inert gas. Figure 3b shows the structure of the equipment, in which the mass filter selects the vaporized metal atoms. This equipment can control the number of atoms in the cluster by mass. In this way, only the selected atoms can “land” on the carrier. This method can be used to prepare both single-atom catalysts and cluster catalysts containing different elements.

To verify the catalytic mechanism of clusters with different numbers of atoms, Abbet et al. [192] employed the mass-separated soft-landing method to prepare  $\text{Pd}_n$  clusters (where  $n$  is the number of Pd atoms,  $1 \leq n \leq 30$ ) on the MgO (100) crystal plane and used the as-synthesized catalyst to catalyze the trimerization of acetylene into benzene. Their study found that when  $n = 1–3$ , the reaction could be catalyzed at approximately 300 K, which was approximately  $130\text{ }^\circ\text{C}$  lower than the reaction temperature of other catalysts containing more Pd atoms ( $n > 3$ ). Single-atom catalysts can significantly reduce the energy barrier of reactions. The defects on the MgO surface transfer charge to

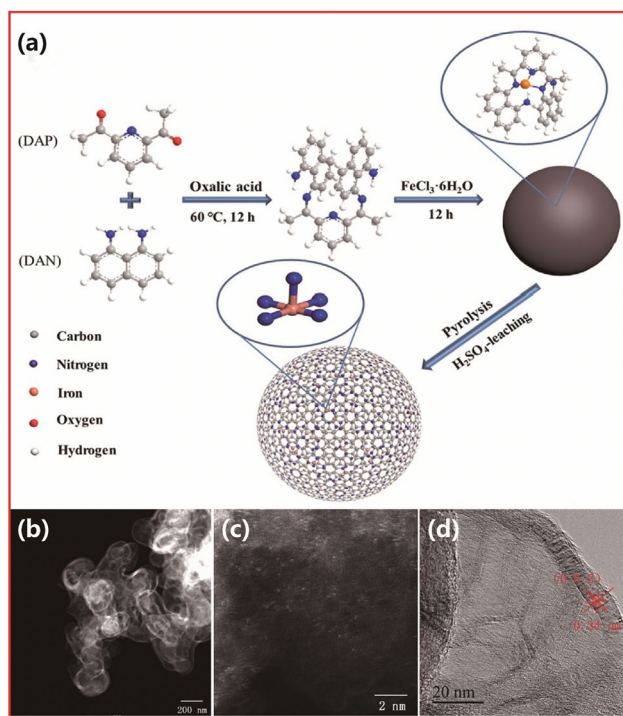


**Fig. 2** a Preparation of the Fe–N–C catalyst. b, c HAADF-STEM images of the Fe–N–C catalyst at different magnifications. d TEM images of the Fe–N–C catalyst. Reprinted with permission from Ref. [179]. Copyright © 2018, Elsevier Inc.

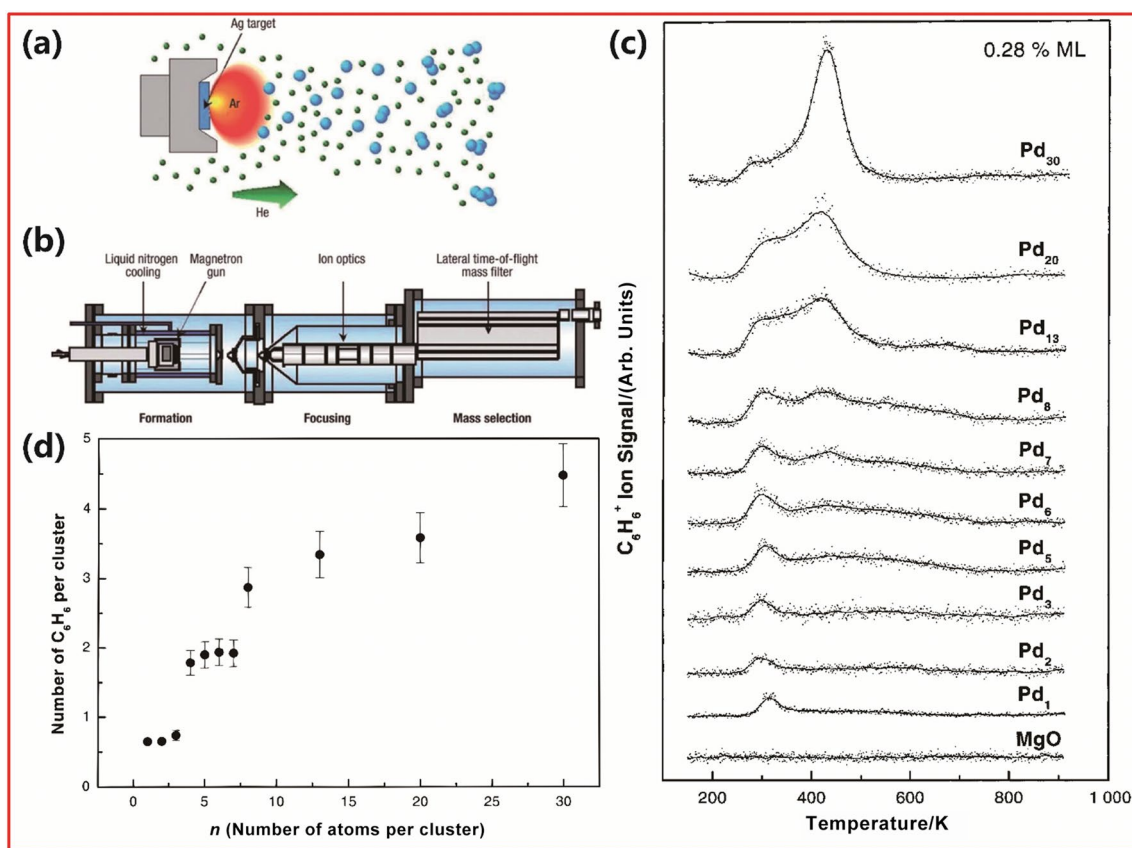


**Fig. 3** Schematic of the mass-separated soft-landing method. **a** High-temperature vaporized solid metal. Vaporized metal atoms are transmitted and aggregated to form clusters by argon gas. **b** The structure of the equipment contains three parts: formation, focusing, and mass selection. Reprinted with permission from Ref. [181]. Copyright ©

2018, The Royal Society of Chemistry. **c** The C<sub>6</sub>H<sub>6</sub><sup>+</sup> ion signals of various Pd clusters with different sizes at different reaction temperatures. **d** The total amount of C<sub>6</sub>H<sub>6</sub> produced by various Pd clusters with different molecules. Reprinted with permission from Ref. [192]. Copyright © 2000, American Chemical Society

single-atom Pd to bind Pd on the MgO surface so that the MgO carrier helps increase the catalytic activity of single-atom Pd. Benzene can be generated at 300 K with the aid of small clusters up to Pd<sub>3</sub>, as shown in Fig. 3c. In Fig. 3d, the number of C<sub>6</sub>H<sub>6</sub> molecules generated by catalytic transformation of Pd<sub>*n*</sub> (4 ≤ *n* ≤ 7) is twice that of Pd<sub>*n*</sub> (1 ≤ *n* ≤ 3) because some C<sub>6</sub>H<sub>6</sub> molecules will be generated at 430 K by Pd<sub>*n*</sub> (4 ≤ *n* ≤ 7). While the temperature must be elevated to approximately 430 K for the Pd<sub>30</sub> catalyst to catalyze the reaction with high C<sub>6</sub>H<sub>6</sub> generation ability.

With the mass-selective soft-landing method, the number of atoms can be precisely controlled while synthesizing metal clusters, even at the single-atom level [185, 193–195]. This method involves physical deposition, and it can extend the synthesis of single-atom catalysts by using many types of planar carriers. However, this method requires ultrahigh vacuum deposition conditions, and the yield is extremely low [196]. In addition, the single atoms are adsorbed on the carrier through a physical method, suggesting that the single atoms easily aggregate into clusters due to the absence of

strong chemical bonds [181, 197, 198]. The loading of single atoms is limited by the deposition method. Furthermore, this method may not be suitable for carrier materials with high surface areas or mesopores [199].

### 3.2 Atomic Layer Deposition Method

ALD occurs when metal single atoms are loaded on the surface of a carrier with atomic-level precision. A well-defined catalyst can be constructed step by step at the atomic level by ALD due to its unique surface self-limiting characteristic, which allows the catalytic materials to be deposited conformally on the high surface area of carriers [200, 201]. During synthesis, the carrier is alternately exposed to different reactive precursor gases, and the targeted material is deposited on the carrier surface layer by layer in a self-limiting manner. Due to this self-limiting characteristic, the size or thickness of the deposited material at the atomic level can be precisely controlled so that the metal atoms can be deposited uniformly on catalyst carriers with a high surface area. Such

a precise bottom-up construction of the catalytic architecture can be achieved by adjusting the number, the sequence, and the type of the ALD cycle [202]. Therefore, ALD is widely used in the field of nanomaterial synthesis due to its precise and controllable deposition with significant uniformity and reliability [105, 189, 198, 203].

In the field of single-atom catalyst design and manufacture, ALD also shows great practical potential by its ability to fine-tune the carriers [181, 189, 204]. The synthesis process always includes three steps [181]. (1) The initial carrier is first pretreated by a chemical process or heating to obtain a carrier with specific anchor sites required for subsequent ALD operation. (2) Metal precursors are adsorbed on the modified carrier in the ALD metal precursor gas, which is usually an organometallic compound. However, each precursor molecule can be adsorbed on only one active site because the chemical adsorption of each precursor molecule is limited due to steric hindrance. (3) The ALD metal precursor (with a partial distributor) chemically adsorbed on the carrier is exposed to a gas-phase reducing agent or oxidant so that the organic ligand is reduced or oxidized and hence removed to obtain single metal atoms.

To verify that a  $\text{Pt}_1/\text{CeO}_2$  single-atom catalyst can produce approximately 50%  $\text{CO}_2$  by a water-mediated Mars–van Krevelen mechanism, Wang et al. [205] proved the feasibility of preparing a single-atom metal catalyst ( $\text{Pt}/\text{CeO}_2$ ) by ALD, carefully controlling the deposition temperature, density, and the type of nucleation sites. In this synthesis, ALD was performed in a viscous flow reactor by alternately exposing it to (methylcyclopentadienyl)trimethylplatinum ( $\text{MeCpPtMe}_3$ ) and oxygen. During deposition, trimethyl(methylcyclopentadiene) was used as a ligand to protect Pt by binding with the metal center. Organic materials were then removed by calcination. The surface Ce vacancies substituted by single Pt atoms were found to be stable, where the lattice oxygen can stabilize the positively charged Pt atoms with six Pt–O bonds. The anchor sites are uniform, and the atoms efficiency is maximized, with a remarkably enhanced activity and 100% CO conversion at 98 °C.

Although Pt catalysts often have high catalytic activity, their high cost and resource scarcity compared to those of other metal elements have significantly limited their practical application on a large scale. Therefore, other types of metal catalysts have been explored to replace Pt catalysts through ALD fabrication. Different from the adsorption mode on Pd nanoparticles, the adsorption mode of 1,3-butadiene on atomically dispersed Pd atoms is mono- $\pi$ -adsorption with single carbon–carbon double bonds. Thus, this approach represents a great chance to improve the selectivity of butenes, especially 1-butene. To confirm this idea, Yan et al. [206, 207] prepared Pd/graphene single-atom catalysts using ALD, as illustrated by the procedure in Fig. 4a. Graphene nanosheets with isolated phenol groups were thermally

reduced in an argon atmosphere at 1 050 °C to obtain graphene carriers. The Pd single atoms were trapped by the isolated phenolic groups during ALD synthesis because they were reduced to specific oxygen functional groups, which could anchor Pd atoms. This reaction forms one bridging oxygen with a Pd single atom, one surface carbon atom and one oxygen atom between the Pd atom and graphene carrier. The HAADF-STEM image illustrates that dispersed Pd single atoms can be randomly observed on the graphene carrier, as shown in Fig. 4b. In addition, the image clearly shows that there are few clusters on Pd/graphene. For the selective hydrogenation of 1,3-butadiene, an extremely high catalytic performance was observed when the Pd/graphene single-atom catalyst was used, as shown in Fig. 4c. 1,3-Butadiene was almost completely converted into 1-butene at 50 °C, which is a mild reaction condition. When the conversion rate was 95%, the selectivity of butene was 100%, which is much higher than the 70% selectivity for 1-butene. Figure 4d shows that the butene selectivity is improved with the aid of a Pd/graphene single-atom catalyst [207].

To develop an efficient, cost-effective, and chemoselective catalyst for the hydrogenation of nitroarenes, Jiang et al. [208] used ALD to prepare a Ni/SiO<sub>2</sub> single-atom catalyst with SiO<sub>2</sub> as a carrier. In a fluidized bed reactor, Ni ALD was performed at 300 °C using hydrogen and bis(cyclopentadienyl)nickel ( $\text{NiCp}_2$ ) as the precursors. Figure 4e presents high-resolution transmission electron microscopy (HR-TEM) images, which show the morphology of Ni nanoparticles fabricated by ALD on the silica substrate (20–30 nm). The insets of Fig. 4e show that the Ni nanoparticle size in the catalyst is 2.4 nm after 2 cycles and 2.6 nm after 15 cycles. This result also indicates that Ni nanoparticles are dispersed on the silica carrier in the TEM images. The as-prepared Ni/SiO<sub>2</sub> catalyst was used for the electrochemical reduction of 4-fluoronitrobenzene. The selectivity of the catalyst for *p*-fluoroaniline was found to be 98.1%, and the yield was 9.2% at 60 °C. The yield also increased with increasing temperature until 120 °C. Moreover, some side products, such as hydroxylamines, hydrazines, azoarenes, or azoxyarenes, were detected at a higher temperature. For the reduction reaction of nitroaryl, shown in Table 1, the Ni/SiO<sub>2</sub> catalyst has a very good TOF (both greater than 0.71 s<sup>-1</sup>), even at a single-atom Ni catalyst loading of only 0.73 wt.%.

One of the crucial disadvantages of the ALD technique is the low loading amount of single atoms because metal single atoms can form clusters under high loading. Sun et al. [209] prepared a stable single-atom catalyst by ALD via Pt single atoms coordinated with oxygen or nitrogen ligands supported on a graphene carrier, as shown in Fig. 4f. In their experiments, the loading of Pt on graphene was increased from 1.52 wt.% to 10.5 wt.% as the cycling number was increased from 50 to 150. The HAADF-STEM

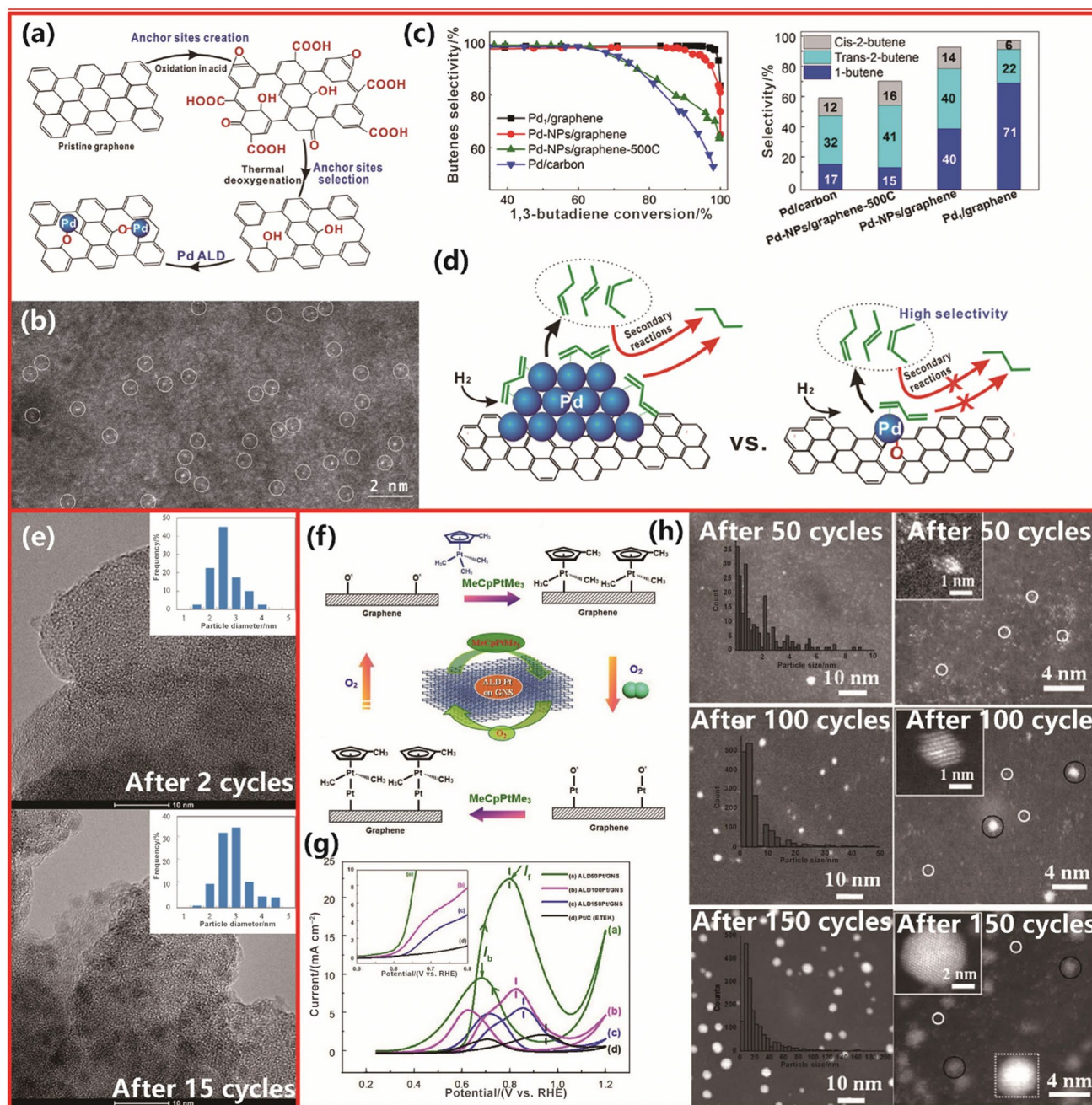


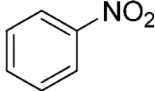
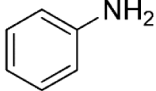
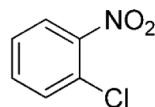
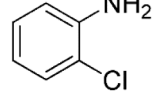
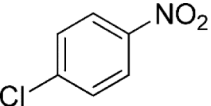
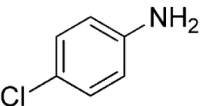
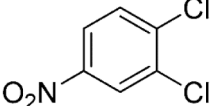
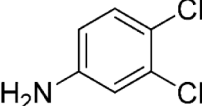
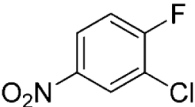
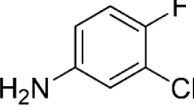
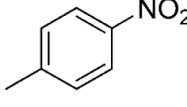
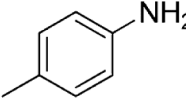
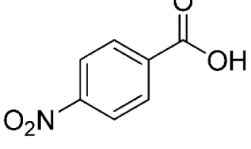
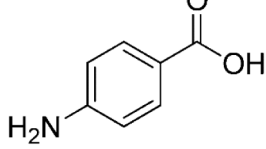
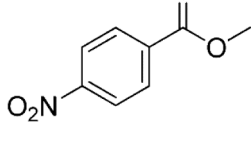
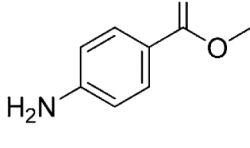
**Fig. 4** **a** Preparation of a Pd/graphene single-atom catalyst by generating anchor positioning and selection sites on the original graphene and performing Pd ALD. **b** Microscopy images of Pd atoms in Pd/graphene with atoms dispersed in the image highlighted with white circles; catalytic performance of different Pd catalysts. **c** Relationship between conversion and selectivity of butene with different reaction temperatures. Different butene selectivity distributions at a 95% conversion rate. **d** The mechanism of butene selectivity enhancement on a single-atom Pd/graphene catalyst. Reprinted with permissions from

Refs. [206, 207]. Copyright © 2018, Elsevier; Copyright © 2015, American Chemical Society. **e** HR-TEM images of Ni/SiO<sub>2</sub> single-atom catalysts after 2 and 15 ALD cycles. Reprinted with permission from Ref. [208]. Copyright © 2015, American Chemical Society. **f** The mechanism of ALD on graphene nanosheets. **g** CV curves of Pt/GNS samples prepared with different numbers of ALD cycles. **h** HAADF-STEM images of Pt/GNS samples with different numbers of ALD cycles. Reprinted with permission from Ref. [209]. Copyright © 2013, Nature Publishing Group

images display the states of Pt on the carrier after three different numbers of Pt ALD cycles, as shown in Fig. 4h. Bright spots, dominantly distributed on the dark background, are Pt single atoms of the Pt/graphene catalyst

(prepared with 50 ALD cycles). Larger clusters can be observed along with single atoms after 100 cycles, indicating the formation of nanoparticles. The particle size is approximately 2–4 nm after 150 cycles, accompanied

**Table 1** Effects of reactants and catalysts on the selectivity, yield, and TOF of amine synthesis by nitro compounds reacting with hydrazine hydrate. Reprinted with permission from Ref. [208]. Copyright © 2015, American Chemical Society

Entry	Reactant	Product	Selectivity/%	Yield/%	TOF/s <sup>-1</sup>
1			95.2 (95.8)	93.8 (45.4)	0.78
2			94.2 (94.5)	92.7 (42.7)	0.75
3			94.0 (95.0)	91.9 (41.5)	0.72
4			95.7 (95.5)	93.7 (42.6)	0.74
5			96.0 (96.3)	94.7 (43.3)	0.74
6			94.8 (94.9)	92.1 (41.1)	0.72
7			87.1 (89.3)	74.8 (37.4)	0.69
8			89.2 (90.5)	76.1 (38.7)	0.71

by single atoms and clusters. Cyclic voltammetry (CV) is used to characterize the catalytic activity and onset potential when applying Pt/graphene catalysts for electrocatalytic methanol oxidation. The peak potentials for methanol oxidation increase with the number of ALD cycles in the forward scan, as shown in Fig. 4g. The peak

potentials for 50, 100 and 150 cycles are 0.79, 0.82, and 0.85 V (vs. RHE), respectively. Compared with the value of 0.96 V for the Pt/C commercial catalyst (vs. RHE), the overpotential for methanol oxidation is reduced by the Pt/graphene catalyst. The peak position shifts to 0.96 V with increasing particle size. There are great advantages

for single-atom catalysts in methanol oxidation, such as superior CO tolerance and higher activity, compared with the actual Pt/C catalyst. However, the loading of Pt atoms was still low, and it was difficult to increase the Pt loading since the aggregation trend of Pt atoms increased with the number of cycles.

ALD, because of its great controllability and repeatability, is the most common method for preparing single-atom metal catalysts. In the future, several limitations of ALD need to be addressed, including the need for strict synthetic conditions, the low loading of the metal catalyst, and high cost [80, 190, 196].

### 3.3 One-Pot Pyrolysis Method

The one-pot pyrolysis method has been developed to prepare single-atom catalysts with high loading. The broken metal–metal or metal–O–metal bonds may lead to the detachment of isolated metal species during high-temperature treatment, forming stable single-atom catalysts via the enhanced metal–support interaction [100, 210, 211]. Cui et al. [212] prepared a nitrogen-doped carbon-carried Zn single-atom catalyst by a one-pot pyrolysis method, and the metal loading reached 1.56 wt.%. The authors believed that this catalyst represents the first Zn catalyst without Zn nanoparticles or clusters. Zhao et al. [213] successfully synthesized several Ni single-atom catalysts, of which the Ni loading reached 20.3 wt.%, supported on nitrogen-doped carbon nanotubes (N-CNTs), called NiSA-N-CNT. In particular, instead of being confined between the carbon layers, the single Ni atoms were combined with the layered carbon. Figure 5a shows a schematic diagram of single Ni atoms on CNTs formed by one-step pyrolysis, after which the layered Ni-g-C<sub>3</sub>N<sub>4</sub> rolls up, forming a CNT structure. The length of bamboo-like CNTs can reach 5 μm, and their average diameters are 20–50 nm (Fig. 5b). The uniform distribution of Ni and N by elemental mapping reveals that this catalyst has a typical tubular structure. Nanoparticles were not observed in this catalyst. The TOF of NiSA-N-CNT, 11.7 s<sup>-1</sup>, was higher than that of Ni nanoparticles (Ni–N–CNT) in the CO<sub>2</sub>RR at 0.55 V. These data demonstrate that single Ni atoms have high intrinsic catalytic activity (Fig. 5c). This TOF value was also better than those of Ni single-atom catalysts reported recently for the CO<sub>2</sub>RR, with TOF values of 1.46 and 4.11 s<sup>-1</sup> [148, 214]. The higher TOF may be attributed to the fine-tuned coordination environment. The onset potentials of the NiSA-N-CNT catalyst for OER and ORR are 25 and 30 mV, respectively, which are both lower than that of Ni–N–CNT in alkaline solution (Fig. 5d). The activities of NiSA-N-CNT for the OER and ORR are lower than those of Ni–N–CNT, probably because the chemical and

electronic environments of Ni single atoms and Ni nanoparticles are significantly different.

As identified, Fe single atoms easily agglomerate during the fabrication process, which limits the loading of Fe single atoms to within 1.9 wt.%–2.5 wt.% [215–218]. Cheng et al. [219] synthesized an Fe single-atom catalyst anchored on nitrogen-doped graphene (FeSA-G) by one-pot pyrolysis, where the loading of Fe atoms was 7.7 wt.%. Microscopy images (Fig. 5e) show the 2D graphene structure, which is formed by a porcine hemin precursor. HR-TEM images show only Fe single atoms on the graphene carriers. STEM with energy-dispersive spectroscopy (STEM-EDS) reveals that the N and Fe atoms are dispersed in the graphene sheets, with N and Fe distributed homogeneously. The AC-STEM results further confirm that Fe atoms are also atomically dispersed, even though Fe atoms have a high loading. Figure 5f–i shows that the half-wave potential and onset potential of FeSA-G for the ORR in an acid electrolyte are 0.804 and 0.950 V, respectively. This catalyst is stable, and compared to the Pt/C catalyst, it has much higher phosphate anion tolerance and the same catalytic performance. The stability test was carried out at 230 °C, and the results indicated that the FeSA-G cathode imparts the battery with stabler performance than the Pt/C cathode.

To fabricate single-atom catalysts by the one-pot pyrolysis technique, metal complexes are often used as precursors, and polymer monomers are employed as carrier precursors. The results all prove that the one-pot pyrolysis method is suitable for fabricating single-atom catalysts with high activity and loading. The addition of polymers as part of the synthesis precursors can significantly overcome the shortcomings of a low loading of single atoms. Notably, the high loading may be attributed to the metals doped in the carrier matrix during pyrolysis.

### 3.4 Co-precipitation Method

The co-precipitation method can be used to prepare supported metal catalysts with uniform dispersions of several active elements simultaneously. For example, two or more types of metal cations dissolved in precipitating agents can generate a precipitation reaction to achieve the molecular-level distribution of different elements through a co-precipitation process. The characteristics of catalysts fabricated by co-precipitation depend on many factors, including the pH of the base solution, aging time, temperature, effective mixing, order and speed of component solution addition, and the number of defects and distribution on the substrate.

To study the structural features of Pt species, Derevyankova et al. [220] prepared a series of Pt/CeO<sub>2</sub> catalysts with different Pt loadings from 1 wt.% to 30 wt.% by the co-precipitation method, and the high loading was attributed to the formation of nanoclusters. Their catalysts were either

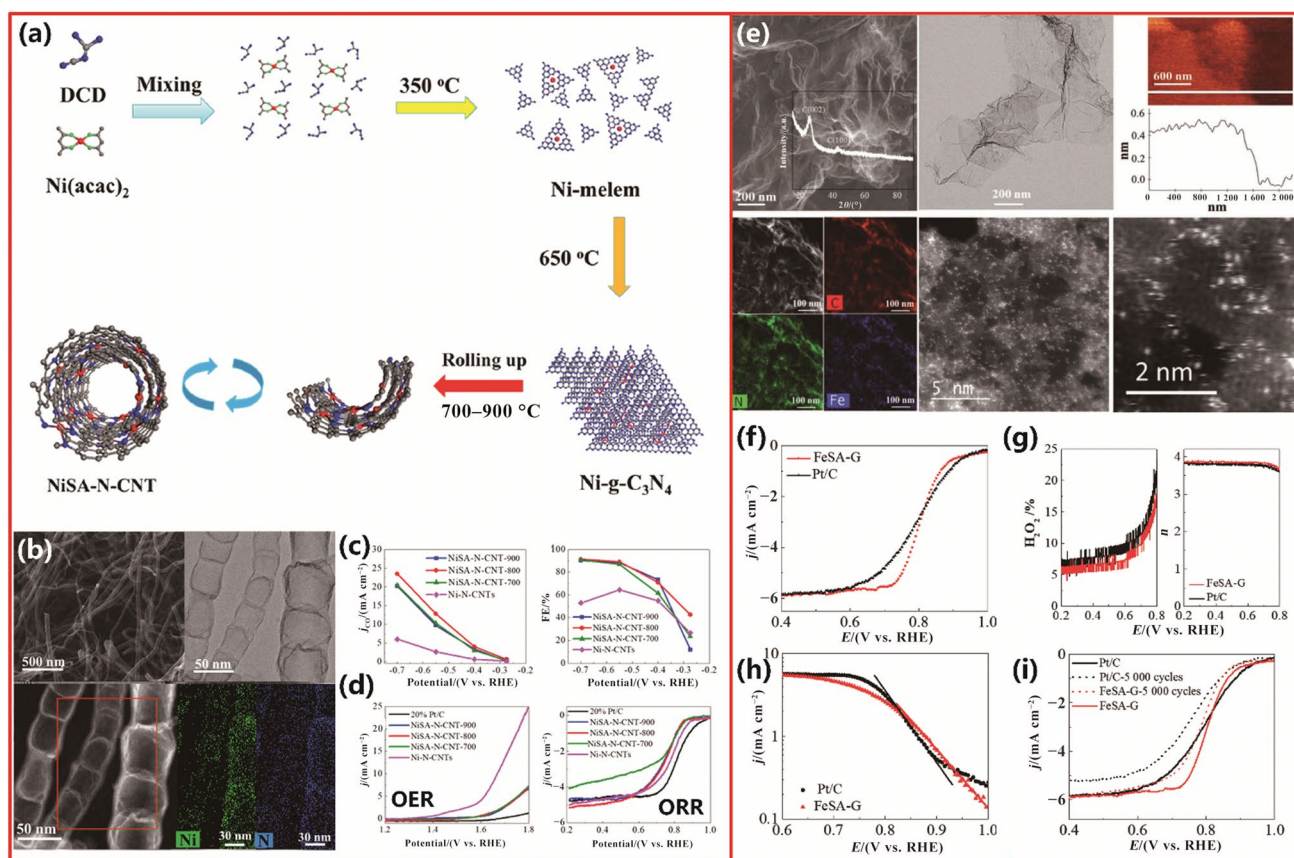


**Fig. 5** **a** The preparation of NiSA-N-CNT with a tubular structure. **b** Microscopy images of NiSA-N-CNT. **c** Faradaic efficiency and  $j_{\text{CO}}$  at different applied potentials of Ni-N-CNT and NiSA-N-CNT-T for the  $\text{CO}_2\text{RR}$ . **d** Linear sweep voltammetry curves of Ni-N-CNTs and NiSA-N-CNT-T for the OER and ORR. Reprinted with permission from Ref. [213]. Copyright © 2018, American Chemical Society. **e** Microscopy images of FeSA-G for the oxygen reduction reaction. **f**

Linear sweep voltammetry curves of FeSA-G and Pt/C in acidic solution. **g** Electron transfer number and yield of  $\text{H}_2\text{O}_2$  for the ORR. **h** Tafel slopes of FeSA-G and Pt/C for the ORR. **i** Linear sweep voltammetry curves of FeSA-G and Pt/C in acidic solution, which are compared with those of these catalysts after 5 000 cycles. Reprinted with permission from Ref. [219]. Copyright © 2019, WILEY-VCH

single atoms or  $\text{PtO}_x$  clusters trapped by  $\text{CeO}_2$  defects and/or epitaxially attached on the  $\text{CeO}_2$  surface. Figure 6a displays TEM images of Pt/ $\text{CeO}_2$  (15 wt.%) and Pt/ $\text{CeO}_2$  (30 wt.%) samples calcined at 450 °C. In Pt/ $\text{CeO}_2$  (15 wt.%), both Pt clusters and their single atoms are distinctly observed in carrier defects and on the surface. In Pt/ $\text{CeO}_2$  (30 wt.%), only Pt clusters are observed. The reactivity of oxygen species of Pt- $\text{CeO}_2$  was analyzed by temperature-programmed reduction (TPR) analysis. Figure 6b illustrates hydrogen consumption during TPR analysis. The hydrogen consumption was triggered at temperatures below 150 °C for all Pt- $\text{CeO}_2$  samples. The reduction in Pt-containing species is responsible for the hydrogen consumption below 350 °C. Pt/ $\text{CeO}_2$  (1 wt.%) has a broad reduction peak at approximately 125 °C, which comes from the reduction of Pt single-atom ions. The increase in Pt loading promotes low-temperature reduction. Pt/ $\text{CeO}_2$  (5 wt.%) has two peaks at 15 and 45 °C, which correspond to the presence of nanoclusters and single

atoms, respectively. The presence of  $\text{Pt}^0$  species accelerates the low-temperature reduction of Pt ionic species in Pt/ $\text{CeO}_2$  catalysts. The reduced species in Pt/ $\text{CeO}_2$  (15 wt.%) and Pt/ $\text{CeO}_2$  (30 wt.%) induce the exothermic and fast reduction of  $\text{PtO}_x$  clusters, and the single-atom signals merge into that of the dominant cluster at 27 and 6 °C. Jan et al. [221] also successfully synthesized a Pt/ $\text{CeO}_2$  single-atom catalyst by a co-precipitation method. It was observed that the strong Pt-O-Ce bond in this single metal catalyst could yield sinter-resistant thermal stability. As presented in Fig. 6c, the STEM micrograph of the Pt/ $\text{CeO}_2$  composite shows that Pt nanoparticles are absent, while Pt is adsorbed on the ceria nanoparticles, forming well-dispersed single atoms. This catalyst can achieve a complete conversion for the CO shift reaction at 200 °C, as shown in Fig. 6d. The catalytic performance of the Pt single-atom catalyst is better than that of pure  $\text{CeO}_2$  and the other samples. This great performance may be attributed to two points: (1) the interaction between

Pt and its nearby highly reducible O atom of  $\text{CeO}_2$  and (2) the preference of CO to adsorb on Pt rather than on the  $\text{CeO}_2$  free surface.

To produce  $\text{SiO}_2$ -supported metal single atoms with high loading in an atomically dispersed manner, Zhu et al. [222] anchored 15 wt.% atomically dispersed Cu on  $\text{SiO}_2$  through the formation of Cu–O–Si covalent bonds between  $\text{Cu}^{2+}$  and silanol (Si–OH) groups on  $\text{SiO}_2$  using a urea hydrolysis-assisted co-precipitation method, as illustrated in Fig. 6e. The TOF of the Cu/ $\text{SiO}_2$  catalyst is  $127.8 \text{ h}^{-1}$  for the low-temperature hydrogenation of 5-hydroxymethylfurfural (HMF). The HR-TEM images in Fig. 6f reveal that the reduced  $\text{SiO}_2$  traps the atomically dispersed Cu with the aid of electron beam exposure. The reduced Cu/ $\text{SiO}_2$  exhibits an ordered hexagonal mesoporous structure, and Cu nanoparticles cannot be detected directly (initial in Fig. 6g). The electron beam irradiation tests indicate that exposure to irradiation destroys the ordered mesoporous structure, forming a condensed matrix when the exposure time reaches 300 s. Cu atoms do not show obvious change or agglomeration. Highly dispersed Cu nanoparticles can be observed when the irradiation time is prolonged to 960 s. The tests show a stable coordination environment and high chemical bonding energy of Cu atoms in the catalysts.

In summary, co-precipitation is one of the most common methods widely applied to prepare single-atom catalysts because of its relatively simple procedure and high catalytic performance of the product. However, this method still has some disadvantages. For example, a highly diluted solution of the target metal must be used to avoid the agglomeration of individual atoms. In addition, at the interface area of the carrier, some metal atoms are anchored during co-precipitation. This is the reason why the metal loadings are apparently higher as observed with this method. These hidden

metal single atoms do not participate in catalytic reactions because of the absence of effective contact.

### 3.5 Impregnation Method

For heterogeneous catalysts, one of the classic preparation methods is the impregnation method [97, 223]. In a typical synthesis procedure, the carrier is impregnated in a solution containing an active component (metal salt). The active component is gradually adsorbed on the carrier surface or restricted to the pore structure after the carrier contacts the solution. Then, the solution is filtered or dried to remove the excess solution. The obtained solid is dried, calcined, and activated to obtain the target catalyst. The metal dispersion depends on the characteristics of the anchoring sites, which are derived from precursor–carrier interactions.

To produce methyl acetate in a fixed-bed reactor with highly selective and high-yielding catalysts, Feng et al. [224] used the impregnation method to synthesize an Ir and La combined catalyst loaded on coconut shell activated carbon (AC) particles, i.e., Ir–La/AC (Ir loading of 1 wt.%). The precursors  $\text{IrCl}_3$  and  $\text{La}_2\text{O}_3$  were dissolved in an aqueous mixture of hydrochloric acid (12% HCl) and AC of 20–40 mesh. HR-TEM images (Fig. 7a–c) show that nanoparticles with sizes of approximately 1–2 nm are uniformly dispersed in the fresh Ir–La/AC catalyst. The nanoparticles are not distinguishable after the catalytic reaction, except for the AC texture, indicating that the nanoparticles were dispersed on the carbon carrier during the reaction. Well-distributed Ir and La atoms on the AC surface can be observed in the HAADF-STEM image (Fig. 7d), suggesting that the active sites of the Ir–La/AC catalyst are in single-atom states. For heterogeneous methanol carbonylation, the space–time yield is 8 200 g

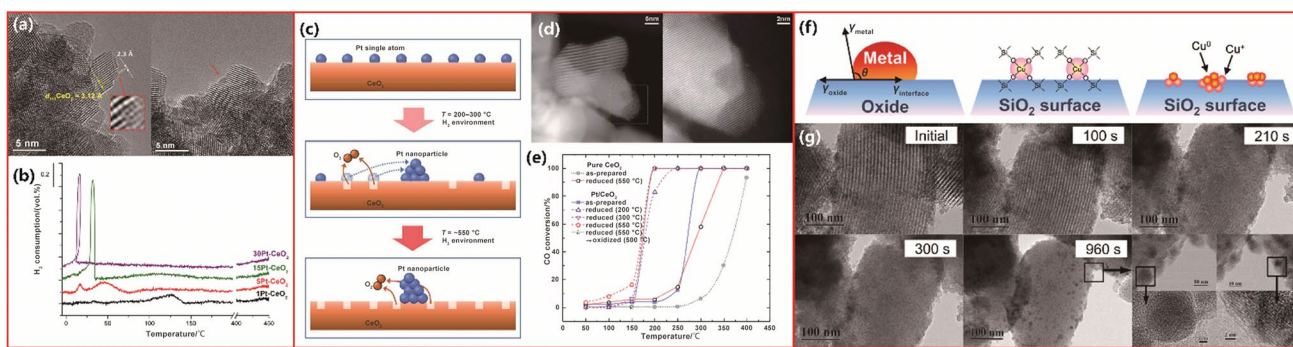


**Fig. 6** **a** HR-TEM images of the Pt/ $\text{CeO}_2$  (15 and 30 wt.%) samples calcined at  $450^\circ\text{C}$ . **b** TPR- $\text{H}_2$  profiles of the Pt– $\text{CeO}_2$  catalysts heated at  $450^\circ\text{C}$ , vol.% means volume percentage. Reprinted with permission from Ref. [220]. Copyright © 2018, American Chemical Society. **c** Schematic of the state of Pt nanoparticles after heat treatment at different temperatures. **d** STEM images of Pt/ $\text{CeO}_2$  showing Pt single atoms adsorbed on the ceria particles. **e** The conversion of CO ox-

idation, which is catalyzed by  $\text{CeO}_2$ -base species reduced at different temperatures. Reprinted with permission from Ref. [221]. Copyright © 2019, The Royal Society of Chemistry. **f** Schematic representation of the synthesis mechanism of the reduced Cu- $\text{SiO}_2$  catalyst. **g** HR-TEM images of the electron beam irradiation-aided Cu/ $\text{SiO}_2$  reduction. Reprinted with permission from Ref. [222]. Copyright © 2017, Elsevier Inc

$\text{kg}_{\text{cat}}^{-1} \text{h}^{-1}$  with the Ir–La/AC catalyst. This process can achieve a relatively high TOF,  $2\,200 \text{ h}^{-1}$ , with over 90% selectivity for methyl acetate. The catalyst shows high stability, as shown in Fig. 7e. For the catalytic reaction, the promoter La can stabilize the single atom of this catalyst, and the active sites are single Ir atoms. The possible mechanism is shown in Fig. 7f.

Although the impregnation method has become indispensable for preparing single-atom catalysts, it still faces the unavoidable disadvantage of low metal loading [106, 225, 226]. To overcome this challenge, Kwon et al. [227] prepared single-atom Rh catalysts (Rh/ZrO<sub>2</sub>) with loadings of 0.3 wt.% and 2 wt.%, respectively. The HR-TEM images indicate that Rh single atoms are the active species in 0.3 wt.% Rh/ZrO<sub>2</sub> and that nanosized Rh clusters are the active materials in 2 wt.% Rh/ZrO<sub>2</sub>, as shown in Fig. 7g, h. Different coordination environments induce different catalytic performance. For example, for direct methane conversion, CO<sub>2</sub> is produced only by Rh nanoparticles, while methanol or ethane is produced in the aqueous phase or gas phase by the single-atom Rh catalyst, as shown in Fig. 7i. For the stability test, the single-atom Rh catalysts were collected by centrifugation and washed with deionized water after one batch of reactions. The yield of the oxygenated products was quite similar even after five reaction–collection cycles. Methyl alcohol was not observed when the centrifuged supernatant without the solid catalyst was used under the same reaction conditions. Single-atomic Rh has been confirmed as an effective catalyst for the conversion of methane to methanol. Hai et al. [228] synthesized single-atom catalysts with a high metal content exceeding 20 wt.% loading of Co, Ni, Zn, Pd and Pt by the impregnation method. The authors tested the combination of 15 different metals with three different carriers, including nitrogen-doped carbon, polymeric carbon nitride, and metal oxides. All 15 metals can exist at the single-atom level with high loading on these carriers. The impregnation method is one of the most effective methods to fabricate single-atom catalysts with high loading.

Polymers can also be used as carriers to stabilize single-atom catalysts in the impregnation method. For example, Kaiser et al. [229] designed carriers with functionalized carbons and controlled thermal activation for Pt single-atom catalysts, which can adjust the oxidation states and coordination environments (–Cl, –N neighborhood). The obtained carbon nitride polymer carrier was polyaniline-derived N-doped carbon. The authors proved that suitable metal anchoring sites, such as nitrogen-containing functional groups, can stabilize metal atoms of the single-atom catalyst and maintain the single-atom form at high temperatures.

In summary, the impregnation method is appropriate for fabricating single-atom catalysts on some carriers with nanostructures. In the impregnation step, the interaction between metal atoms and the anchor points as well as the selection

of proper metal precursors can control the position of single metal atoms. Isolated individual metal atoms can be formed and anchored on the carrier surface through further dispersal of the metal precursor by a subsequent calcination process.

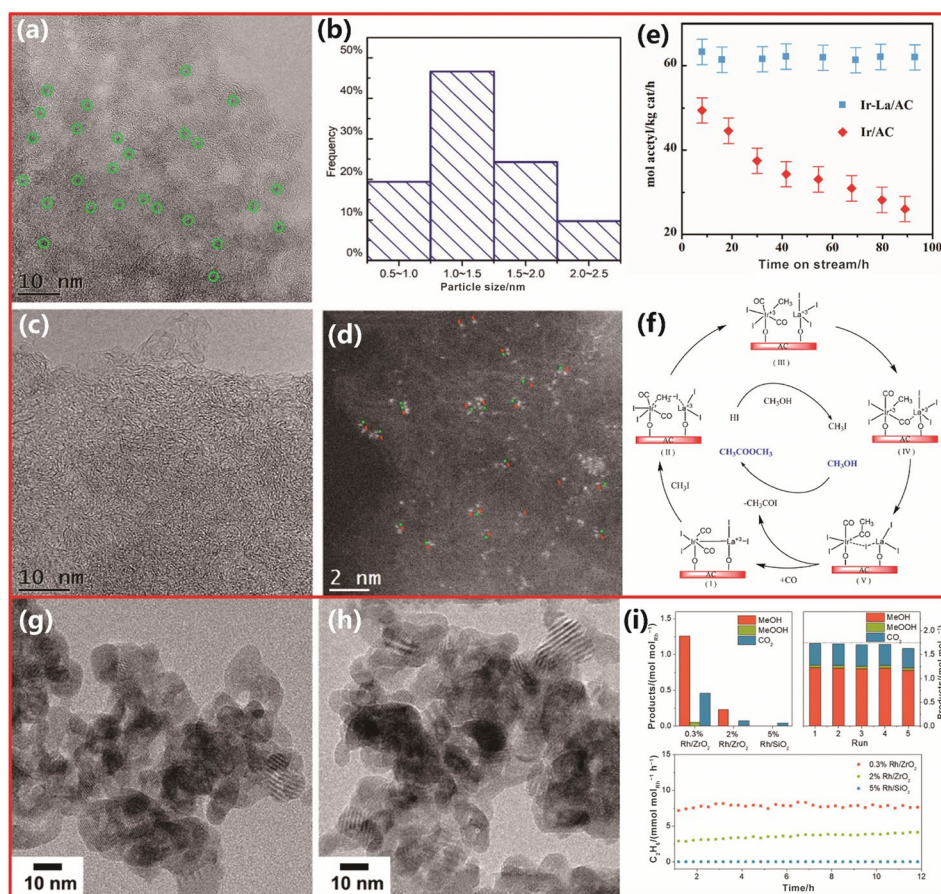
### 3.6 Organometallic Complex Approach

The organometallic complex approach has been employed to prepare single-atom catalysts based on their subtle structure. The metal of a molecular complex with a defined structure can coordinate with a functional group on the carrier surface. This approach can anchor metal atoms in an accurately controlled manner regarding the position and number of metal atoms. Pd single atoms stabilized, supported, and isolated by functionalized MOFs have been tested. For example, Szilágyi et al. [230] used a metal–organic complex Pd(CH<sub>3</sub>COO)<sub>2</sub> as the precursor and the MOF NH<sub>2</sub>-MIL-101 (Cr) as the carrier so that –NH<sub>2</sub> groups coordinate with Pd atoms to fix the metal atoms and obtain a stable Pd single-atom catalyst (0.85 wt.%). The NH<sub>2</sub> groups of the MOF matrix have strong interactions with Pd atoms by providing coordination sites, which can form coordinate bonds to stabilize Pd single atoms. The HAADF-STEM micrographs in Fig. 8a reveal that the pores of NH<sub>2</sub>-MIL-101(Cr) contain a substantial number of single atoms. By integrating the thermal desorption spectra data in Fig. 8b, c, it was determined that half of the Pd remains in the single-atom form. In this way, the authors have proved that such an organometallic complex method can immobilize single metal catalysts on a carrier via chemical bonds to improve stability.

The organometallic complex approach can prepare site-isolated metal single-atom catalysts by utilizing a molecular complex with a uniform structure. This method can accurately control the structure of the anchored complex and the number of metal atoms. A suitable ligand and strong interaction between the ligand and functional group are essential factors in maintaining the original properties of the molecular complex. For example, Liu et al. [231] used an organometallic complex (PhPCP)Pt–OH to prepare a Pt single-atom catalyst through the procedure shown in Fig. 8d. HR-TEM images reveal that 70% of the Pt species are single atoms, and no nanoparticles are observed, as shown in Fig. 8e. Figure 8f shows the CO adsorption/diffuse reflectance infrared Fourier transform spectroscopy (DRIFTS) results. For these Pt catalysts, the peak of single atoms is intenser than the peak of nanoparticles. In particular, the overall IR signal intensities of the overcoated samples are lower than those of the other samples due to the overcoats limiting accessibility to a portion of the Pt species. The metal species have comparable chemical environments in the bare and coated samples judging from their similar CO adsorption peak positions.

Sun et al. [232] encapsulated single Rh atoms within zeolites using [Rh(NH<sub>2</sub>CH<sub>2</sub>CH<sub>2</sub>NH<sub>2</sub>)<sub>3</sub>]Cl<sub>3</sub> as a precursor

**Fig. 7** **a** HR-TEM images of the fresh Ir–La/AC catalyst, **b** corresponding particle size distribution, **c** spent Ir–La/AC catalyst, and **d** spent Ir–La/AC catalyst (the atom size in the red-dotted region is larger than that in the green-dotted region; red dots represent Ir atoms, and green dots represent La atoms). **e** Test of Ir/AC and Ir–La/AC for heterogeneous methanol carbonylation. **f** The mechanism of methanol carbonylation by the Ir–La/AC catalyst. Reprinted with permission from Ref. [224]. Copyright © 2019, American Chemical Society. HR-TEM images of **g** 0.3 wt.% Rh/ZrO<sub>2</sub> and **h** 2 wt.% Rh/ZrO<sub>2</sub>. **i** The results of direct methane oxidation. The results of the recyclability test performed with the 0.3 wt.% Rh/ZrO<sub>2</sub> catalyst. Yield of methane conversion to ethane. Reprinted with permission from Ref. [227]. Copyright © 2017, American Chemical Society



accompanied by a ligand-protected direct hydrogen reduction, as shown in Fig. 8g. Inductively coupled plasma atomic emission spectroscopy (ICP-AES) verifies that the Rh loading is 0.28 wt.% in all the samples. Scanning transmission electron microscopy observation and extended X-ray absorption analysis indicate that every individual Rh atom is trapped in the 5-membered ring and that the oxygen atom of the zeolite skeleton can stabilize these atoms. As shown in Fig. 8h, a few atomically dispersed Rh atoms can be observed in some regions of the zeolite framework by Cs-corrected STEM. Elemental mapping analysis of the Rh catalyst further confirms the homogeneous distribution of Rh single atoms throughout the zeolite crystals (Fig. 8i). As shown in Fig. 8j, the Rh catalyst exhibits a superior H<sub>2</sub> generation rate for ammonia borane (AB). The TOF value of AB hydrolysis is 432 mol<sub>H<sub>2</sub></sub> mol<sub>Rh</sub><sup>-1</sup> min<sup>-1</sup> at 298 K. Most significantly, for the tandem hydrogenation of nitroarenes, zeolite-encaged Rh single-atom catalysts show superior efficiency. The H<sub>2</sub> generation rates can be improved by increasing the reaction temperature. The TOF value can reach 1 829 min<sup>-1</sup> with Rh@S-1-H at 313 K, with a calculated apparent activation energy of 75.5 kJ mol<sup>-1</sup> for the catalyzed reaction. Furthermore, Rh@S-1-H possesses excellent recycling stability because the size of Rh species, crystallinity of zeolites, and

the H<sub>2</sub> generation rate do not show obvious changes after five AB hydrolysis cycles. Nitrobenzene is converted to aniline with more than 99% selectivity by such a Rh catalyst. This catalyst also has selectivity for different nitroarenes with reliable recycling stability. The authors also researched AB hydrolysis under nitroarene hydrogenation conditions with the aid of Rh@S-1-H. As shown in Fig. 8j, the involvement of nitrobenzene decreases the volume of generated H<sub>2</sub> to 66 mL. AB hydrolysis and nitroarene hydrogenation follow the tandem catalytic process because nitrobenzene reduction consumes part of the AB hydrolysis-generated H<sub>2</sub>. The involvement of 4-nitroxyline does not influence H<sub>2</sub> evolution, suggesting that zeolites prevent the Rh species from contacting with 4-nitroxyline in the tandem reaction.

Some researchers have explored transition metal single-atom catalysts with large-scale synthesis through a universal ligand-mediated method. Yang et al. [233] used the coordination ability between metals and nitrogen to synthesize transition metal single-atom catalysts by complexing and coordinating metal cations with 1,10-phenanthroline hydrate. The synthesis procedure is shown in Fig. 9a. Metal atoms are atomically dispersed on the carbon carrier, which is confirmed by HAADF-STEM, as shown in Fig. 9b. Single atoms of Mn, Cr, Co, Fe, Ni, Zn, and Cu on the carbon substrate are observed

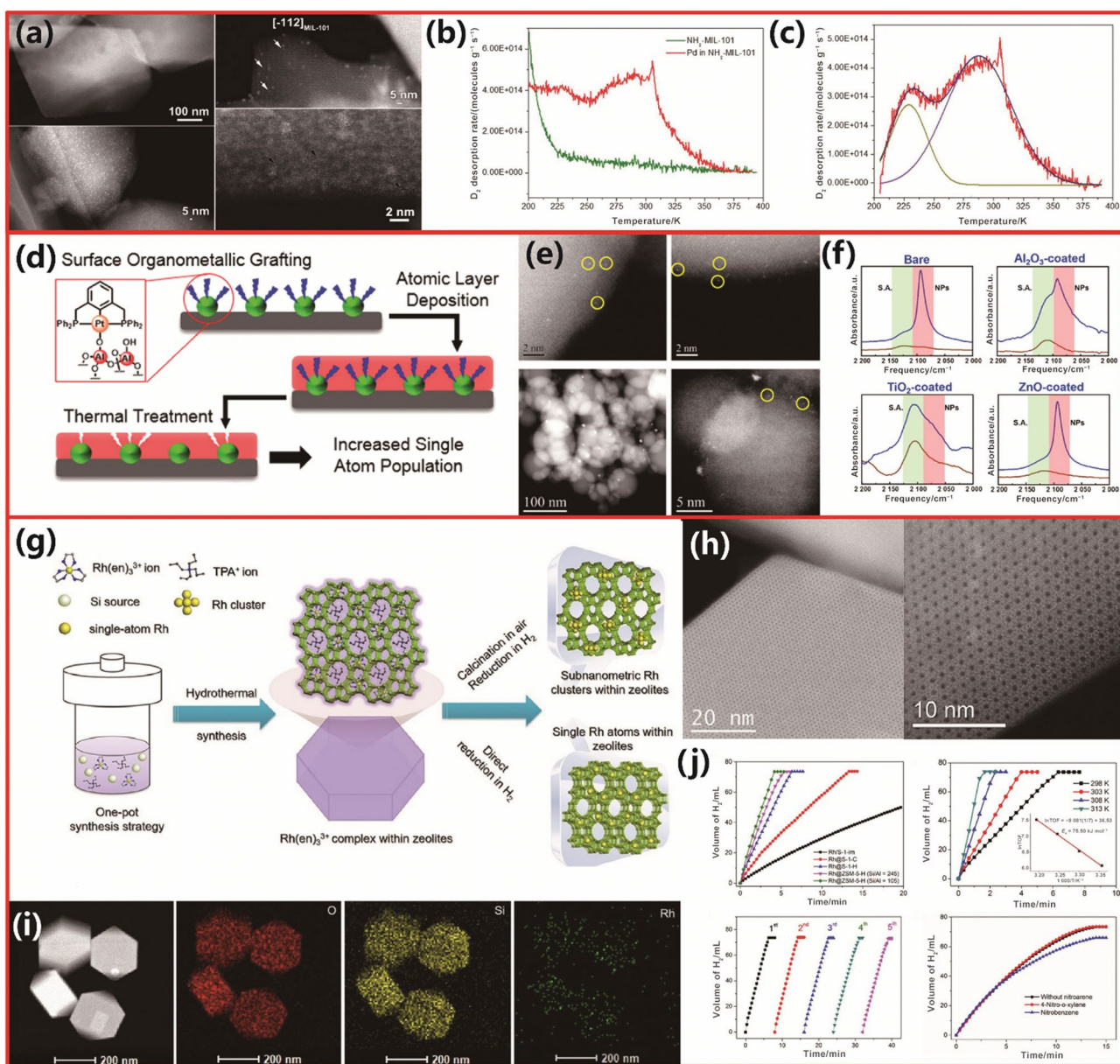


**Fig. 8** **a** HAADF-STEM images of MIL-101 crystals, well-dispersed Pd clusters and individual Pd atoms. **b** Near-ambient-temperature thermal desorption spectroscopy spectra of  $\text{NH}_2$ -MIL-101 with/without Pd. **c** Gaussian fit of  $\text{NH}_2$ -MIL-101(Cr) with Pd. Reprinted with permission from Ref. [230]. Copyright © 2017, The Royal Society of Chemistry. **d** Preparation of oxide-supported single-atom Pt materials. **e** HAADF images of the  $(^{\text{Ph}}\text{PCP})\text{Pt-Al}_2\text{O}_3$  precursor and  $(^{\text{Ph}}\text{PCP})\text{Pt-Al}_2\text{O}_3$ . **f** CO adsorption (blue)/desorption (brown) and DRIFTS spectra of  $(^{\text{Ph}}\text{PCP})\text{Pt-Al}_2\text{O}_3$  with different numbers of ALD cycles and oxide. Reprinted with permission from Ref. [231]. Copyright ©

2017, American Chemical Society. **g** Schematic diagram of the preparation of the Rh@MFI single-atom catalyst. **h** Cs-corrected STEM images of Rh@S-1-H. **i** The corresponding O, Si, and Rh EDX elemental mapping images of Rh@S-1-H. **j** The hydrolysis effects of AB (1 M, 1 mL) catalyzed by Rh@S-1-H and the other catalysts (1 M = 1 mol L<sup>-1</sup>). Temperature influence on the hydrolysis of AB (1 M, 1 mL) catalyzed by Rh@S-1-H. Recycling stability of Rh@S-1-H. Comparison of nitroarene involvement in AB hydrolysis in a water/methanol mixed solution catalyzed by Rh@S-1-H. Reprinted with permission from Ref. [232]. Copyright © 2019, Wiley-VCH

based on the high density of bright dots in the images. For Ru and Pt noble metal single-atom catalysts, the results are similar. From 0.7 to 1.5 V versus RHE, a wide potential range, Ni single atoms display excellent CO<sub>2</sub>RR performance, with high Faradaic efficiency to CO (FE<sub>CO</sub>) exceeding 90%, as indicated

in Fig. 9c. The CO<sub>2</sub>RR performance of these single-metal catalysts (M-SACs), with similar metal loadings of 2.5 wt.%–5.3 wt.%, was tested at 1.2 V versus RHE. For the CO<sub>2</sub>RR, Ni-SAC displays the highest activity among these M-SACs, while the curve of FE<sub>CO</sub> shows that the value of FE<sub>CO</sub> is related to

the metal atomic number (Fig. 9c). The  $FE_{CO}$  increases with the use of Cr to Ni. When using Ni to Zn, the  $FE_{CO}$  decreases abruptly.

As discussed above, due to the involvement of organometallic ligands, the organometallic complex approach has the advantage of obtaining single-atom catalysts with high metal loading. To maintain the structural characteristics of the molecular complexes, a strong interaction on the carrier surface between the functional groups and ligands is needed. This method uses precise molecular complexes to prepare isolated active center catalysts, which are ideal model catalysts to study catalytic mechanisms, by precisely controlling the structure of single-atom catalysts and the position and number of metal atoms. The organic precursors can be designed and synthesized to obtain the target structure and the related performance, such as by introducing nitrogen- or oxygen-containing groups. For example, Gao et al. [234] immobilized single Co atoms by a simple thermal treatment approach for photocatalytic  $CO_2$  conversion on partially oxidized graphene nanosheets. The nanosheets offer C/O functional groups as rigid ligands to catch Co single atoms. Abdel et al. [235] anchored Cu single atoms on the oxygen atoms of  $-OH/-OH_2$  species on UiO-66 (Zr) to cover the defect sites. The researchers obtained a Cu/UiO-66 (Zr) single-atom catalyst with an atomic ratio of Cu/Zr<sub>6</sub> = 0.8. Razmjooei et al. [236] designed a Fe-based nitrogenous carbon single-atom catalyst with high micro- and mesoporosity as well as a high active site density, where Fe could be easily trapped with two nitrogen atoms and four oxygen atoms of EDTA. All these examples of single-atom catalysts highlight their flexibility in fabrication and design with different active metals.

### 3.7 Freestanding Single Metals, Clusters, Nanoparticles, or Dopants in Carriers

The selectivity and catalytic activity are determined by the single-atom coordination environment, depending on the fabrication technique and the number of loaded single atoms. The mass-separated soft-landing method and the ALD method are typical surface modulation techniques used to fabricate single-atom catalysts. The deposited metals react with the carriers in a very limited range through electronic interaction with limited spatial mass transfer. The freestanding single atoms can be stabilized on the carrier surface, and the metal doping effect should be quite rare in the matrix. A high deposition amount generates metal clusters, nanoparticles, and even films. Both methods can reflect the real loading amount of the single atoms on a specific surface. The difference is that the chemical bonds between the single atoms and the carriers may promote a higher loading amount in the ALD method. It should be noted that the deposition surface in ALD can have any morphology, which may induce a

higher loading amount in complex three-dimensional frameworks. The loading amount in a specific area should still be very limited by the mass-separated soft-landing method because the chemical bonds energy is just due to electron exchange and not strong lattice confinement. This kind of dangling-like bonds cannot compete with the high surface free energy-induced agglomeration once the loading amount reaches its limit.

The active metal states are complex in catalysts fabricated with the one-pot pyrolysis method, co-precipitation method, impregnation method, and organometallic complex approach because the precursors of active metals are mixed with carrier precursors. Metal precursors can be adsorbed by the surface of carriers or carrier precursors. Some other metal precursors may participate in the formation of carriers and become dopants in the carriers. This portion of the metal will increase the apparent loading of metals if it cannot be distinguished from the freestanding and agglomerated metals. Furthermore, the reaction conditions cannot be controlled as precisely as those in the mass-separated soft-landing method and the ALD method. The formation of freestanding single atoms, nanoclusters, nanoparticles, and doped metals may occur simultaneously during these chemical-reaction-intensive fabrication methods. In-depth analysis of the coordination environments of the metals in single-atom catalysts is necessary to explore the spatial distribution and electronic structure. Clarifying the contribution of the actual portion of single atoms will benefit the theoretical exploration of single-atom catalysis. Relatively higher loadings can be detected in catalysts fabricated by the co-precipitation method, the one-pot pyrolysis method and the impregnation method. However, the metal species include single atoms, clusters, nanoparticles, and even dopants.

## 4 Roles of Polymers in the Preparation of Single-Atom Catalysts

The application of polymers in the fabrication of single-atom catalysts is inspired by two basic structural properties, i.e., the variety of structures and the abundant functional groups [237]. Four basic structures can be deconvoluted from various polymer structures including linear, branched, crosslinked, and network structures, as shown in Fig. 10a. Linear polymers are constructed with long chains that are linked by hydrogen bonding or van der Waals forces. Branched polymers are constructed based on the linear polymer by linking short chains hanging from the main chains. Crosslinked polymers are constructed by linking many long chains with short chains to form ladder structures, in which the chains are connected by strong covalent bonds. Networked polymers have complex networks

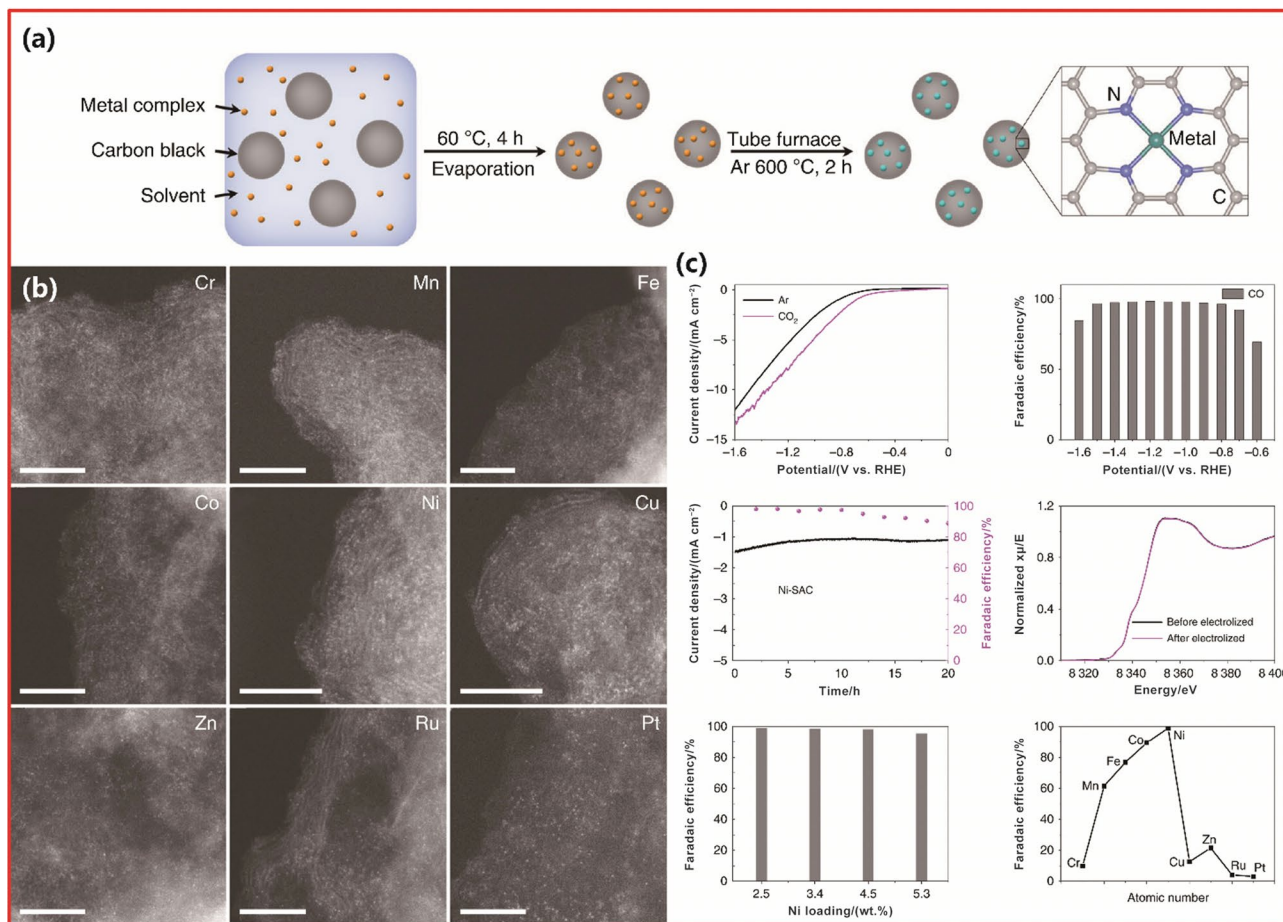


**Fig. 9** **a** Schematic of M-SAC synthesis. **b** Microscopy images induced by different metals. **c** CO<sub>2</sub>RR performance. LSV of Ni-SAC. FE<sub>CO</sub> of Ni-SAC at different potentials. Stability tests for Ni-SAC. XANES spectra before and after CO<sub>2</sub>RR tests with Ni-SAC. FE<sub>CO</sub> of

Ni-SAC with different Ni loadings. FE<sub>CO</sub> of M-SACs. Reprinted with permission from Ref. [233]. Copyright © 2019, Nature Publishing Group

of three-dimensional linkages. The polymer structures can also be composed of different fragments. The assembly of these fragments includes four basic types of copolymer, i.e., random, alternating, block, and graft, as shown in Fig. 10b. Polymers can be applied to construct various spatial structures for carriers of single atoms. Oisaki et al. [238] fabricated organometallic complexes immobilized in the pores of MOFs by covalent linkage. The authors initially prepared a precursor, namely, a N-heterocyclic carbene containing a chain of 4,7-bis(4-carboxyphenyl)-1,3-dimethylbenzimidazolium tetrafluoroborate. Then, they assembled the precursor into a MOF-5-type structure without covalent bonds (IRMOF-76), which could not be involved in organometallic reactions. To obtain a MOF with catalytic activity, the researchers used [4,7-bis(4-carboxyphenyl)-1,3-dimethylbenzimidazol-2-ylidene](pyridyl)palladium(II) iodide as a metal complex to react with Zn(NO<sub>3</sub>)<sub>2</sub>·6H<sub>2</sub>O in N,N-diethylformamide and pyrrole to bind Pd onto IRMOF-77, which

immobilized the Pd organometallic complex in the MOFs with corresponding MOF structural order and porosity.

The specific structures of polymers are natural carrier templates for catalysts with high specific areas [239]. High molecular weight polymers with abundant anchor sites are suitable for forming strong metal–matrix interactions to suppress metal–metal interactions during the fabrication process and in a catalytic environment [97, 114, 240–245]. For example, Liu et al. [246] and Chen et al. [247] investigated, for Pt single-atom catalysts, whether single-layer TM-Pcs (TM for transition metals Sc to Zn and Pc for phthalocyanine) can be used as potential substrates based on first-principles calculations. Pt atoms can firmly bind to Ti-Pc to form a high diffusion barrier, while the strong interaction between Ti and Pc can prevent the formation of Pt clusters. Abel et al. [248] successfully synthesized a single layer of polymerized Fe–Pc through a metal-oriented surface reaction and pointed out that the  $\pi$ -conjugate system was a completely delocalized two-dimensional electronic system.

The functional groups in polymers are abundant, containing oxygen, nitrogen, sulfur, phosphorus, boron, halogen, hydrocarbon, metal, and even radicals. Figure 10c shows several functional groups that have been employed in single-atom catalysis research [234, 249, 250]. Some of these groups have the potential to be strong trapping centers for metal atoms, and naturally, the metal functional groups can be part of the catalysts [243, 245, 251, 252]. Sulfur and nitrogen functional groups have been proved to be effective trapping centers for metal atoms. These abundant heteroatoms can coordinate with single metals by lone pairs of electrons via strong coordination interactions. For instance, Wu et al. [252] prepared single-atom Fe/N-codoped porous carbon composites by a coordination polymer strategy. A silica colloid can serve as a high-quality template to produce carbon-based porous nanomaterials. An Fe single-atom catalyst was synthesized using *o*-phenylenediamine (oPD),  $(\text{NH}_4)_2\text{S}_2\text{O}_8$ , and  $\text{K}_3[\text{Fe}(\text{CN})_6]$  as the precursors. The coordination environments of Fe, S, and N were investigated by X-ray photoelectron spectroscopy (XPS). Fe–N<sub>x</sub> species were characterized as active sites, and S was found to be buried within the carbon matrix, weakening O–O bonding during the ORR. The successful application of polymers

with various functional groups has demonstrated that these various structures of polymers are of great use in synthesizing single-atom catalysts.

In particular, to synthesize single-atom catalysts, polymers with nitrogen-containing groups have been intensively employed as carriers, synthetic templates, encapsulation agents, and protection agents because the coordination and spatial confinement functions of the nitrogen-containing groups play critical roles in the fabrication and catalyst performance [253]. For instance, He et al. [249] used a precursor dilution strategy to fabricate single-atom catalysts supported on N-doped porous carbon. The metal precursor is tetraphenylporphyrin (TPP) with chelated metal cations through N atoms. Pt atoms are supported by N atoms, as observed through X-ray diffraction (XRD), extended X-ray absorption fine structure (EXAFS), and XPS characterizations. Wu et al. [251] synthesized a Cu single-metal catalyst whose Cu(I)–N active sites were exposed through pyrolysis of Cu phthalocyanine and dicyandiamide. HAADF-STEM, scanning tunneling microscopy (STM), and XAFS were employed to identify the isolated Cu(I)–N coordination environment, which contributed to the high ORR stability and activity, as demonstrated by density functional theory

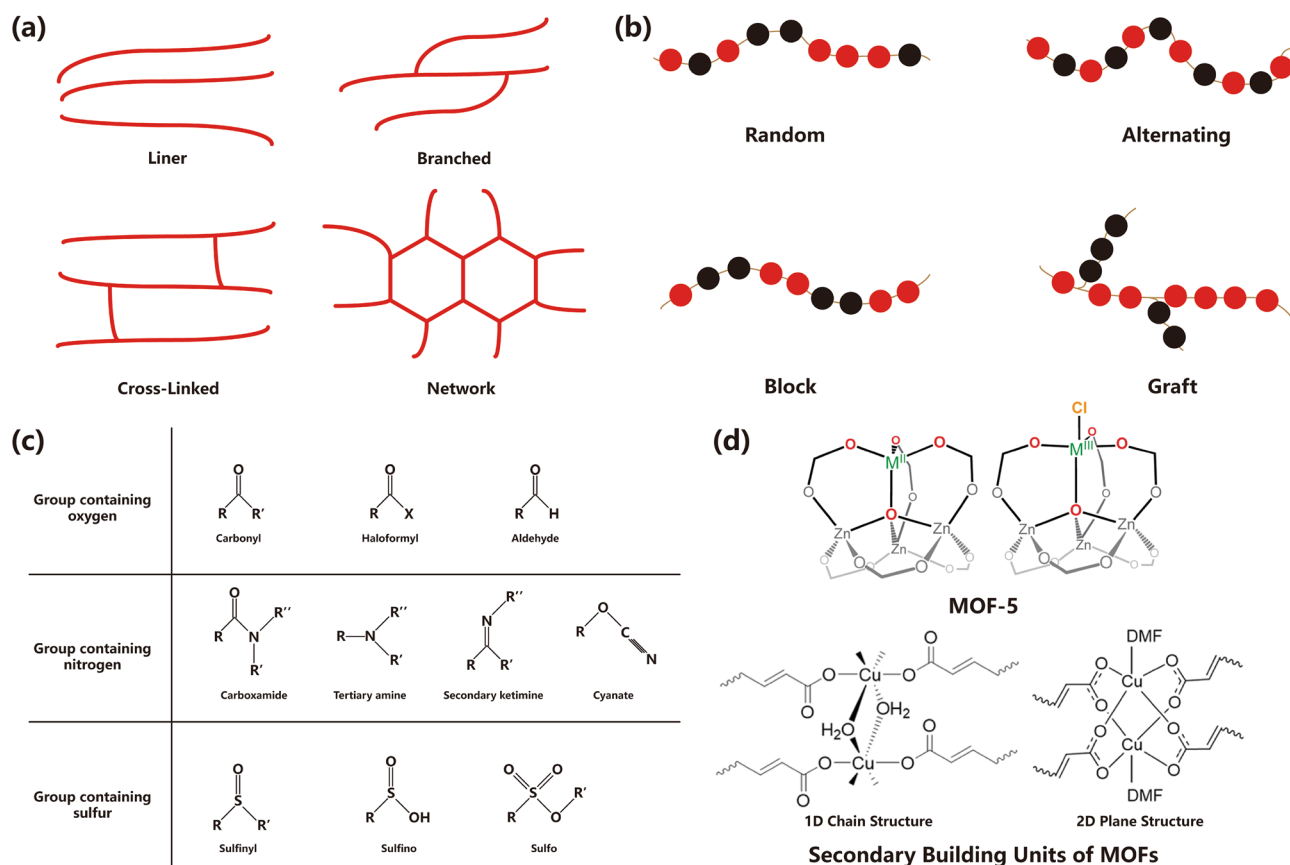


**Fig. 10** **a** Diagrams of linear, branched, crosslinked, and networked polymer structures. **b** Four basic copolymer structures. **c** Functional groups containing oxygen, nitrogen, and sulfur. **d** MOF-5 and secondary building units of MOFs

(DFT) calculations and electrochemical measurements. Pan et al. [250] prepared atomically dispersed Fe–N<sub>4</sub> catalysts with porous N-doped carbon by a polymerization-pyrolysis-evaporation strategy. Experiments and DFT calculations illustrated that the Fe–N<sub>4</sub> sites exhibit superior trifunctional ORR, OER, and HER catalytic performance. Moreover, Co, Ni, and Mn single-atom catalysts were fabricated by this method with metal–N<sub>4</sub> coordination environments. Metal ions in the ligands, which are provided by pyridine-like nitrogen, can be captured by abundant electron lone pairs. Zhang et al. [254] deposited a high content of pyridine heterocycles on carbonitride (g-C<sub>3</sub>N<sub>4</sub>) sheets. The g-C<sub>3</sub>N<sub>4</sub> sheets can host empty d-orbitals for strong N<sub>2</sub> and N<sub>2</sub>H<sub>4</sub> adsorption because of their negative valence. Single d-electrons can engage in back-donation to activate the nitrogen-nitrogen triple bond [255]. The authors synthesized several g-C<sub>3</sub>N<sub>4</sub>-coordinated transition metal single-atom catalysts, and the ligand species were attached to the surface of CNT carriers using a graphene skeleton containing periodic heptazine units linked by tertiary amines. The researchers confirmed that metal atoms could coordinate with N atoms to overcome aggregation and thus stabilize the single-atom catalysts [97].

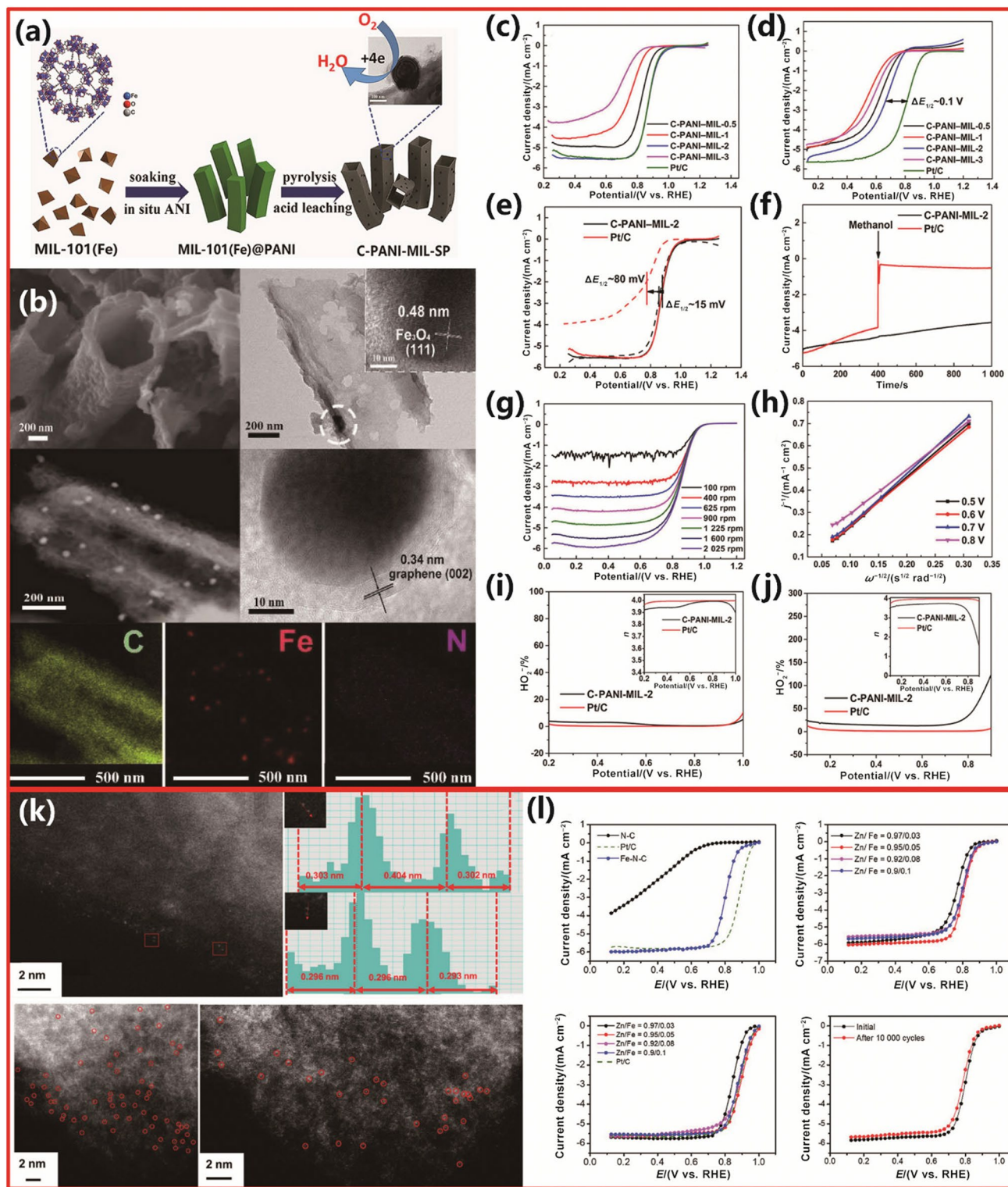
#### 4.1 Synthetic Templates

Many polymers with specific spatial structures can be used as templates for the synthesis of monatomic catalysts, such as lamellar materials, covalent organic frameworks (COFs), MOFs, and zeolites [97]. Interlayered ions and 2D layers form lamellar two-dimensional (2D) materials. The interlayered ions can effectively suppress agglomeration by enlarging the adjacent distances of precursors during posttreatment. Suitable spaces are provided by the 2D layer, which can encapsulate precursors [256]. The microporous crystalline aluminosilicate, which is called zeolite, contains SiO<sub>4</sub> and AlO<sub>4</sub> tetrahedra crystalline networks linked by oxygen bridges forming well-developed pores [257–259]. Zeolite can largely stabilize many single active site species because of the high content of hydroxyl groups [260]. COFs confine mononuclear metal precursors by a well-defined porous structure. Moreover, other light elements (such as B, C, N, and O) contained within COFs can capture metal single atoms, serving as coordination sites to prevent agglomeration [217, 261–267]. Similar to COFs, MOFs are emphasized as a special category of polymers containing metal nodes, and these materials have an extremely high surface area, highly ordered arrangements of organic linkers, distinct designability, and well-defined porous structures [237, 268–270]. MOFs have attracted intensive research interest for constructing various microstructures to support single atoms [82]. The spatial structures of MOFs also provide the possibility to modulate the textural characteristics of the desired catalysts [240]. Researchers have found that the

original metal nodes, which are in the secondary building units (SBUs) of MOFs, can be replaced partially by the target metal atoms (Fig. 10d). Normally, high-temperature pyrolysis and reduction can convert MOF-coordinated metal precursors into supported metal single-atom catalysts [82, 271, 272].

To design catalysts on hollow carbon tubes for fuel cells with nonprecious metal-based microstructures, Yang et al. [273] synthesized hollow carbon microtubes doped with nitrogen as carriers to prepare Fe single-atom catalysts by a self-sacrificial template synthesis approach called C-PANI-MIL (Materiaux de l'Institute Lavosier)-SP (second pyrolysis). Figure 11a illustrates the fabrication procedure, in which Fe-MOF nanocrystals are used as the self-sacrifice template. Polyaniline (PANI) is deposited on the Fe-MOF nanocrystal surface in situ. Fe<sub>3</sub>O<sub>4</sub> nanoparticles are anchored inside the carbon tubes after self-sacrificial template decomposition through two-step pyrolysis. The abundant N atoms in pyrrole and graphite can coordinate with metal atoms to avoid aggregation. In addition, the conjugated  $\pi$  orbitals in the carbon matrix attract electrons on N atoms, causing electron population rise of the  $\pi^*$  orbitals of O<sub>2</sub> molecules, which enables the O–O bonds to be cleaved and further improves the ORR performance. The HR-TEM images reveal that the nanoparticle is composed of Fe<sub>3</sub>O<sub>4</sub>, as shown in Fig. 11b. Metal particles are wrapped by approximately 14-layer graphene sheets on the carbon microtube walls. The elemental analysis results clearly show that the ferruginous particles are buried within the walls of the carbon microtubes. Figure 11c, d shows that the onset potential and half-wave potential of the C-PANI-MIL-2 catalyst (number 2 indicates that MIL is soaked in PANI for two days in the synthetic process) are 1.0 and 0.87 V, respectively. These values are similar to those of 20 wt.% Pt/C in alkaline solution. Figure 11e shows that C-PANI-MIL-2 has a superior current density. Methanol (10 vol.%) was introduced into the electrolyte to test the anti-methanol property with chronoamperometry. The methanol tolerance of C-PANI-MIL-2 is stronger than that of commercial Pt/C in alkaline solution, as shown in Fig. 11f. Figure 11g–j indicates that the direct and indirect 4e<sup>−</sup> reduction processes determine the ORR behaviors on the C-PANI-MIL-2 catalyst in KOH or HClO<sub>4</sub>, respectively.

To find a synthesis route without tedious acid washing steps and to avoid uncontrollable morphologies and undesirable compounds, Xiao et al. [274] synthesized Fe–N–C catalysts using a zeolite imidazolate skeleton (ZIF-8) as a self-template. The cavity diameter and pore size of ZIF-8, which is a typical MOF, are 11 Å and 3.4 Å, respectively [275–278]. The uniformly dispersed Fe atoms are bonded with four N atoms in the porous nitrogen-doped carbon framework. Moreover, the main active sites are pyridinic-N and graphite-N under acidic and alkaline conditions,



respectively. However, the catalyst without Fe doping (N-C catalyst) exhibits a low ORR activity in acidic solution, as indicated in Fig. 11i. Based on different activities between N-C and Fe-N-C catalysts, the addition of Fe accelerates the formation of active sites. Figure 11k shows the presence

of single Fe atoms detected by HAADF-STEM observation. The Fe single atoms are distributed along the carbon matrix edge and highlighted as bright dots. Axially, each Fe atom is connected to two O atoms, while equatorially, it is connected to four N atoms. Both in acidic and alkaline electrolytes,

**Fig. 11** **a** Synthesis procedure of C-PANI-MIL. **b** Microscopy images of C-PANI-MIL accompanied by elemental mappings of C, Fe, and N. RDE polarization curves of C-PANI-MIL in **c** alkaline solution or **d** acidic solution for different ANI soaking times. **e** 10 000-cycle stability tests of C-PANI-MIL-2 and Pt/C in alkaline solution. **f** Chronoamperometric (0.6 V) response at 1 600 rpm (1 rpm = 1 r min<sup>-1</sup>) in alkaline solution. **g** Current densities at different rotating speeds for the C-PANI-MIL-2 catalyst in alkaline solution. **h** K–L plots at different potentials. % H<sub>2</sub>O<sub>2</sub> and transferred electron number (*n*) during the ORR **i** in alkaline solution and **j** in acidic solution. Reprinted with permission from Ref. [273]. Copyright © 2018, Wiley–VCH. **k** HAADF-STEM images of the Fe–N–C catalyst. **l** Electrocatalytic performance of electrocatalysts. Steady-state polarization curves for N–C-, Fe–N–C-, and Pt/C-catalyzed ORR processes in Ar recorded in acidic electrolyte. Variable Zn/Fe composition in an O<sub>2</sub>-saturated acidic electrolyte. Variable Zn/Fe composition and Pt/C in alkaline electrolytes. Fe–N–C catalysts (Zn/Fe=0.95/0.05) after different CV cycles in acidic electrolytes. Reprinted with permission from Ref. [274]. Copyright © 2019, Elsevier Ltd.

the ORR performance of the catalyst is excellent, as shown in Fig. 11l. The catalyst shows, in acidic solution, an onset ORR potential ( $E_{\text{onset}}$ ) of 0.95 V and a half-wave potential ( $E_{1/2}$ ) of 0.81 V. In alkaline solution, the Fe–N–C catalyst has an  $E_{\text{onset}}$  above 1.0 V, which is even much better than that of commercialized Pt/C, while the  $E_{1/2}$  value of the Fe–N–C catalyst (0.90 V) is better than that of commercial Pt/C ( $E_{1/2}$ =0.875 V). The Fe–N–C catalyst has comparable or better stability than the PANI pyrolysis samples and other ZIF samples reported in the literature [90, 279–281].

In summary, the tunable chemical composition of MOF precursors, large surface area, and well-defined pore structure, which are some of the advantages of metal–organic hybrids, can help MOF-derived single-atom catalysts achieve diverse microstructures and coordination environments [82, 282]. Similar to the N atoms in nitrogen-containing groups, MOFs usually contain abundant ligands with coordination atoms. Thus, MOF ligand-derived materials can also stabilize target metal single atoms with rich anchoring sites [99]. Posttreatment can stabilize target metal atoms on the carrier by coordination interactions, which occur between the ligands of MOFs and these metal atoms.

## 4.2 Carriers for Metal Atoms of Single-Atom Catalysts

Polymer materials also have great application prospects as carriers of single atoms because of their unique structural characteristics and high specific surface area. The ordered structure of polymers and their vacancy-abundant surface enable these materials to provide numerous highly uniform attachment sites for the metal active components. The polymer structures can maintain the initial states of the single-atom metal after loading the active components and even retain the original frameworks after calcination or oxidation, which makes polymers excellent catalyst carriers to achieve

high loading with various microstructures [283, 284]. In this subsection, the polymers used as supports are introduced in terms of different metals.

### 4.2.1 Co Single-Atom Catalyst

A stable electrocatalyst anchored on polymer-derived hollow N-doped porous carbon spheres (HNPCSs) has been designed for the CO<sub>2</sub>RR by atomically dispersing Co–N<sub>5</sub> sites. Pan et al. [285] used HNPCSs as carriers with high electrical conductivity, a large surface area, and abundant coordination N sites to prepare Co single-atom catalysts (Co–N<sub>5</sub>/HNPCSs). The synthesis procedures are shown in Fig. 12a. For a typical synthesis, SiO<sub>2</sub>@melamine-resorcinol–formaldehyde polymer spheres are pyrolyzed under Ar at 700 °C to obtain SiO<sub>2</sub>@nitrogen-doped porous carbon spheres. The silicon dioxide core is then etched by HF. The single Co atoms of CoPc can coordinate with N atoms to prepare Co–N<sub>5</sub>/HNPCS catalysts. The hollow spherical structure is uniform, as shown in Fig. 12b, indicated by both SEM and TEM. Co, N, and C are observed in the EDS images and are uniformly distributed across the load over the whole HNPCSs. High-density bright dots in the HAADF-STEM images correspond to single Co atoms. Electrochemical measurements for the CO<sub>2</sub>RR show that the catalytic current density of Co–N<sub>5</sub>/HNPCSs is 6.2 mA cm<sup>-2</sup> at 0.73 V (vs. RHE), which is 15.5-fold higher than that of pure CoPc, as indicated in Fig. 12c. The Faradaic efficiencies for CO production (FE<sub>CO</sub>) of Co–N<sub>5</sub>/HNPCSs are 99.2% and 99.4% at 0.73 and 0.79 V (vs. RHE), respectively. These values are much higher than those of CoPc (Fig. 12d). Co–N<sub>5</sub>/HNPCSs also show FE<sub>CO</sub> values superior to those of Fe-, Ni-, and Cu–N<sub>5</sub>/HNPCS catalysts (Fig. 12e), indicating the positive role of single Co atoms in CO production. Figure 12f shows that the FE<sub>CO</sub> drops with decreasing CoN<sub>x</sub> coordination. Figure 12g shows that after electrolysis for 10 h at 0.73 V, the CO current density value and FE<sub>CO</sub> of this catalyst present no significant changes. The K-edge XANES peak positions of Co are higher energies than those of the ex situ state, indicating that the valence state of Co is higher during electrolysis than in the ex situ state (Fig. 12h). However, because the potential increases and the electrons are transferred, the Co K-edge has a significant blueshift at a higher potential. Suitable electronic structures are vital for the CO<sub>2</sub>RR, which can be summarized based on the observed changes.

A general strategy has been proposed to prepare single-atom catalysts by metal-catalyzed thermal polymerization. Chen et al. [286] explored a polymer carrier, polyphenanthroline, which could carry a high Co atom content above 2.0 wt.%, to form a Co-PPhen-*X* catalyst (where *X* is the temperature of thermopolymerization). The fabrication process shown in Fig. 12i involves dehalogenation polymerization

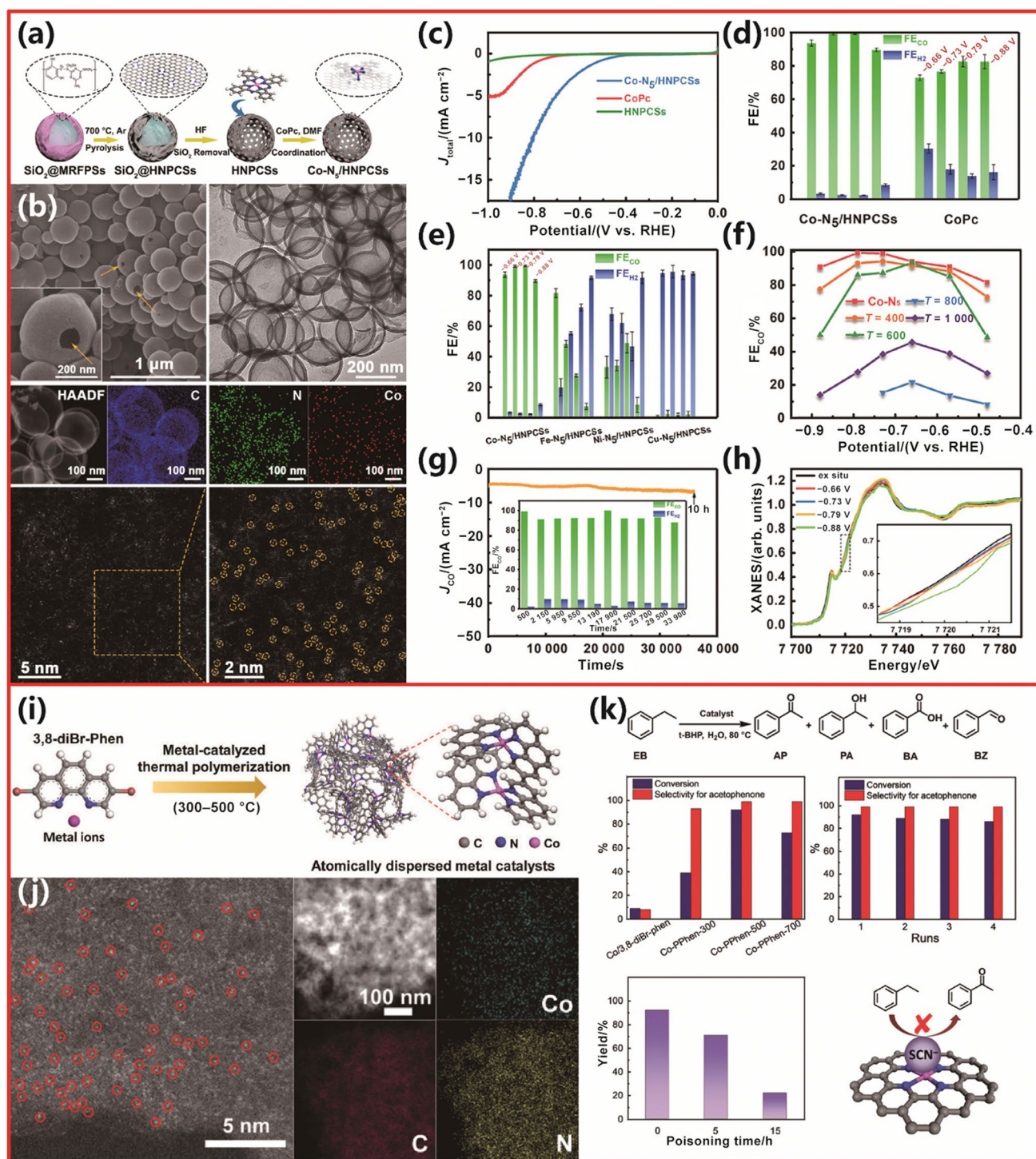


**Fig. 12** **a** Schematic illustration of the catalyst. **b** Microscopy images of  $\text{Co-N}_5/\text{HNPCs}$  catalysts. **c** LSV curves of the  $\text{CO}_2\text{RR}$ . **d**  $\text{FE}_{\text{H}_2}$  and  $\text{FE}_{\text{CO}}$  of Co-base catalysts. **e**  $\text{FE}_{\text{CO}}$  and  $\text{FE}_{\text{H}_2}$  of M- $\text{N}_5/\text{HNPCs}$ . **f**  $\text{FE}_{\text{CO}}$  of  $\text{Co-N}_5/\text{HNPCs}$ - $T$ . **g** Chronoamperograms of  $\text{Co-N}_5/\text{HNPCs}$  catalysts after treatment at different temperatures. **h** Ex situ and in situ XANES of the  $\text{Co-N}_5/\text{HNPCs}$  catalyst at different potentials. Reprinted with permission from Ref. [285]. Copyright © 2018, American Chemical Society. **i** Synthetic process of Co catalyst formation. **j** Microscopy images of the Co-PPhen catalyst. **k** Model of

the ethylbenzene selective oxidation reaction. The selectivity for acetophenone and conversion of ethylbenzene oxidation with Co-PPhen-X. The performance of Co-PPhen-500 after different cycle numbers. The yield of ethylbenzene conversion catalyzed by Co-PPhen-500 after introducing  $\text{SCN}^-$  ions for different amounts of time. Schematic diagram of  $\text{SCN}^-$  ions affecting the catalyst performance. Reprinted with permission from Ref. [286]. Copyright © 2019, The Royal Society of Chemistry

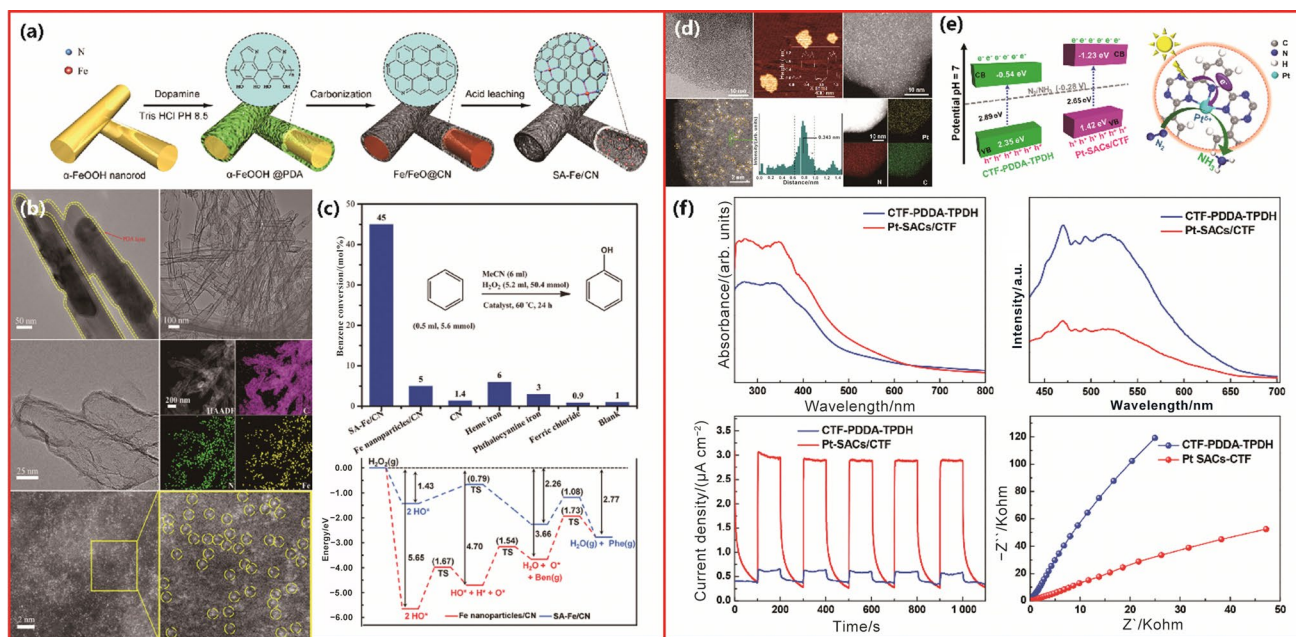


**Fig. 13** **a** Synthesis of SA-Fe/CN. **b** Microscopy photographs of SA-Fe/CN. **c** Benzene conversion of SA-Fe/CN and other catalysts, mol% means molar fraction. Reaction mechanisms of benzene oxidation and  $\text{H}_2\text{O}_2$  activation. Reprinted with permission from Ref. [287]. Copyright © 2017, American Chemical Society. **d** Microscopy pho-

tographs of the Pt-SAC/CTF catalyst. **e** Band diagram and the photocatalytic  $\text{N}_2$  fixation mechanism. **f** DRS spectra, PL spectra with excitation at 400 nm, and  $I-t$  and EIS curves of Pt-SACs/CTF and CTF-PDDA-TPDH catalysts. Reprinted with permission from Ref. [288]. Copyright © 2020, American Chemical Society

with 3,8-dibromo-1,10-phenothroline by metal catalysis. This process ensures in situ formation of the catalyst and high atom loading and dispersion because the phenanthroline structure coordinates with the metal and is strong and stable during the monomer thermal polymerization. The Co species in the catalyst can be identified as isolated single atoms without agglomeration by HAADF-STEM, as shown in Fig. 12j. C, N, and Co are distributed uniformly on the carrier by STEM-EDS elemental mapping. For aromatic alkane selective oxidation, as shown in Fig. 12k, the Co-PPhen-X catalyst exhibits an increased catalytic activity with a conversion efficiency of 92% and an excellent selectivity of 99% to acetophenone (AP) compared with the unreacted blank experiment. After four recycles with the Co-PPhen-500 catalyst, the loss of selectivity and activity was not significant. In addition, the catalytic performance of ethylbenzene conversion decreases sharply after introducing  $\text{SCN}^-$  ions. This result indicates the poisoning effect of  $\text{SCN}^-$  by occupying the active positions of Co, further demonstrating that Co atomically dispersed sites are vital in catalysis.

#### 4.2.2 Fe Single-Atom Catalysts

To develop a novel core-shell strategy to prepare stable single-atom catalysts with nitrogen-doped polymers, Zhang et al. [287] carbonized and acid-treated polydopamine

(PDA) to obtain hollow nitrogen-doped carbon as a carrier for Fe single-atom catalysts (SA-Fe/CN). Figure 13a shows the synthesis procedure. Fe clusters are absent in the TEM image (Fig. 13b). EDX mapping analysis reveals that uniform distributions of Fe, C, and N occur along with the carbon and nitrogen skeleton ( $-\text{CN}-$ ). In HAADF-STEM images, single Fe atoms are highlighted by yellow circles. For hollow nitrogen-doped carbon, single Fe atoms are found on its inner wall. All characterizations indicate that isolated metal single atoms can be anchored firmly with  $-\text{CN}-$ . The SA-Fe/CN catalyst was used for the hydroxylation of benzene to phenol. These results show that the benzene conversion rate is 45% and that the selectivity for phenol is 94%. The conversion rate values are much higher than those of samples with heme iron addition, phthalocyanine iron addition, and without Fe addition, which are 6%, 3%, and 1%, respectively. These results demonstrate that for catalyzing the direct oxidation of benzene to phenol, the energy barrier of this Fe single-atom catalyst is much lower than those with the addition of Fe nanoparticles on CN, which was further confirmed by DFT simulations, as shown in Fig. 13c.

#### 4.2.3 Pt Single-Atom Catalysts

Li et al. [288] used a stable and ultrathin covalent triazine backbone polymer (CTF-PDDA-TPDH) with a nanosheet morphology as a carrier containing  $-\text{N}_3$  groups for anchoring

Pt atoms, forming a Pt-SAC/CTF catalyst. As shown by the HR-TEM image in Fig. 13d, only single-atom Pt can be observed. The HADDF-STEM images show that Pt atoms are dispersed in the Pt-SAC/CTF catalyst. The corresponding EDS mapping images indicate that the entire carrier is covered with uniform distributions of Pt, N, and C. Electrochemical impedance spectroscopy (EIS) testing confirms the fast charge transfer capability, as shown in Fig. 13e. The conversion from  $N_2$  to  $NH_3$  is thermodynamically accelerated because the catalyst has a higher negative conduction band position  $E_0$  ( $N_2/NH_3 = 0.28$  V vs. NHE). Figure 13e demonstrates the photocatalytic  $N_2$  fixation mechanism. The light-harvesting capability of the catalyst was measured by using diffuse reflectance spectroscopy (DRS) (Fig. 13f), indicating a visible light photocatalytic potential. The measured photoluminescence (PL) spectra indicate that Pt single-atom involvement decreases the intrinsic emission peaks, which implies that the Pt-SAC/CTF catalyst has a low electron–hole recombination rate. This catalyst also shows a higher capability for photocatalytic  $N_2$  fixation than the pristine CTF-PDDA-TPDH nanosheets because of the high electron–hole separation rate. The chronoamperometric  $I-t$  curves were plotted to analyze the photoresponse of Pt-SACs/CTF and CTF-PDDATPDH under chopped illumination conditions. Pt-SACs/CTF has a higher electron–hole separation efficiency, so the photoresponse of Pt-SACs/CTF is higher than that of the pristine sample. The EIS test confirms the fast charge transfer capability, as indicated by the small arc radius in the Nyquist plot of the Pt-SAC/CTF electrode.

Zhou et al. [289] explored a porous organic polymer (POL-2BPY) as a catalyst carrier with a high pyridinic nitrogen content, which could coordinate with many Rh atoms to form a POL-2BPY material (Rh-POL-2BPY). Rh coordinates with the N atom of bipyridine during vapor-phase methanol carbonylation. The porous organic ligand of the carrier can modify the monomer at the molecular level. The framework of the porous organic ligand contains P or N ligand coordination sites so that the strong electron-donating groups can tune the electronic state of the supported single atoms in the framework of the porous organic ligand polymers.

#### 4.2.4 Other Single-Atom Catalysts

The catalytic performance can be correlated with the coordination environment at the atomic scale. Wang et al. [290] used  $g-C_3N_4$  as the carrier to prepare a Cu single-atom catalyst called Cu-NGS. As shown in Fig. 14a, Cu atoms are coordinated with N, and the coordination number of Cu single atoms is tailored by using thiourea as a reducing agent. The brighter dots shown in Fig. 14b are recognized as single Cu atoms anchored on the carbon network. STEM-EDS

mapping confirms the homogeneous distribution of Cu, C, N, and S in Cu-NGS. The half-wave potential of the Cu-NGS catalyst is 0.81 V (vs. RHE) for the ORR. The value is higher than that of NGS, 0.63 V (vs. RHE). This result is comparable to that of a commercial Pt/C catalyst (vs. RHE) (Fig. 14c). At low overpotentials, the Tafel slope of this catalyst is  $54$  mV  $dec^{-1}$ , which is smaller than that of Pt/C ( $84$  mV  $dec^{-1}$ ). The kinetic ORR current density ( $J_k$ ) value is  $15.36$  mA  $cm^{-2}$  due to its superior intrinsic electrocatalytic activity. The catalytic pathway of this catalyst involves a 4-electron process because the electron transfer number is approximately 3.8, and the yield of  $H_2O_2$  is below 7%. The Cu-NGS catalyst is very stable, with 73% of the initial current retained in an alkaline solution after 9 000 s. This result suggests that the catalyst has a high methanol tolerance ability because the CV measurements do not show obvious differences for Cu-NGS in alkaline solution with/without methanol addition.

N species are strong anchoring sites of Cu ions. Yang et al. [291] used through-hole polymer nanofibers as carriers to prepare Cu single-atom catalysts called CuSAs/TCNFs. Cu/ZIF-8 was formed after Cu ions were trapped in the ZIF-8 pores during precursor preparation. As shown in Fig. 14d, Cu/ZIF-8 nanoparticles are embedded into PAN nanofibers by electrospinning and then carbonized into carbon with N dopants. Cu ions are reduced in a reducing atmosphere and anchored by nitrogen during carbonization. Clusters and nanoparticles are observed to be absent in CuSAs/TCNFs (Fig. 14e), and only carbon diffraction fringes can be distinguished in the selected area electron diffraction (SAED) pattern. The above results corroborate that Cu atoms did not agglomerate into particles. Dispersions of N and Cu are observed to be uniform on the carbon nanofibers by EDS. The white dots are atomically dispersed Cu atoms. CuSAs/TCNFs can catalyze the  $CO_2RR$  at a low onset potential (0.41 V vs. RHE), as shown in Fig. 14f, which is much more positive than that with TCNFs. The gas-phase products were found to be  $H_2$  and CO, and the liquid-phase product was methanol based on gas chromatography and  $^1H$  nuclear magnetic resonance (NMR) spectroscopy characterizations. The FE for methanol production reached the maximum value of 44%, and that of CO production was 56% at 0.9 V (vs. RHE). The methanol formation rate was  $68.4$   $\mu mol$   $m^{-2}$   $s^{-1}$  when using CuSAs/TCNFs as the cathode, demonstrating its high catalytic activity toward the  $CO_2RR$ .

### 4.3 Other Applications of Polymers

#### 4.3.1 Encapsulation Agents for Single-Atom Catalysts

Confining the active metals in micropores is one of the most effective strategies to prevent their migration, leakage, and aggregation during fabrication and catalysis. Microporous

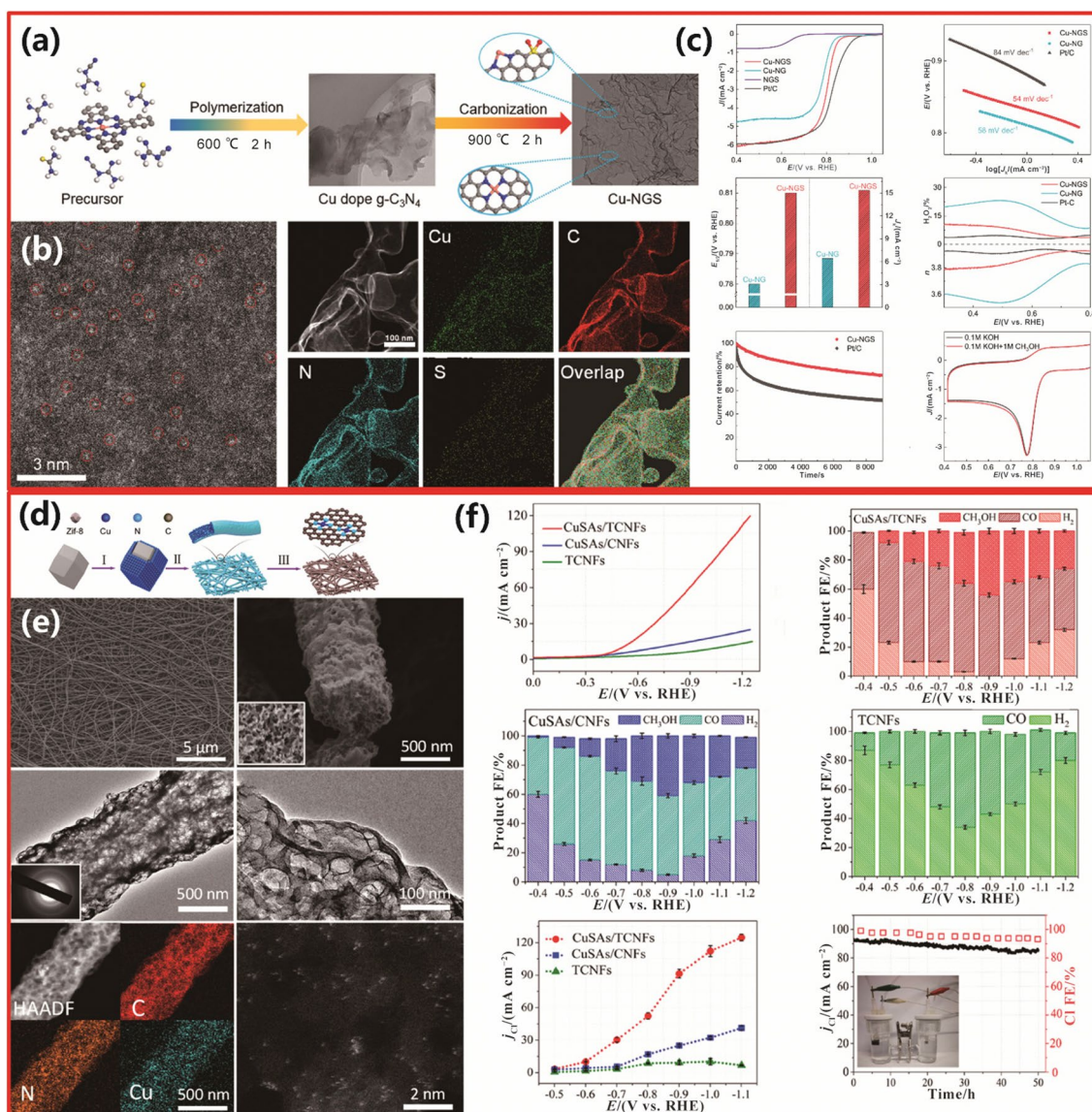


**Fig. 14** **a** Synthetic process of Cu-NGS. The H, S, N, O, Cu, and C atoms are represented by white, yellow, blue, red, pink, and gray balls, respectively. **b** Microscopy images of Cu-NGS. **c** Performance of Cu-NGS. Steady-state ORR polarization plots of NGS, Cu-NG, Cu-NGS, and Pt/C. The corresponding Tafel plots. Half-wave potentials and kinetic currents of Cu-NG and Cu-NGS. Electron transfer number ( $n$ ) and  $\text{H}_2\text{O}_2$  yield in the RRDE tests of Cu-NG, Cu-NGS, and Pt/C. Chronoamperometric responses of Cu-NGS and Pt/C at

0.8 V. Methanol tolerance tests of Cu-NGS. Reprinted with permission from Ref. [290]. Copyright © 2019, American Chemical Society. **d** Synthesis process of CuSAs/TCNFs. **e** Microscopy image of CuSAs/TCNFs. **f** LSV curves of CuSAs/TCNFs. Faradaic efficiencies of different products. Partial current densities. Stability of CuSAs/TCNFs. Reprinted with permission from Ref. [291]. Copyright © 2019, American Chemical Society

polymer materials have been widely used as carriers to prepare atomically dispersed metal-based catalysts [292, 293]. Functional groups containing N atoms on the interior of the cavity can pull metal precursors into the cavity. Metal complexes are trapped in the cages in situ once they are bound within the cage structures. The molecular cage as the encapsulation agent can control the metal particle size to obtain the desired single-atom catalyst [132].

Mo-based catalysts can be controllably synthesized at multiscale levels by a novel cage confinement pyrolysis route. Kou et al. [294] prepared Mo-based single-atom catalysts (called Mo SACs/N-C), as shown in Fig. 15a, b. N atoms of N-C carrier structures can controllably trap and isolate single atoms, clusters, and nanoparticles.  $[\text{MoO}_4]^{2-}$  was confined within the cavity of ZIF-8 to spatially separate Mo metal species of various sizes from the

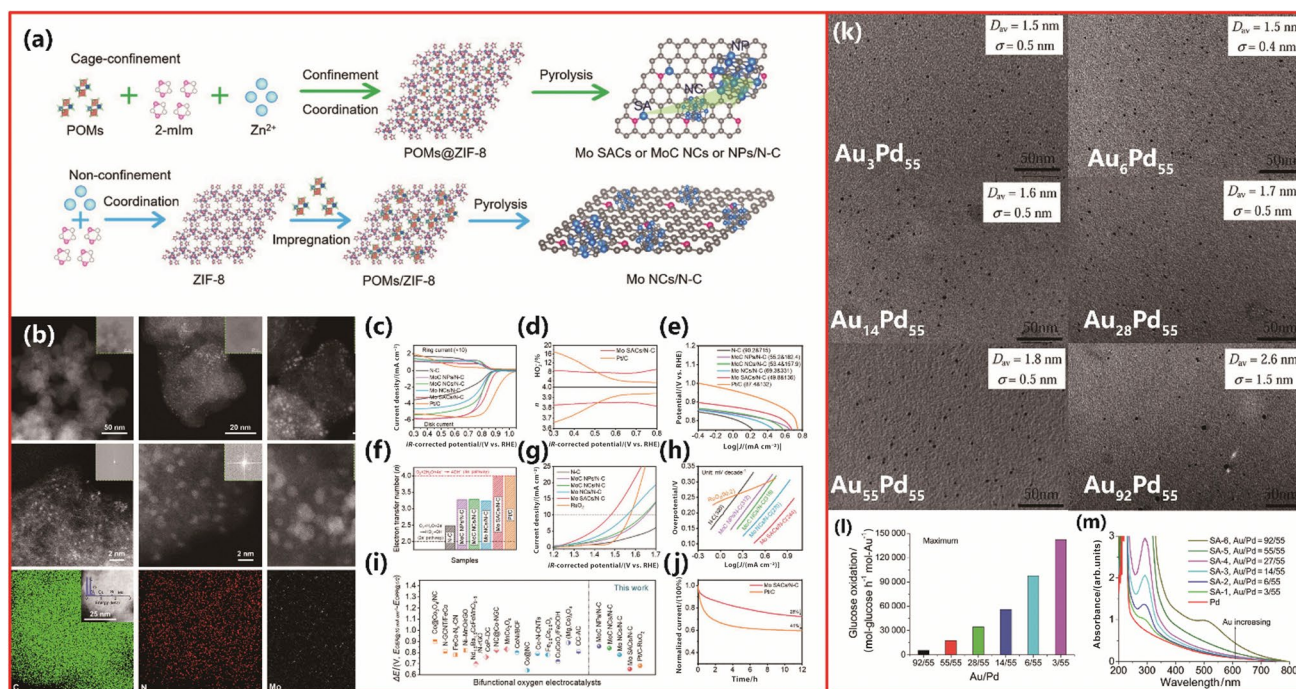


**Fig. 15** **a** Schematic diagram of the synthesis routes for selective cage confinement and nonconfinement. **b** Microscopy images of Mo-based catalysts. **c** Rotating ring-disk electrode voltammograms in alkaline solution. **d** The relationship between the electric potential, the electron transfer number and peroxide yield of Pt/C and Mo SAC/N–C catalysts. **e** Tafel plots of all catalysts for the ORR. **f** Electron transfer number of all catalysts. **g** Voltammograms of all catalysts for the OER with  $iR$  correction. **h** Tafel plots of all catalysts for

the OER. **i**  $\Delta E$  values of Mo-based catalysts and other ORR electrocatalysts. **j** Comparison of the current–time response curve. Reprinted with permission from Ref. [294]. Copyright © 2019, Elsevier Ltd. **k** TEM images of different Au/Pd SACs. **l** UV–vis spectra of different Au/Pd SACs in colloidal dispersions. **m** Catalytic activity of different Au/Pd SACs. Reprinted with permission from Ref. [295]. Copyright © 2014, The Royal Society of Chemistry

precursors. Then, on the nitrogen-doped carbon, a Mo-based catalyst was anchored during pyrolysis. Mo could be in the states of nanoparticles (11.73 wt.%), subnanometer clusters (7.57 wt.%), and single atoms (0.76 wt.% and 2.51 wt.%). As shown in Fig. 15b, in all samples, N, C, and Mo are distributed uniformly by EDS mapping of Mo SACs/N–C. Mo single atoms of Mo SACs/N–C are isolated bright dots in HAADF-STEM. As presented in Fig. 15c–i, the high half-wave potential ( $E_{1/2}$ ) of the ORR is 0.83 V when mediated by Mo SACs/N–C catalysis. This value is lower than that of Pt/C (0.90 V). At low overpotentials, the Tafel slope of Mo SACs/N–C is the lowest (49.8 mV dec<sup>-1</sup>), which confirms the excellent ORR performance. Moreover, this result suggests that the catalytic performance of the Mo SAC/N–C catalyst is extremely stable through a 12-h stability test at a current density of 10 mA cm<sup>-2</sup>, while the current loss of Mo SACs/N–C is 28%, which is lower than that of the reference Pt/C catalyst (41%) (Fig. 15j).

#### 4.3.2 Protection Agents for Single-Atom Catalysts

Polymers can be used as protective agents to protect metal particles, avoiding atom bonding during the preparation of

metal single-atom catalysts. Zhang et al. [295] used a step-wise reduction method with a reducing agent (L-ascorbic acid) and protection agent [polyvinyl pyrrolidone (PVP)] to prepare Au/Pd single-atom catalysts called Au/Pd SACs. In the synthesis, Pd nanoclusters were prepared as carriers by alcohol reduction. The obtained Pd clusters were then dispersed into the PVP solution and stirred sufficiently so that PVP could fully protect the metal particles. The Au atoms were reduced on the Pd clusters to obtain an Au/Pd single-atom catalyst. Depending on the molar ratio of starting materials Au<sup>3+</sup> and Pd at preparation, the catalysts are named SA-1 (3/55), SA-2 (6/55), SA-3 (14/55), SA-4 (28/55), SA-5 (55/55), and SA-6 (92/55). Figure 15k displays the deposited Au atoms on the Pd nanocluster surface. Figure 15l compares the UV–vis absorption spectra of Au/Pd SACs and Pd<sub>55</sub> clusters in aqueous dispersions. An increase in the Au content leads to an increased absorption intensity. The SA-1, SA-2, SA-3, SA-4, and SA-5 nanoclusters do not show a surface plasmon peak at 520 nm, which indicates that the Pd<sub>55</sub> nanoclusters are not fully covered with Au. However, for SA-6 nanoclusters, a core–shell structure is formed, based on the intense plasmon peak at 550 nm. In this core–shell structure, Au is the shell, and Pd is the core. For Au/Pd

SACs, the catalytic activity of aerobic glucose oxidation can be evaluated. As shown in Fig. 15m, for aerobic glucose oxidation, the composition variation in Au/Pd SACs changes the initial catalytic activity. This result indicates that the Au atom activity decreases with increasing Au content.

## 5 Summary and Outlook

### 5.1 Summary

The application of supporting materials (carriers) including polymers has shown a comprehensive impact on the catalytic performance, stability, and loading amount for single-atom catalysts. Research on single-atom catalysis involves condensed matter and chemical engineering, revealing the influence of the material structure on the performance in catalytic reactions. Single-atom catalysts have the highest utilization rate, which is superior to that of conventional heterogeneous catalysts, such as nanoparticles and nanoclusters [186]. The catalytic performance of a single-atom catalyst depends on the coordination environment rather than the traditional concepts of particle size, shape, and exposed facet(s) [188]. Single-atom catalysts, representing the lower limit of particle size, have attracted intensive attention for further improving the catalytic efficiency, increasing the abundance of active components, and effectively reducing the consumption of noble metals; moreover, such research necessitates studies for a fundamental understanding of the catalysis mechanisms.

In recent years, various single-atom catalytic materials have been successfully designed, fabricated, and characterized, as summarized in Table 2. The fabrication methods are based on two main strategies, i.e., bottom-up and top-down, depending on the conditions that form the single atoms. One of the most interesting advantages of bottom-up synthesis is the precise control of single atoms on the supports. This advantage benefits the selectivity of the catalysts and enables them to be suitable for complex organic reactions. In contrast, the disadvantages of this approach include the low loading of single atoms and harsh fabrication conditions, which subsequently increase the cost of catalyst fabrication. The advantage of top-down methods is high single-atom loading on the supports. However, the high loading inevitably induces agglomeration of the single atoms. The organometallic complex approach also faces the necessity of developing appropriate organic complexes to satisfy the fabrication conditions. Top-down methods use more polymers with many coordination functional groups as carriers, which may be a better way to prepare single-atom catalysts with abundant types and contents of functional groups.

The functions of polymers in single-atom catalysis include acting as synthetic templates, carriers for metal atoms, encapsulation agents, and protection agents, as shown in Fig. 16. These organic materials have flexible tunability, well-defined porosity, high surface area, and many unique functional groups. These features of polymers can anchor more active sites because of the generation of a larger support surface area. Polymers can also provide effective interactions between single atoms and their supports to balance catalytic activity and stability. Another feature of polymers and polymer-derived materials is that they usually contain abundant heteroatoms possessing lone electron pairs, such as N. The intensive coordination interaction of single metal atoms with lone electron pairs can anchor the metal atoms on the carrier to increase metal dispersion and density. Notably, these introduced heteroatoms can adjust the electronic structure of individual atoms. The lone electron pair coordination environment benefits the formation of single-atom catalysts because it can enlarge the average distance of a single precursor adsorbed on the polymer matrix [296–298]. Polymers with nitrogen groups are favorable candidates for dispersing active single atoms with weak aggregation and can influence charge distribution to improve the performance of catalysts. The innovative synthesis strategy of single-atom catalysts takes advantage of the N species in polymers.

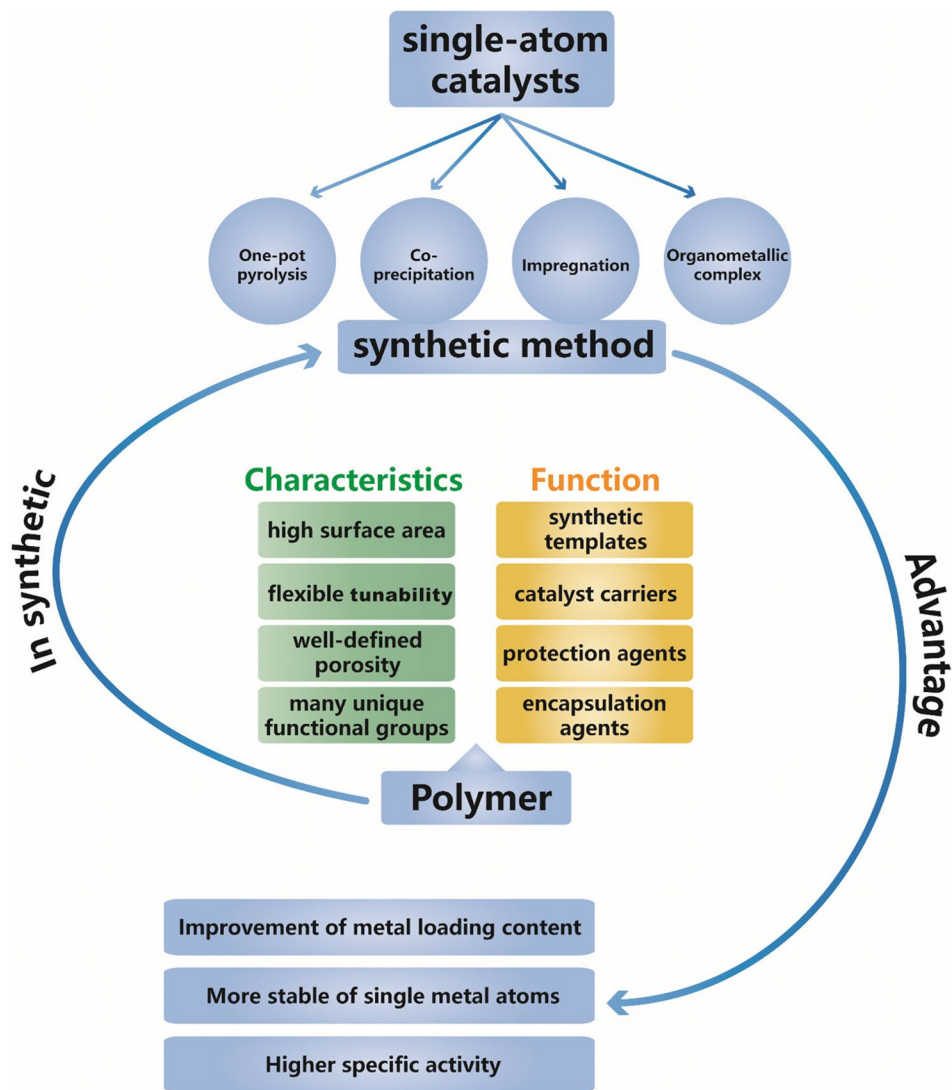
The well-defined structures and coordination environment on the polymer carriers can deliver greatly enhanced catalytic performance for single-atom catalysts. However, minor changes in the coordination environment can alter the electronic structure of single atoms, which in turn can change the intrinsic properties of the active sites. The accurate design and control of the coordination environments of active sites at the atomic scale on polymer carriers is a very important and challenging research field for the application of these carriers in the synthesis of single-atom catalysts. Research interests in this field include several aspects. For example, the immobilization of functional metal species (metal ions/clusters or organic ligands) depends on the exploration of combinations of metal species and carriers. Another aspect is how to control the spatial position and orientation of active sites in diverse polymers to generate synergistic catalysis and cascade reactions. Furthermore, techniques to tune the microenvironment around active metal centers need to be developed to enhance the reactivity and selectivity of single-atom catalysts.

The controllable synthesis of single-atom catalysts with an accurate metal content and distribution is an urgent challenge for the practical application of single-atom catalysts, although many synthesis techniques have been developed. Most synthesis methods are difficult to scale up for three

**Table 2** Comparison of different strategies for stabilizing single-atom catalysts

Stabilizing strategies	Synthesis methods	Single metals	Carriers	Catalyzed reactions	Advantages	Disadvantages	References
Bottom-Up Strategies	Mass-separated soft-landing method	Pd	Any substrate without high-surface-area carriers, such as MgO	Transforming acetylene trimerization to benzene	Precisely controlled deposition parameters at the atomic level	1. Ultrahigh vacuum deposition conditions 2. Extremely low yield 3. Easy aggregation	[192]
	Atomic layer deposition method	Pt, Ni	Catalyst carrier materials, such as CeO <sub>2</sub> , SiO <sub>2</sub> , and graphene	Methanol oxidation, Electrochemical reduction of 4-fluoronitrobenzene, Selective hydrogenation of 1,3-butadiene	1. Precisely controlled deposition parameters at the atomic level 2. The uniformity and repeatability of deposition	1. Low loading of single atoms 2. Strict synthetic conditions 3. High costs	[205–209]
	Co-precipitation method	Pt, Cu	Any catalyst carriers, such as CeO <sub>2</sub> and SiO <sub>2</sub>	CO shift reaction, Hydrogenation of 5-hydroxymethylfurfural	Simple procedure	Used a highly diluted solution of the target metal	[220–222]
	Impregnation method	Ir, La, Rh, Pt	Almost any metal species and carrier materials, such as activated carbon, ZrO <sub>2</sub> , and N-doped carbon	Heterogeneous methanol carbonylation, Methane oxidation	1. Suitable for preparing catalysts on open carriers 2. Controlled position of single metal atoms	The low loading of single atoms	[224, 227, 229]
Top-Down Strategies	One-pot pyrolysis method	Zn, Ni, Fe	Mostly carbon-based carriers, such as 1,10-phenanthroline, CNTs, and nitrogen-doped graphene	ORR, OER, CO <sub>2</sub> RR	The high loading of single atoms	The presence of clusters	[213, 215–219]
	Organometallic complexes approach	Pd, Pt, Rh, Fe, Co, Cr, Mn, Cu, Ni, Zn, Ru	Catalyst carrier materials, such as MOFs, zeolites, 1,10-phenanthroline hydrate, Al <sub>2</sub> O <sub>3</sub> , and TiO <sub>2</sub>	HER, Ammonia borane hydrolysis	The high loading of single atoms	Finding or designing a suitable organic complex	[230–234]

**Fig. 16** Characteristics and application of polymers and the advantages of using polymers to synthesize single-atom catalysts



main reasons. First, single-atom catalysts are not stable enough to meet the industrial requirements for long-term cycling stability, especially for high metal loading or high reaction temperature. Furthermore, the high price makes industrial-scale fabrication difficult. Thus, developing new methods to overcome these challenges is of great practical significance for the large-scale synthesis and applications of single-atom catalysts. Most importantly, the process of fabricating single-atom catalysts is complicated and not environmentally friendly, such as the heat treatment of polymer precursors. In particular, polymers doped with S or P will lead to negative effects, including low efficiency, harmful element/composite emissions, water pollution, and so on. Therefore, green, facile, and general strategies are under exploration to synthesize single-atom catalysts with good stability and high loading amounts.

## 5.2 Technical Challenges and the Corresponding Analysis

### 5.2.1 Improvement in the Metal Loading Content

The catalytic activity significantly depends on the content of metal loading because a high loading will generate more active sites in catalytic reactions. However, the metal loading amount is less than 1% in almost all cases. Heteroatoms can be employed as stabilizing centers, which are anchored on defect sites of the carrier. Metal atoms can coordinate with heteroatoms to achieve high metal loadings [97, 101]. Nitrogen atoms are effective in anchoring single metal atoms. Metal atoms can be fixed on the carrier by nitrogen atoms in a variety of nitrogen-containing carriers, such as  $C_3N_4$ , pyrrole, phenanthroline, and graphene. As the nitrogen

content increases, the metal atom loading in the catalyst can be effectively increased. It should be noted that some of the reported high loading amounts are attributed to metals buried within the carriers or binding agents. Therefore, the loading amount of single atoms exposed to the reactants needs further research.

### 5.2.2 Stabilization

Another important issue of single-atom catalysts is stability. The metal atoms on the surface should remain in single-atom states. The activity and stability of surface reactions are determined by the interaction degree between the carrier and metal atom. It is easy to form nanoparticles due to agglomeration without stronger interactions between surface metal atoms and carriers. When defect sites of a carrier trap single atoms, a single atomic structure can remain thermodynamically stabilized, which has been confirmed by many recent studies [188, 299]. Defective carrier design is vital for controlling the atomic structure of the metal. Furthermore, the stability under the appropriate reaction conditions should be evaluated. Under certain reaction conditions, including redox reactions, hydrothermal treatments, and high temperatures or voltages, the catalysts endure harsh environments. Under such harsh conditions, defect sites can be stabilized by metal atoms with catalytic activity. Therefore, after metal deposition, the overall structure can be stabilized.

### 5.2.3 Oxidic Electronic States

The specific activity of a single-atom catalyst is higher than that of its corresponding nanoparticles, which is often debated. Surface reactions would be affected by the electronic state of the surrounding atoms. The single atom will become oxidic due to the intensive interaction between the single atoms and carriers, stabilizing metal single atoms on defects. It is easy to form nanoparticles because oxidic single atoms are not stable in a reducing environment. Studies on controlling the electronic state of single atoms are rare. The catalytic activity and selectivity will be further improved under highly reducing conditions if single atoms remain stable.

### 5.2.4 Absence of Ensemble Sites

A disadvantage of single-atom catalysts may be the lack of ensemble sites. Ensemble sites are required in some reactions. For example, two adjacent adsorption sites are generally required for C–C coupling, for example, in the electroreduction of CO<sub>2</sub> to C<sub>2</sub> hydrocarbons [300, 301]. Moreover, single-atom catalysts show activity at much higher overpotentials or temperatures for such reactions. Even when single-atom catalysts are widely dispersed, some single atoms are trapped in the micropore network and cannot form ensemble

sites for the catalytic reaction. In contrast, it is beneficial to design raft structures for single-atom catalysts. In the raft structure, even the metal atoms that are buried deeply inside the carrier can participate in the catalytic reaction. As such, this system can significantly improve the atomic efficiency of the monatomic catalyst. In summary, precise control of ensemble sites will benefit the catalytic reaction.

## 5.3 Proposed Future Research Directions

### 5.3.1 Further Studying the Catalytic Mechanisms of Single-Atom Catalysts

Compared to that of regular catalysts, the catalytic mechanism of single-atom catalysts needs further study. Most mechanistic studies are based on DFT calculations, and reaction energy diagrams have been reported for several transition metal single-atom catalysts [101]. Vijay et al. [302] used DFT to investigate the catalytic mechanisms of CO<sub>2</sub>RR by transition metal catalysts. The results show that materials with similar narrow d states, such as ionic compounds, supporting clusters, molecules and single atoms, can be optimized to be large dipoles, achieving higher catalytic activity beyond the transition metal scale. This principle also applies to other processes in which the decisive factor is the interaction of adsorbed species. DFT simulations are often implemented based on the most simplistic conditions. Some important parameters are absent in the simulation, such as water involvement, cations, pH value, and electric field. The reaction energy diagram should be improved to realistically reflect the single-atom catalytic process. A large gap exists between the understanding of the mechanism on single-atom catalysts compared to heterogeneous catalysis and homogeneous catalysis, which might be filled by machine learning based on a large quantity of published data. The fundamental understanding of single-atom catalysis can improve the accuracy of data analysis and lead to advances in single-atom catalyst design.

### 5.3.2 Further Increasing the Loading Content of Single-Atom Catalysts

Single-atom catalysts demonstrate excellent performance, but they also have some strict requirements, for example, ensuring that the loading content for practical applications is high enough while keeping the reaction sites isolated under catalytic conditions. Some challenges remain in actual preparations of single-atom catalysts with a high loading content. (a) The binding sites, which can coordinate with single atoms, are few. (b) No ideal species isolate individual metal atoms anchored to the carrier. (c) The distribution of anchoring sites on carrier surfaces is heterogeneous, which leads to nonuniform metal sites. The functionalization of carrier surfaces is in high demand for the accurate trapping

of single metal atoms. With breakthroughs in carrier materials via functionalization and nanostructure design, single-atom catalysts can be developed for practical applications.

### 5.3.3 Further Development Toward Large-Scale Implementation of Single-Atom Catalysts

Practical applications require the large-scale fabrication of single-atom catalysts via simple and economical methods. With the development of single-atom catalysts, researchers are gradually beginning to understand the complex reaction systems and dynamic structure evolution of these catalysts in depth. Single-atom catalysts should be combined with practical applications of industrial chemical catalysis. Technical issues, including the capacity of equipment and the reactor size, should be considered more in the preparation of single-atom catalysts. Some industrial parameters, such as large-scale production, space–time yield, and stability, are significant indexes for evaluating the economy of reactions. Few studies have been reported on the large-scale production of single-atom catalysts with stability and high loading. Hence, it is highly desirable to develop universal and simple methods that can be used to prepare single-atom catalysts.

**Acknowledgements** This work is financially supported by the National Natural Science Foundation of China (Grant No. 51572166). W.X. Li acknowledges research supported by the Program for Professor of Special Appointment (Eastern Scholar: TP2014041) at Shanghai Institutions of Higher Learning.

**Author Contributions** W.X. Li conceived of the presented idea. Z.H. Guo and W.X. Li wrote the manuscript with support from J. Yang, Y. Li, and H.Y. He. X.L. Sun, S. Li, and J.J. Zhang proposed research summaries and directions. All authors discussed the contents and contributed to the final manuscript.

**Funding** Open Access funding enabled and organized by CAUL and its Member Institutions.

### Declarations

**Conflict of interest** The authors declare that they have no conflict of interest.

**Ethics approval** Not applicable.

**Open Access** This article is licensed under a Creative Commons Attribution 4.0 International License, which permits use, sharing, adaptation, distribution and reproduction in any medium or format, as long as you give appropriate credit to the original author(s) and the source, provide a link to the Creative Commons licence, and indicate if changes were made. The images or other third party material in this article are included in the article's Creative Commons licence, unless indicated otherwise in a credit line to the material. If material is not included in the article's Creative Commons licence and your intended use is not permitted by statutory regulation or exceeds the permitted use, you will need to obtain permission directly from the copyright holder. To view a copy of this licence, visit <http://creativecommons.org/licenses/by/4.0/>.

## References

- Jansi Rani, B., Ravi, G., Yuvakkumar, R., et al.: CoNiSe<sub>2</sub> nanostructures for clean energy production. *ACS Omega* **5**, 14702–14710 (2020). <https://doi.org/10.1021/acsomega.0c01476>
- Olivos-Suarez, A.I., Szécsényi, À., Hensen, E.J.M., et al.: Strategies for the direct catalytic valorization of methane using heterogeneous catalysis: challenges and opportunities. *ACS Catal.* **6**, 2965–2981 (2016). <https://doi.org/10.1021/acscatal.6b00428>
- Hosseini, S.E., Abdul Wahid, M.: The role of renewable and sustainable energy in the energy mix of Malaysia: a review. *Int. J. Energy Res.* **38**, 1769–1792 (2014). <https://doi.org/10.1002/er.3190>
- Dincer, I., Acar, C.: A review on clean energy solutions for better sustainability. *Int. J. Energy Res.* **39**, 585–606 (2015). <https://doi.org/10.1002/er.3329>
- Sørensen, B.: A sustainable energy future: construction of demand and renewable energy supply scenarios. *Int. J. Energy Res.* **32**, 436–470 (2008). <https://doi.org/10.1002/er.1375>
- Duan, J., Tang, X., Dai, H.F., et al.: Building safe lithium-ion batteries for electric vehicles: a review. *Electrochem. Energy Rev.* **3**, 1–42 (2020). <https://doi.org/10.1007/s41918-019-00060-4>
- Wu, D., Peng, C., Yin, C., et al.: Review of system integration and control of proton exchange membrane fuel cells. *Electrochem. Energy Rev.* **3**, 466–505 (2020). <https://doi.org/10.1007/s41918-020-00068-1>
- Lokhande, P.E., Chavan, U.S., Pandey, A.: Materials and fabrication methods for electrochemical supercapacitors: overview. *Electrochem. Energy Rev.* **3**, 155–186 (2020). <https://doi.org/10.1007/s41918-019-00057-z>
- Lu, J.J., Yin, S.B., Shen, P.K.: Carbon-encapsulated electrocatalysts for the hydrogen evolution reaction. *Electrochem. Energy Rev.* **2**, 105–127 (2019). <https://doi.org/10.1007/s41918-018-0025-9>
- Jia, Y.F., Yuan, Y., Sun, J., et al.: Porous PEDOT network coated on MoS<sub>2</sub> nanobelts toward improving capacitive performance. *ACS Sustain. Chem. Eng.* **8**, 12696–12705 (2020). <https://doi.org/10.1021/acssuschemeng.0c04791>
- Friedl, J., Lebedeva, M.A., Porfyrakis, K., et al.: All-fullerene-based cells for nonaqueous redox flow batteries. *J. Am. Chem. Soc.* **140**, 401–405 (2018). <https://doi.org/10.1021/jacs.7b11041>
- Braun, P.V., Cook, J.B.: Deterministic design of chemistry and mesostructure in Li-ion battery electrodes. *ACS Nano* **12**, 3060–3064 (2018). <https://doi.org/10.1021/acsnano.8b01885>
- Zhou, G.M., Xu, L., Hu, G.W., et al.: Nanowires for electrochemical energy storage. *Chem. Rev.* **119**, 11042–11109 (2019). <https://doi.org/10.1021/acs.chemrev.9b00326>
- Wang, Y.J., Yang, Y., Zou, L.L., et al.: Carbon-supported W@Pt nanoparticles with a Pt-enriched surface as a robust electrocatalyst for oxygen reduction reactions. *ChemistrySelect* **3**, 1056–1061 (2018). <https://doi.org/10.1002/slct.201702493>
- Li, Y.W., Zhang, W.J., Li, J., et al.: Fe-MOF-derived efficient ORR/OER bifunctional electrocatalyst for rechargeable zinc–air batteries. *ACS Appl. Mater. Interfaces* **12**, 44710–44719 (2020). <https://doi.org/10.1021/acsami.0c11945>
- Vinod Selvaganesh, S., Selvarani, G., Sridhar, P., et al.: Graphitic carbon as durable cathode-catalyst support for PEFCs. *Fuel Cells* **11**, 372–384 (2011). <https://doi.org/10.1002/fuce.201000151>
- Chen, C., Kang, Y.J., Huo, Z.Y., et al.: Highly crystalline multi-metallic nanoframes with three-dimensional electrocatalytic surfaces. *Science* **343**, 1339–1343 (2014). <https://doi.org/10.1126/science.1249061>
- Mohanta, P.K., Regnet, F., Jörissen, L.: Impact of highly stable catalyst support materials on polymer electrolyte membrane fuel

- cell performance. *Energy Technol.* **8**, 2000081 (2020). <https://doi.org/10.1002/ente.202000081>
19. Sun, R.L., Xia, Z.X., Qi, F.L., et al.: Efficient design for a high-energy and high-power capability hybrid electric power device with enhanced electrochemical interfaces. *ACS Appl. Mater. Interfaces* **11**, 19943–19949 (2019). <https://doi.org/10.1021/acscami.9b01863>
  20. Yao, Y., Wang, J., Shahid, U.B., et al.: Electrochemical synthesis of ammonia from nitrogen under mild conditions: current status and challenges. *Electrochem. Energy Rev.* **3**, 239–270 (2020). <https://doi.org/10.1007/s41918-019-00061-3>
  21. Wang, X.Q., Li, Z.J., Qu, Y.T., et al.: Review of metal catalysts for oxygen reduction reaction: from nanoscale engineering to atomic design. *Chem* **5**, 1486–1511 (2019). <https://doi.org/10.1016/j.chempr.2019.03.002>
  22. Wang, Y., Wang, D.S., Li, Y.D.: A fundamental comprehension and recent progress in advanced Pt-based ORR nanocatalysts. *SmartMat* **2**, 56–75 (2021). <https://doi.org/10.1002/smm2.1023>
  23. Keith, J.A., Jacob, T.: Theoretical studies of potential-dependent and competing mechanisms of the electrocatalytic oxygen reduction reaction on Pt(111). *Angew. Chem. Int. Ed.* **49**, 9521–9525 (2010). <https://doi.org/10.1002/anie.201004794>
  24. Zhang, B.W., Wang, Y.X., Chou, S.L., et al.: Fabrication of superior single-atom catalysts toward diverse electrochemical reactions. *Small Methods* **3**, 1800497 (2019). <https://doi.org/10.1002/smt.201800497>
  25. Zhu, C.Z., Fu, S.F., Shi, Q.R., et al.: Single-atom electrocatalysts. *Angew. Chem. Int. Ed.* **56**, 13944–13960 (2017). <https://doi.org/10.1002/anie.201703864>
  26. Wang, Y.X., Su, H.Y., He, Y.H., et al.: Advanced electrocatalysts with single-metal-atom active sites. *Chem. Rev.* **120**, 12217–12314 (2020). <https://doi.org/10.1021/acs.chemrev.0c00594>
  27. Hlatky, G.G.: Heterogeneous single-site catalysts for olefin polymerization. *Chem. Rev.* **100**, 1347–1376 (2000). <https://doi.org/10.1021/cr9902401>
  28. Ye, R., Zhao, J., Wickemeyer, B.B., et al.: Foundations and strategies of the construction of hybrid catalysts for optimized performances. *Nat. Catal.* **1**, 318–325 (2018). <https://doi.org/10.1038/s41929-018-0052-2>
  29. Wang, M., Chen, L., Sun, L.C.: Recent progress in electrochemical hydrogen production with earth-abundant metal complexes as catalysts. *Energy Environ. Sci.* **5**, 6763–6778 (2012). <https://doi.org/10.1039/c2ee03309g>
  30. He, Q., Lee, J.H., Liu, D.B., et al.: Accelerating CO<sub>2</sub> electroreduction to CO over Pd single-atom catalyst. *Adv. Funct. Mater.* **30**, 2000407 (2020). <https://doi.org/10.1002/adfm.202000407>
  31. Jiao, J., Lin, R., Liu, S., et al.: Copper atom-pair catalyst anchored on alloy nanowires for selective and efficient electrochemical reduction of CO<sub>2</sub>. *Nat. Chem.* **11**, 222–228 (2019). <https://doi.org/10.1038/s41557-018-0201-x>
  32. Sun, L.B., Reddu, V., Fisher, A.C., et al.: Electrocatalytic reduction of carbon dioxide: opportunities with heterogeneous molecular catalysts. *Energy Environ. Sci.* **13**, 374–403 (2020). <https://doi.org/10.1039/c9ee03660a>
  33. Wang, X., Peng, X., Chen, W., et al.: Insight into dynamic and steady-state active sites for nitrogen activation to ammonia by cobalt-based catalyst. *Nat. Commun.* **11**, 653 (2020). <https://doi.org/10.1038/s41467-020-14287-z>
  34. Yang, Y.L., Li, F., Chen, J., et al.: Single Au atoms anchored on amino-group-enriched graphitic carbon nitride for photocatalytic CO<sub>2</sub> reduction. *ChemSuschem* **13**, 1979–1985 (2020). <https://doi.org/10.1002/cssc.202000375>
  35. Zhong, L.X., Zhang, L.M., Li, S.Z.: Understanding the activity of carbon-based single-atom electrocatalysts from ab initio simulations. *ACS Mater. Lett.* **3**, 110–120 (2021). <https://doi.org/10.1021/acsmaterialslett.0c00419>
  36. Singh, B., Sharma, V., Gaikwad, R.P., et al.: Single-atom catalysts: a sustainable pathway for the advanced catalytic applications. *Small* **17**, 2006473 (2021). <https://doi.org/10.1002/smll.202006473>
  37. Xie, C., Yan, D.F., Li, H., et al.: Defect chemistry in heterogeneous catalysis: recognition, understanding, and utilization. *ACS Catal.* **10**, 11082–11098 (2020). <https://doi.org/10.1021/acscatal.0c03034>
  38. Zhang, B.L., Yu, H.Y., Wang, J.Q., et al.: Synthesis of CeO<sub>2</sub> nanoparticles with different morphologies and their properties as peroxidase mimic. *J. Am. Ceram. Soc.* **102**, 2218–2227 (2019). <https://doi.org/10.1111/jace.16071>
  39. Jin, R.C., Li, G., Sharma, S., et al.: Toward active-site tailoring in heterogeneous catalysis by atomically precise metal nanoclusters with crystallographic structures. *Chem. Rev.* **121**, 567–648 (2021). <https://doi.org/10.1021/acs.chemrev.0c00495>
  40. Ma, Z., Dai, S.: Development of novel supported gold catalysts: a materials perspective. *Nano Res.* **4**, 3–32 (2011). <https://doi.org/10.1007/s12274-010-0025-5>
  41. Zuliani, A., Ivars, F., Luque, R.: Advances in nanocatalyst design for biofuel production. *ChemCatChem* **10**, 1968–1981 (2018). <https://doi.org/10.1002/cctc.201701712>
  42. Srinivasan, S., Demirocak, D.E., Kaushik, A., et al.: Reversible hydrogen storage using nanocomposites. *Appl. Sci.* **10**, 4618 (2020). <https://doi.org/10.3390/app10134618>
  43. Gadipelly, C., Mannepalli, L.K.: Nano-metal oxides for organic transformations. *Curr. Opin. Green Sustain. Chem.* **15**, 20–26 (2019). <https://doi.org/10.1016/j.cogsc.2018.08.002>
  44. Vignarooban, K., Lin, J., Arvay, A., et al.: Nano-electrocatalyst materials for low temperature fuel cells: a review. *Chin. J. Catal.* **36**, 458–472 (2015). [https://doi.org/10.1016/S1872-2067\(14\)60175-3](https://doi.org/10.1016/S1872-2067(14)60175-3)
  45. Thoda, O., Xanthopoulou, G., Vekinis, G., et al.: Review of recent studies on solution combustion synthesis of nanostructured catalysts. *Adv. Eng. Mater.* **20**, 1800047 (2018). <https://doi.org/10.1002/adem.201800047>
  46. Niemann, M.U., Srinivasan, S.S., Phani, A.R., et al.: Nanomaterials for hydrogen storage applications: a review. *J. Nanomater.* **2008**, 950967 (2008). <https://doi.org/10.1155/2008/950967>
  47. Mohamed, R.M., McKinney, D.L., Sigmund, W.M.: Enhanced nanocatalysts. *Mater. Sci. Eng. R Rep.* **73**, 1–13 (2012). <https://doi.org/10.1016/j.mser.2011.09.001>
  48. Jung, N., Chung, D.Y., Ryu, J., et al.: Pt-based nanoarchitecture and catalyst design for fuel cell applications. *Nano Today* **9**, 433–456 (2014). <https://doi.org/10.1016/j.nantod.2014.06.006>
  49. Ambat, I., Srivastava, V., Sillanpää, M.: Recent advancement in biodiesel production methodologies using various feedstock: a review. *Renew. Sustain. Energy Rev.* **90**, 356–369 (2018). <https://doi.org/10.1016/j.rser.2018.03.069>
  50. Fukuzumi, S., Yamada, Y., Suenobu, T., et al.: Catalytic mechanisms of hydrogen evolution with homogeneous and heterogeneous catalysts. *Energy Environ. Sci.* **4**, 2754–2766 (2011). <https://doi.org/10.1039/c1ee01551f>
  51. Shen, H., Li, Y.J., Shi, Z.Q.: A novel graphdiyne-based catalyst for effective hydrogenation reaction. *ACS Appl. Mater. Interfaces* **11**, 2563–2570 (2019). <https://doi.org/10.1021/acscami.8b00566>
  52. Liang, H., Li, T.R., Zhang, J., et al.: 3-D hierarchical Ag/ZnO@CF for synergistically removing phenol and Cr(VI): heterogeneous vs. homogeneous photocatalysis. *J. Colloid Interface Sci.* **558**, 85–94 (2020). <https://doi.org/10.1016/j.jcis.2019.09.105>
  53. Zhou, J., Zhang, Y., Li, S., et al.: Ni/NiO nanocomposites with rich oxygen vacancies as high-performance catalysts for

- nitrophenol hydrogenation. *Catalysts* **9**, 944 (2019). <https://doi.org/10.3390/catal9110944>
54. de Vos, A., Lejaeghere, K., Muniz Miranda, F., et al.: Electronic properties of heterogenized Ru(II) polypyridyl photoredox complexes on covalent triazine frameworks. *J. Mater. Chem. A* **7**, 8433–8442 (2019). <https://doi.org/10.1039/c9ta00573k>
55. Ge, R.Y., Huo, J.J., Liao, T., et al.: Hierarchical molybdenum phosphide coupled with carbon as a whole pH-range electrocatalyst for hydrogen evolution reaction. *Appl. Catal. B Environ.* **260**, 118196 (2020). <https://doi.org/10.1016/j.apcatb.2019.118196>
56. Ge, R.Y., Li, W.X., Huo, J.J., et al.: Metal-ion bridged high conductive RGO-M-MoS<sub>2</sub> (M = Fe<sup>3+</sup>, Co<sup>2+</sup>, Ni<sup>2+</sup>, Cu<sup>2+</sup> and Zn<sup>2+</sup>) composite electrocatalysts for photo-assisted hydrogen evolution. *Appl. Catal. B Environ.* **246**, 129–139 (2019). <https://doi.org/10.1016/j.apcatb.2019.01.047>
57. Zhu, M.Y., Yu, S.J., Ge, R.Y., et al.: Cobalt oxide supported on phosphorus-doped g-C<sub>3</sub>N<sub>4</sub> as an efficient electrocatalyst for oxygen evolution reaction. *ACS Appl. Energy Mater.* **2**, 4718–4729 (2019). <https://doi.org/10.1021/acsaem.9b00273>
58. Huo, J.J., Chen, Y.L., Liu, Y., et al.: Bifunctional iron nickel phosphide nanocatalysts supported on porous carbon for highly efficient overall water splitting. *Sustain. Mater. Technol.* **22**, e00117 (2019). <https://doi.org/10.1016/j.susmat.2019.e00117>
59. Li, W.X., He, X.F., Ge, R.Y., et al.: Cobalt porphyrin (CoTCPP) advanced visible light response of g-C<sub>3</sub>N<sub>4</sub> nanosheets. *Sustain. Mater. Technol.* **22**, e00114 (2019). <https://doi.org/10.1016/j.susmat.2019.e00114>
60. Ge, R.Y., Huo, J.J., Sun, M.J., et al.: Surface and interface engineering: molybdenum carbide-based nanomaterials for electrochemical energy conversion. *Small* **17**, 1903380 (2021). <https://doi.org/10.1002/sml.201903380>
61. Desalegn, B.Z., Jadhav, H.S., Seo, J.G.: Highly efficient g-C<sub>3</sub>N<sub>4</sub> nanorods with dual active sites as an electrocatalyst for the oxygen evolution reaction. *ChemCatChem* **11**, 2870–2878 (2019). <https://doi.org/10.1002/cctc.201900330>
62. Liu, M.M., Wang, L.L., Zhao, K.N., et al.: Atomically dispersed metal catalysts for the oxygen reduction reaction: synthesis, characterization, reaction mechanisms and electrochemical energy applications. *Energy Environ. Sci.* **12**, 2890–2923 (2019). <https://doi.org/10.1039/c9ee01722d>
63. Liu, Q., Zhang, Z.L.: Platinum single-atom catalysts: a comparative review towards effective characterization. *Catal. Sci. Technol.* **9**, 4821–4834 (2019). <https://doi.org/10.1039/c9cy01028a>
64. Vancsó, P., Popov, Z.I., Pető, J., et al.: Transition metal chalcogenide single layers as an active platform for single-atom catalysis. *ACS Energy Lett.* **4**, 1947–1953 (2019). <https://doi.org/10.1021/acseenergylett.9b01097>
65. Qiao, B., Wang, A., Yang, X., et al.: Single-atom catalysis of CO oxidation using Pt<sub>1</sub>/FeO<sub>x</sub>. *Nat. Chem.* **3**, 634–641 (2011). <https://doi.org/10.1038/nchem.1095>
66. Lin, J., Wang, A.Q., Qiao, B.T., et al.: Remarkable performance of Ir<sub>1</sub>/FeO<sub>x</sub> single-atom catalyst in water gas shift reaction. *J. Am. Chem. Soc.* **135**, 15314–15317 (2013). <https://doi.org/10.1021/ja408574m>
67. Wang, Y., Arandiyán, H., Scott, J., et al.: Single atom and nanoclustered Pt catalysts for selective CO<sub>2</sub> reduction. *ACS Appl. Energy Mater.* **1**, 6781–6789 (2018). <https://doi.org/10.1021/acsaem.8b00817>
68. Sun, M.H., Ji, J.P., Hu, M.Y., et al.: Overwhelming the performance of single atoms with atomic clusters for platinum-catalyzed hydrogen evolution. *ACS Catal.* **9**, 8213–8223 (2019). <https://doi.org/10.1021/acscatal.9b02305>
69. Zhang, X., Zhang, Z.H., Wu, D.H., et al.: K<sub>1-x</sub>Mo<sub>3</sub>P<sub>2</sub>O<sub>14</sub> as support for single-atom catalysts. *J. Phys. Chem. C* **121**, 22895–22900 (2017). <https://doi.org/10.1021/acs.jpcc.7b07643>
70. Sun, J.F., Xu, Q.Q., Qi, J.L., et al.: Isolated single atoms anchored on N-doped carbon materials as a highly efficient catalyst for electrochemical and organic reactions. *ACS Sustain. Chem. Eng.* **8**, 14630–14656 (2020). <https://doi.org/10.1021/acssuschemeng.0c04324>
71. Kunwar, D., Zhou, S.L., DeLaRiva, A., et al.: Stabilizing high metal loadings of thermally stable platinum single atoms on an industrial catalyst support. *ACS Catal.* **9**, 3978–3990 (2019). <https://doi.org/10.1021/acscatal.8b04885>
72. Han, C.W., Iddir, H., Uzun, A., et al.: Migration of single iridium atoms and tri-iridium clusters on MgO surfaces: aberration-corrected STEM imaging and ab initio calculations. *J. Phys. Chem. Lett.* **6**, 4675–4679 (2015). <https://doi.org/10.1021/acs.jpcclett.5b01884>
73. Kwon, K.C., Suh, J.M., Varma, R.S., et al.: Electrocatalytic water splitting and CO<sub>2</sub> reduction: sustainable solutions via single-atom catalysts supported on 2D materials. *Small Methods* **3**, 1800492 (2019). <https://doi.org/10.1002/smt.20180492>
74. Büchele, S., Chen, Z.P., Mitchell, S., et al.: Tailoring nitrogen-doped carbons as hosts for single-atom catalysts. *ChemCatChem* **11**, 2812–2820 (2019). <https://doi.org/10.1002/cctc.201900547>
75. Sharifi, T., Gracia-Espino, E., Chen, A.R., et al.: Oxygen reduction reactions on single- or few-atom discrete active sites for heterogeneous catalysis. *Adv. Energy Mater.* **10**, 1902084 (2020). <https://doi.org/10.1002/aenm.201902084>
76. Wang, A., Li, J., Zhang, T.: Heterogeneous single-atom catalysis. *Nat. Rev. Chem.* **2**, 65–81 (2018). <https://doi.org/10.1038/s41570-018-0010-1>
77. Li, Z., Ji, S.F., Liu, Y.W., et al.: Well-defined materials for heterogeneous catalysis: from nanoparticles to isolated single-atom sites. *Chem. Rev.* **120**, 623–682 (2020). <https://doi.org/10.1021/acs.chemrev.9b00311>
78. Wang, L.Q., Huang, L., Liang, F., et al.: Preparation, characterization and catalytic performance of single-atom catalysts. *Chin. J. Catal.* **38**, 1528–1539 (2017). [https://doi.org/10.1016/S1872-2067\(17\)62770-0](https://doi.org/10.1016/S1872-2067(17)62770-0)
79. Lang, R., Li, T.B., Matsumura, D., et al.: Hydroformylation of olefins by a rhodium single-atom catalyst with activity comparable to RhCl(PPh<sub>3</sub>)<sub>3</sub>. *Angew. Chem. Int. Ed.* **55**, 16054–16058 (2016). <https://doi.org/10.1002/anie.201607885>
80. Li, J.C., Wei, Z.D., Liu, D., et al.: Dispersive single-atom metals anchored on functionalized nanocarbons for electrochemical reactions. In: Shao, M.H. (ed.) *Electrocatalysis*. Topics in Current Chemistry Collections, pp. 127–148. Springer, Cham (2020). [https://doi.org/10.1007/978-3-030-43294-2\\_5](https://doi.org/10.1007/978-3-030-43294-2_5)
81. Wang, Q., Astruc, D.: State of the art and prospects in metal-organic framework (MOF)-based and MOF-derived nanocatalysis. *Chem. Rev.* **120**, 1438–1511 (2020). <https://doi.org/10.1021/acs.chemrev.9b00223>
82. Song, Z.X., Zhang, L., Doyle-Davis, K., et al.: Recent advances in MOF-derived single atom catalysts for electrochemical applications. *Adv. Energy Mater.* **10**, 2001561 (2020). <https://doi.org/10.1002/aenm.202001561>
83. Wang, H.F., Chen, L.Y., Pang, H., et al.: MOF-derived electrocatalysts for oxygen reduction, oxygen evolution and hydrogen evolution reactions. *Chem. Soc. Rev.* **49**, 1414–1448 (2020). <https://doi.org/10.1039/c9cs00906j>
84. Lu, X.F., Xia, B.Y., Zang, S.Q., et al.: Metal-organic frameworks based electrocatalysts for the oxygen reduction reaction. *Angew. Chem. Int. Ed.* **59**, 4634–4650 (2020). <https://doi.org/10.1002/anie.201910309>
85. Guo, J.J., Huo, J.J., Liu, Y., et al.: Nitrogen-doped porous carbon supported nonprecious metal single-atom electrocatalysts: from synthesis to application. *Small Methods* **3**, 1900159 (2019). <https://doi.org/10.1002/smt.201900159>

86. Xu, J.T., Ouyang, J.Y., Fan, Z.Q., et al.: Polymer-supported half-titanocene catalysts for the syndiospecific polymerization of styrene. *J. Polym. Sci. A Polym. Chem.* **38**, 127–135 (2000). [https://doi.org/10.1002/\(SICI\)1099-0518\(20000101\)38:1%3c127::AID-POLA17%3e3.0.CO;2-8](https://doi.org/10.1002/(SICI)1099-0518(20000101)38:1%3c127::AID-POLA17%3e3.0.CO;2-8)
87. Chen, W.X., Pei, J.J., He, C.T., et al.: Rational design of single molybdenum atoms anchored on N-doped carbon for effective hydrogen evolution reaction. *Angew. Chem. Int. Ed.* **56**, 16086–16090 (2017). <https://doi.org/10.1002/anie.201710599>
88. Wei, Y.S., Zhang, M., Zou, R.Q., et al.: Metal–organic framework-based catalysts with single metal sites. *Chem. Rev.* **120**, 12089–12174 (2020). <https://doi.org/10.1021/acs.chemrev.9b00757>
89. Chen, Y., Ji, S., Zhao, S., et al.: Enhanced oxygen reduction with single-atomic-site iron catalysts for a zinc-air battery and hydrogen-air fuel cell. *Nat. Commun.* **9**, 5422 (2018). <https://doi.org/10.1038/s41467-018-07850-2>
90. Wang, X., Chen, W.X., Zhang, L., et al.: Uncoordinated amine groups of metal–organic frameworks to anchor single Ru sites as chemoselective catalysts toward the hydrogenation of quinoline. *J. Am. Chem. Soc.* **139**, 9419–9422 (2017). <https://doi.org/10.1021/jacs.7b01686>
91. Wang, J.P., Han, G.K., Wang, L.G., et al.: ZIF-8 with ferrocene encapsulated: a promising precursor to single-atom Fe embedded nitrogen-doped carbon as highly efficient catalyst for oxygen electroreduction. *Small* **14**, 1704282 (2018). <https://doi.org/10.1002/sml.201704282>
92. Chen, Y.J., Ji, S.F., Wang, Y.G., et al.: Isolated single iron atoms anchored on N-doped porous carbon as an efficient electrocatalyst for the oxygen reduction reaction. *Angew. Chem. Int. Ed.* **56**, 6937–6941 (2017). <https://doi.org/10.1002/anie.201702473>
93. Ji, S.F., Chen, Y.J., Fu, Q., et al.: Confined pyrolysis within metal–organic frameworks to form uniform Ru<sub>3</sub> clusters for efficient oxidation of alcohols. *J. Am. Chem. Soc.* **139**, 9795–9798 (2017). <https://doi.org/10.1021/jacs.7b05018>
94. He, Y.H., Hwang, S., Cullen, D.A., et al.: Highly active atomically dispersed CoN<sub>4</sub> fuel cell cathode catalysts derived from surfactant-assisted MOFs: carbon–shell confinement strategy. *Energy Environ. Sci.* **12**, 250–260 (2019). <https://doi.org/10.1039/c8ee02694g>
95. Zhao, J., Wang, Y.N., Dong, W.W., et al.: A new surfactant-introduction strategy for separating the pure single-phase of metal–organic frameworks. *Chem. Commun. Camb. Engl.* **51**, 9479–9482 (2015). <https://doi.org/10.1039/c5cc02043c>
96. Pan, Y.C., Heryadi, D., Zhou, F., et al.: Tuning the crystal morphology and size of zeolitic imidazolate framework-8 in aqueous solution by surfactants. *CrystEngComm* **13**, 6937–6940 (2011). <https://doi.org/10.1039/c1ce05780d>
97. Ji, S.F., Chen, Y.J., Wang, X.L., et al.: Chemical synthesis of single atomic site catalysts. *Chem. Rev.* **120**, 11900–11955 (2020). <https://doi.org/10.1021/acs.chemrev.9b00818>
98. Jeong, H., Shin, S., Lee, H.: Heterogeneous atomic catalysts overcoming the limitations of single-atom catalysts. *ACS Nano* **14**, 14355–14374 (2020). <https://doi.org/10.1021/acsnano.0c06610>
99. Kaiser, S.K., Chen, Z.P., Faust Akl, D., et al.: Single-atom catalysts across the periodic table. *Chem. Rev.* **120**, 11703–11809 (2020). <https://doi.org/10.1021/acs.chemrev.0c00576>
100. Lang, R., Du, X.R., Huang, Y.K., et al.: Single-atom catalysts based on the metal–oxide interaction. *Chem. Rev.* **120**, 11986–12043 (2020). <https://doi.org/10.1021/acs.chemrev.0c00797>
101. Nguyen, T.N., Salehi, M., Le, Q.V., et al.: Fundamentals of electrochemical CO<sub>2</sub> reduction on single-metal-atom catalysts. *ACS Catal.* **10**, 10068–10095 (2020). <https://doi.org/10.1021/acscatal.0c02643>
102. Zhuo, H.Y., Zhang, X., Liang, J.X., et al.: Theoretical understandings of graphene-based metal single-atom catalysts: stability and catalytic performance. *Chem. Rev.* **120**, 12315–12341 (2020). <https://doi.org/10.1021/acs.chemrev.0c00818>
103. Liao, Y.Z., Cheng, Z.H., Zuo, W.W., et al.: Nitrogen-rich conjugated microporous polymers: facile synthesis, efficient gas storage, and heterogeneous catalysis. *ACS Appl. Mater. Interfaces* **9**, 38390–38400 (2017). <https://doi.org/10.1021/acsami.7b09553>
104. Li, C.: Single Co atom catalyst stabilized in C/N containing matrix. *Chin. J. Catal.* **37**, 1443–1445 (2016). [https://doi.org/10.1016/S1872-2067\(16\)62520-2](https://doi.org/10.1016/S1872-2067(16)62520-2)
105. Wu, G.H., Huang, H., Rong, J.F., et al.: Recent advances in non-noble metal single atom catalysts. *Acta Petrolei Sinica* **34**, 639–650 (2018)
106. Zhang, H.B., Liu, G.G., Shi, L., et al.: Single-atom catalysts: emerging multifunctional materials in heterogeneous catalysis. *Adv. Energy Mater.* **8**, 1701343 (2018). <https://doi.org/10.1002/aenm.201701343>
107. Zhang, R.G., Peng, M., Ling, L.X., et al.: PdIn intermetallic material with isolated single-atom Pd sites: a promising catalyst for direct formic acid fuel cell. *Chem. Eng. Sci.* **199**, 64–78 (2019). <https://doi.org/10.1016/j.ces.2019.01.018>
108. Ling, C.Y., Li, Q., Du, A.J., et al.: Computation-aided design of single-atom catalysts for one-pot CO<sub>2</sub> capture, activation, and conversion. *ACS Appl. Mater. Interfaces* **10**, 36866–36872 (2018). <https://doi.org/10.1021/acsami.8b10394>
109. Zhang, J., Sun, P., Zhao, Z.L., et al.: Application of heterogeneous catalysts in olefin hydroformylation. *Chin. Sci. Bull.* **64**, 3173–3187 (2019). <https://doi.org/10.1360/N972019-00160>
110. Zhong, W.H., Zhang, G.Z., Zhang, Y.C., et al.: Enhanced activity of C<sub>2</sub>N-supported single Co atom catalyst by single atom promoter. *J. Phys. Chem. Lett.* **10**, 7009–7014 (2019). <https://doi.org/10.1021/acs.jpcclett.9b02906>
111. Liu, C.G., Jiang, M.X., Su, Z.M.: Computational study on M<sub>1</sub>/POM single-atom catalysts (M = Cu, Zn, Ag, and Au; POM = [PW<sub>12</sub>O<sub>40</sub>]<sup>3-</sup>): metal-support interactions and catalytic cycle for alkene epoxidation. *Inorg. Chem.* **56**, 10496–10504 (2017). <https://doi.org/10.1021/acs.inorgchem.7b01480>
112. Karmakar, S., Chowdhury, C., Datta, A.: Noble-metal-supported GeS monolayer as promising single-atom catalyst for CO oxidation. *J. Phys. Chem. C* **122**, 14488–14498 (2018). <https://doi.org/10.1021/acs.jpcc.8b02442>
113. Liu, S.Q., Liu, Y.W., Gao, X.P., et al.: Two-dimensional transition metal porphyrin sheets as a promising single-atom-catalyst for dinitrogen electrochemical reduction to ammonia: a theoretical study. *J. Phys. Chem. C* **124**, 1492–1499 (2020). <https://doi.org/10.1021/acs.jpcc.9b10294>
114. Ling, C.Y., Ouyang, Y.X., Li, Q., et al.: A general two-step strategy-based high-throughput screening of single atom catalysts for nitrogen fixation. *Small Methods* **3**, 1800376 (2019). <https://doi.org/10.1002/smt.201800376>
115. Liao, T., Kou, L.Z., Du, A.J., et al.: H<sub>2</sub>S sensing and splitting on atom-functionalized carbon nanotubes: a theoretical study. *Adv. Theory Simul.* **1**, 1700033 (2018). <https://doi.org/10.1002/adts.201700033>
116. Liao, T., Sun, Z.Q., Kim, J.H., et al.: Theoretically designed metal-welded carbon nanotubes: extraordinary electronic properties and promoted catalytic performance. *Nano Energy* **32**, 209–215 (2017). <https://doi.org/10.1016/j.nanoen.2016.12.033>
117. Chen, L.N., Hou, K.P., Liu, Y.S., et al.: Efficient hydrogen production from methanol using a single-site Pt<sub>1</sub>/CeO<sub>2</sub> catalyst. *J. Am. Chem. Soc.* **141**, 17995–17999 (2019). <https://doi.org/10.1021/jacs.9b09431>
118. Liu, K., Hou, G., Mao, J., et al.: Genesis of electron deficient Pt<sub>1</sub>(0) in PDMS-PEG aggregates. *Nat. Commun.* **10**, 996 (2019). <https://doi.org/10.1038/s41467-019-08804-y>

119. Song, H., Rioux, R.M., Hoefelmeyer, J.D., et al.: Hydrothermal growth of mesoporous SBA-15 silica in the presence of PVP-stabilized Pt nanoparticles: synthesis, characterization, and catalytic properties. *J. Am. Chem. Soc.* **128**, 3027–3037 (2006). <https://doi.org/10.1021/ja057383r>
120. Wu, C.Q., Li, D.D., Ding, S.Q., et al.: Monoatomic platinum-anchored metallic MoS<sub>2</sub>: correlation between surface dopant and hydrogen evolution. *J. Phys. Chem. Lett.* **10**, 6081–6087 (2019). <https://doi.org/10.1021/acs.jpclett.9b01892>
121. Zhao, D., Chen, Z., Yang, W.J., et al.: MXene (Ti<sub>3</sub>C<sub>2</sub>) vacancy-confined single-atom catalyst for efficient functionalization of CO<sub>2</sub>. *J. Am. Chem. Soc.* **141**, 4086–4093 (2019). <https://doi.org/10.1021/jacs.8b13579>
122. Zhang, Y.L., Li, X.K., Li, K., et al.: Novel Au catalysis strategy for the synthesis of Au@Pt core-shell nanoelectrocatalyst with self-controlled quasi-monolayer Pt skin. *ACS Appl. Mater. Interfaces* **9**, 32688–32697 (2017). <https://doi.org/10.1021/acsami.7b08210>
123. Zhang, L., Doyle-Davis, K., Sun, X.L.: Pt-based electrocatalysts with high atom utilization efficiency: from nanostructures to single atoms. *Energy Environ. Sci.* **12**, 492–517 (2019). <https://doi.org/10.1039/c8ee02939c>
124. Tang, Y., Wang, Y.G., Li, J.: Theoretical investigations of Pt<sub>1</sub>@CeO<sub>2</sub> single-atom catalyst for CO oxidation. *J. Phys. Chem. C* **121**, 11281–11289 (2017). <https://doi.org/10.1021/acs.jpcc.7b00313>
125. Yang, S., Kim, J., Tak, Y.J., et al.: Single-atom catalyst of platinum supported on titanium nitride for selective electrochemical reactions. *Angew. Chem. Int. Ed Engl.* **55**, 2058–2062 (2016). <https://doi.org/10.1002/anie.201509241>
126. Yan, D.X., Chen, J., Jia, H.P.: Temperature-induced structure reconstruction to prepare a thermally stable single-atom platinum catalyst. *Angew. Chem. Int. Ed.* **59**, 13562–13567 (2020). <https://doi.org/10.1002/anie.202004929>
127. Woo, H., Lee, E.K., Yun, S.W., et al.: Platinum single atoms on carbon nanotubes as efficient catalyst for hydroalkoxylation. *Bull. Korean Chem. Soc.* **38**, 1221–1225 (2017). <https://doi.org/10.1002/bkcs.11252>
128. Langer, R., Fako, E., Błoński, P., et al.: Anchoring of single-platinum-adatoms on cyanographene: experiment and theory. *Appl. Mater. Today* **18**, 100462 (2020). <https://doi.org/10.1016/j.apmt.2019.100462>
129. Peng, Y.H., Geng, Z.G., Zhao, S.T., et al.: Pt single atoms embedded in the surface of Ni nanocrystals as highly active catalysts for selective hydrogenation of nitro compounds. *Nano Lett.* **18**, 3785–3791 (2018). <https://doi.org/10.1021/acs.nanolett.8b01059>
130. Wang, D.L., Li, H.P., Du, N., et al.: Single platinum atoms immobilized on monolayer tungsten trioxide nanosheets as an efficient electrocatalyst for hydrogen evolution reaction. *Adv. Funct. Mater.* **31**, 2009770 (2021). <https://doi.org/10.1002/adfm.202009770>
131. Harrath, K., Yu, X.H., Xiao, H., et al.: The key role of support surface hydrogenation in the CH<sub>4</sub> to CH<sub>3</sub>OH selective oxidation by a ZrO<sub>2</sub>-supported single-atom catalyst. *ACS Catal.* **9**, 8903–8909 (2019). <https://doi.org/10.1021/acscatal.9b02093>
132. Jongkind, L., Caumes, X., Hartendorp, A.P.T., et al.: Ligand template strategies for catalyst encapsulation. *Acc. Chem. Res.* **51**, 2115–2128 (2018). <https://doi.org/10.1021/acs.accounts.8b00345>
133. Lou, Y., Zheng, Y.P., Li, X., et al.: Pocketlike active site of Rh<sub>1</sub>/MoS<sub>2</sub> single-atom catalyst for selective crotonaldehyde hydrogenation. *J. Am. Chem. Soc.* **141**, 19289–19295 (2019). <https://doi.org/10.1021/jacs.9b06628>
134. Han, B., Lang, R., Tang, H.L., et al.: Superior activity of Rh<sub>1</sub>/ZnO single-atom catalyst for CO oxidation. *Chin. J. Catal.* **40**, 1847–1853 (2019). [https://doi.org/10.1016/S1872-2067\(19\)63411-X](https://doi.org/10.1016/S1872-2067(19)63411-X)
135. Tang, Y., Asokan, C., Xu, M., et al.: Rh single atoms on TiO<sub>2</sub> dynamically respond to reaction conditions by adapting their site. *Nat. Commun.* **10**, 4488 (2019). <https://doi.org/10.1038/s41467-019-12461-6>
136. Kodama, K., Jinnouchi, R., Takahashi, N., et al.: Activities and stabilities of Au-modified stepped-Pt single-crystal electrodes as model cathode catalysts in polymer electrolyte fuel cells. *J. Am. Chem. Soc.* **138**, 4194–4200 (2016). <https://doi.org/10.1021/jacs.6b00359>
137. Chen, Z., Chen, Y.J., Chao, S.L., et al.: Single-atom Au<sup>I</sup>-N<sub>3</sub> site for acetylene hydrochlorination reaction. *ACS Catal.* **10**, 1865–1870 (2020). <https://doi.org/10.1021/acscatal.9b05212>
138. Cao, S.F., Yang, M., Elnabawy, A.O., et al.: Single-atom gold oxo-clusters prepared in alkaline solutions catalyse the heterogeneous methanol self-coupling reactions. *Nat. Chem.* **11**, 1098–1105 (2019). <https://doi.org/10.1038/s41557-019-0345-3>
139. Xi, W., Wang, K., Shen, Y.L., et al.: Dynamic co-catalysis of Au single atoms and nanoporous Au for methane pyrolysis. *Nat. Commun.* **11**, 1919 (2020). <https://doi.org/10.1038/s41467-020-15806-8>
140. Tian, C.C., Zhang, H.Y., Zhu, X., et al.: A new trick for an old support: stabilizing gold single atoms on LaFeO<sub>3</sub> perovskite. *Appl. Catal. B Environ.* **261**, 118178 (2020). <https://doi.org/10.1016/j.apcatb.2019.118178>
141. Liu, D., Li, J.C., Shi, Q.R., et al.: Atomically isolated iron atom anchored on carbon nanotubes for oxygen reduction reaction. *ACS Appl. Mater. Interfaces* **11**, 39820–39826 (2019). <https://doi.org/10.1021/acsami.9b12054>
142. Gao, Y., Cai, Z.W., Wu, X.C., et al.: Graphdiyne-supported single-atom-sized Fe catalysts for the oxygen reduction reaction: DFT predictions and experimental validations. *ACS Catal.* **8**, 10364–10374 (2018). <https://doi.org/10.1021/acscatal.8b02360>
143. Hou, C.C., Zou, L.L., Sun, L.M., et al.: Single-atom iron catalysts on overhang-eave carbon cages for high-performance oxygen reduction reaction. *Angew. Chem. Int. Ed.* **59**, 7384–7389 (2020). <https://doi.org/10.1002/anie.202002665>
144. Li, J.C., Tang, D.M., Hou, P.X., et al.: The effect of carbon support on the oxygen reduction activity and durability of single-atom iron catalysts. *MRS Commun.* **8**, 1158–1166 (2018). <https://doi.org/10.1557/mrc.2018.174>
145. Gole, J.L., White, M.G.: Nanocatalysis: selective conversion of ethanol to acetaldehyde using mono-atomically dispersed copper on silica nanospheres. *J. Catal.* **204**, 249–252 (2001). <https://doi.org/10.1006/jcat.2001.3335>
146. Hajifatheali, H., Ahmadi, E., Wojtczak, A., et al.: The synthesis of N-methylbis[2-(dodecylthio)ethyl]amine (SNS) and investigation of its efficiency as new mononuclear catalyst complex in copper-based ATRP. *Macromol. Res.* **23**, 977–985 (2015). <https://doi.org/10.1007/s13233-015-3132-z>
147. Qin, L., Cui, Y.Q., Deng, T.L., et al.: Highly stable and active Cu<sub>1</sub>/CeO<sub>2</sub> single-atom catalyst for CO oxidation: a DFT study. *ChemPhysChem* **19**, 3346–3349 (2018). <https://doi.org/10.1002/cphc.201800860>
148. Zhao, C.M., Dai, X.Y., Yao, T., et al.: Ionic exchange of metal-organic frameworks to access single nickel sites for efficient electroreduction of CO<sub>2</sub>. *J. Am. Chem. Soc.* **139**, 8078–8081 (2017). <https://doi.org/10.1021/jacs.7b02736>
149. Ling, C.Y., Shi, L., Ouyang, Y.X., et al.: Nanosheet supported single-metal atom bifunctional catalyst for overall water splitting. *Nano Lett.* **17**, 5133–5139 (2017). <https://doi.org/10.1021/acs.nanolett.7b02518>
150. Dai, X.Y., Chen, Z., Yao, T., et al.: Single Ni sites distributed on N-doped carbon for selective hydrogenation of acetylene.

- Chem. Commun. **53**, 11568–11571 (2017). <https://doi.org/10.1039/c7cc04820c>
151. Cao, X.R., Ji, Y.F., Luo, Y.: Dehydrogenation of propane to propylene by a Pd/Cu single-atom catalyst: insight from first-principles calculations. *J. Phys. Chem. C* **119**, 1016–1023 (2015). <https://doi.org/10.1021/jp508625b>
152. Marcinkowski, M.D., Yuk, S.F., Doudin, N., et al.: Low-temperature oxidation of methanol to formaldehyde on a model single-atom catalyst: Pd atoms on Fe<sub>3</sub>O<sub>4</sub>(001). *ACS Catal.* **9**, 10977–10982 (2019). <https://doi.org/10.1021/acscatal.9b03891>
153. Zhou, S.Q., Shang, L., Zhao, Y.X., et al.: Pd single-atom catalysts on nitrogen-doped graphene for the highly selective photothermal hydrogenation of acetylene to ethylene. *Adv. Mater.* **31**, 1900509 (2019). <https://doi.org/10.1002/adma.201900509>
154. Liang, J.X., Lin, J., Yang, X.F., et al.: Theoretical and experimental investigations on single-atom catalysis: Ir<sub>1</sub>/FeO<sub>x</sub> for CO oxidation. *J. Phys. Chem. C* **118**, 21945–21951 (2014). <https://doi.org/10.1021/jp503769d>
155. Lu, Y.B., Kuo, C.T., Kovarik, L., et al.: A versatile approach for quantification of surface site fractions using reaction kinetics: the case of CO oxidation on supported Ir single atoms and nanoparticles. *J. Catal.* **378**, 121–130 (2019). <https://doi.org/10.1016/j.jcat.2019.08.023>
156. Wang, Q., Huang, X., Zhao, Z.L., et al.: Ultrahigh-loading of Ir single atoms on NiO matrix to dramatically enhance oxygen evolution reaction. *J. Am. Chem. Soc.* **142**, 7425–7433 (2020). <https://doi.org/10.1021/jacs.9b12642>
157. Du, Z.Z., Chen, X.J., Hu, W., et al.: Cobalt in nitrogen-doped graphene as single-atom catalyst for high-sulfur content lithium-sulfur batteries. *J. Am. Chem. Soc.* **141**, 3977–3985 (2019). <https://doi.org/10.1021/jacs.8b12973>
158. Kim, K., Kang, T., Kim, M., et al.: Three-dimensional entangled and twisted structures of nitrogen doped poly-(1,4-diethynylbenzene) chain combined with cobalt single atom as a highly efficient bifunctional electrocatalyst. *Appl. Catal. B Environ.* **275**, 119107 (2020). <https://doi.org/10.1016/j.apcatb.2020.119107>
159. Mori, K., Taga, T., Yamashita, H.: Isolated single-atomic Ru catalyst bound on a layered double hydroxide for hydrogenation of CO<sub>2</sub> to formic acid. *ACS Catal.* **7**, 3147–3151 (2017). <https://doi.org/10.1021/acscatal.7b00312>
160. Wang, D.W., Li, Q., Han, C., et al.: Single-atom ruthenium based catalyst for enhanced hydrogen evolution. *Appl. Catal. B Environ.* **249**, 91–97 (2019). <https://doi.org/10.1016/j.apcatb.2019.02.059>
161. Schwerdtfeger, E.D., Irwin, L.J., Miller, S.A.: Highly branched polyethylene from ethylene alone via a single zirconium-based catalyst. *Macromolecules* **41**, 1080–1085 (2008). <https://doi.org/10.1021/ma702213c>
162. Yang, F., Song, P., Liu, X.Z., et al.: Highly efficient CO<sub>2</sub> electroreduction on ZnN<sub>4</sub>-based single-atom catalyst. *Angew. Chem. Int. Ed.* **57**, 12303–12307 (2018). <https://doi.org/10.1002/anie.201805871>
163. Guan, J.Q., Duan, Z.Y., Zhang, F.X., et al.: Water oxidation on a mononuclear manganese heterogeneous catalyst. *Nat. Catal.* **1**, 870–877 (2018). <https://doi.org/10.1038/s41929-018-0158-6>
164. Kong, N.N., Fan, X., Liu, F.F., et al.: Single vanadium atoms anchored on graphitic carbon nitride as a high-performance catalyst for non-oxidative propane dehydrogenation. *ACS Nano* **14**, 5772–5779 (2020). <https://doi.org/10.1021/acsnano.0c00659>
165. Saini, P.K., Romain, C., Williams, C.K.: Dinuclear metal catalysts: improved performance of heterodinuclear mixed catalysts for CO<sub>2</sub>-epoxide copolymerization. *Chem. Commun.* **50**, 4164–4167 (2014). <https://doi.org/10.1039/c3cc49158g>
166. Zhang, W.Y., Chao, Y.G., Zhang, W.S., et al.: Emerging dual-atomic-site catalysts for efficient energy catalysis. *Adv. Mater.* **33**, 2102576 (2021). <https://doi.org/10.1002/adma.202102576>
167. Shi, Q., Ji, Y.J., Chen, W.X., et al.: Single-atom Sn–Zn pairs in CuO catalyst promote dimethyldichlorosilane synthesis. *Natl. Sci. Rev.* **7**, 600–608 (2019). <https://doi.org/10.1093/nsr/nwz196>
168. Bai, L.C., Hsu, C.S., Alexander, D.T.L., et al.: A cobalt-iron double-atom catalyst for the oxygen evolution reaction. *J. Am. Chem. Soc.* **141**, 14190–14199 (2019). <https://doi.org/10.1021/jacs.9b05268>
169. Fan, M.M., Cui, J.W., Wu, J.J., et al.: Improving the catalytic activity of carbon-supported single atom catalysts by polynary metal or heteroatom doping. *Small* **16**, 1906782 (2020). <https://doi.org/10.1002/smll.201906782>
170. Zhang, L.L., Wang, A.Q., Miller, J.T., et al.: Efficient and durable Au alloyed Pd single-atom catalyst for the Ullmann reaction of aryl chlorides in water. *ACS Catal.* **4**, 1546–1553 (2014). <https://doi.org/10.1021/cs500071c>
171. Pei, G.X., Liu, X.Y., Yang, X.F., et al.: Performance of Cu-alloyed Pd single-atom catalyst for semihydrogenation of acetylene under simulated front-end conditions. *ACS Catal.* **7**, 1491–1500 (2017). <https://doi.org/10.1021/acscatal.6b03293>
172. Wang, W.L., Santos, E.J.G., Jiang, B., et al.: Direct observation of a long-lived single-atom catalyst chiseling atomic structures in graphene. *Nano Lett.* **14**, 450–455 (2014). <https://doi.org/10.1021/nl403327u>
173. Alexopoulos, K., Vlachos, D.G.: Surface chemistry dictates stability and oxidation state of supported single metal catalyst atoms. *Chem. Sci.* **11**, 1469–1477 (2020). <https://doi.org/10.1039/c9sc05944j>
174. Yang, X.F., Wang, A.Q., Qiao, B.T., et al.: Single-atom catalysts: a new frontier in heterogeneous catalysis. *Acc. Chem. Res.* **46**, 1740–1748 (2013). <https://doi.org/10.1021/ar300361m>
175. Lai, W.H., Miao, Z.C., Wang, Y.X., et al.: Atomic-local environments of single-atom catalysts: synthesis, electronic structure, and activity. *Adv. Energy Mater.* **9**, 1900722 (2019). <https://doi.org/10.1002/aenm.201900722>
176. Wang, B., Cai, H.R., Shen, S.H.: Single metal atom photocatalysis. *Small Methods* **3**, 1800447 (2019). <https://doi.org/10.1002/smt.201800447>
177. Zheng, N.F., Zhang, T.: Preface: single-atom catalysts as a new generation of heterogeneous catalysts. *Natl. Sci. Rev.* **5**, 625–625 (2018). <https://doi.org/10.1093/nsr/nwy095>
178. Wang, Y., Bao, S.X., Li, R., et al.: Universal strategy for homogeneously doping noble metals into cyano-bridged coordination polymers. *ACS Appl. Mater. Interfaces* **7**, 2088–2096 (2015). <https://doi.org/10.1021/am508246m>
179. Lyu, D.D., Mollamahale, Y.B., Huang, S.L., et al.: Ultra-high surface area graphitic Fe–N–C nanospheres with single-atom iron sites as highly efficient non-precious metal bifunctional catalysts towards oxygen redox reactions. *J. Catal.* **368**, 279–290 (2018). <https://doi.org/10.1016/j.jcat.2018.10.025>
180. Wang, J., Li, Z.J., Wu, Y.E., et al.: Fabrication of single-atom catalysts with precise structure and high metal loading. *Adv. Mater.* **30**, e1801649 (2018). <https://doi.org/10.1002/adma.201801649>
181. Yan, H., Su, C.L., He, J., et al.: Single-atom catalysts and their applications in organic chemistry. *J. Mater. Chem. A* **6**, 8793–8814 (2018). <https://doi.org/10.1039/c8ta01940a>
182. Zhang, Q.Q., Guan, J.Q.: Single-atom catalysts for electrocatalytic applications. *Adv. Funct. Mater.* **30**, 2000768 (2020). <https://doi.org/10.1002/adfm.202000768>
183. Qi, J.L., Xu, Q.Q., Sun, J.F., et al.: Synthesis, characterization and analysis of graphene-supported single-atom catalysts. *Prog. Chem.* **32**, 505–518 (2020)
184. Wu, W.H., Lei, W., Wang, L.Q., et al.: Preparation of single atom catalysts. *Prog. Chem.* **32**, 23–32 (2020). <https://doi.org/10.7536/PC190704>
185. Alarawi, A., Ramalingam, V., He, J.H.: Recent advances in emerging single atom confined two-dimensional materials for

- water splitting applications. *Mater. Today Energy* **11**, 1–23 (2019). <https://doi.org/10.1016/j.mtener.2018.10.014>
186. Guo, W.X., Wang, Z.Y., Wang, X.Q., et al.: General design concept for single-atom catalysts toward heterogeneous catalysis. *Adv. Mater.* **33**, 2004287 (2021). <https://doi.org/10.1002/adma.202004287>
187. Zou, L.L., Wei, Y.S., Hou, C.C., et al.: Single-atom catalysts derived from metal–organic frameworks for electrochemical applications. *Small* **17**, 2004809 (2021). <https://doi.org/10.1002/sml.202004809>
188. Xiong, H.F., Datye, A.K., Wang, Y.: Thermally stable single-atom heterogeneous catalysts. *Adv. Mater.* **33**, 2004319 (2021). <https://doi.org/10.1002/adma.202004319>
189. Han, B., Lang, R., Qiao, B.T., et al.: Highlights of the major progress in single-atom catalysis in 2015 and 2016. *Chin. J. Catal.* **38**, 1498–1507 (2017). [https://doi.org/10.1016/S1872-2067\(17\)62872-9](https://doi.org/10.1016/S1872-2067(17)62872-9)
190. Zhu, Y.Z., Peng, W.C., Li, Y., et al.: Modulating the electronic structure of single-atom catalysts on 2D nanomaterials for enhanced electrocatalytic performance. *Small Methods* **3**, 1800438 (2019). <https://doi.org/10.1002/smt.201800438>
191. Gawande, M.B., Fornasiero, P., Zbořil, R.: Carbon-based single-atom catalysts for advanced applications. *ACS Catal.* **10**, 2231–2259 (2020). <https://doi.org/10.1021/acscatal.9b04217>
192. Abbet, S., Sanchez, A., Heiz, U., et al.: Acetylene cyclotrimerization on supported size-selected Pd<sub>n</sub> clusters (1 ≤ n ≤ 30): one atom is enough! *J. Am. Chem. Soc.* **122**, 3453–3457 (2000). <https://doi.org/10.1021/ja9922476>
193. Tyo, E.C., Vajda, S.: Catalysis by clusters with precise numbers of atoms. *Nat. Nanotechnol.* **10**, 577–588 (2015). <https://doi.org/10.1038/nnano.2015.140>
194. Johnson, G.E., Priest, T., Laskin, J.: Charge retention by gold clusters on surfaces prepared using soft landing of mass selected ions. *ACS Nano* **6**, 573–582 (2012). <https://doi.org/10.1021/nn2039565>
195. Laskin, J., Johnson, G.E., Prabhakaran, V.: Soft landing of complex ions for studies in catalysis and energy storage. *J. Phys. Chem. C* **120**, 23305–23322 (2016). <https://doi.org/10.1021/acs.jpcc.6b06497>
196. Chen, Y.J., Ji, S.F., Chen, C., et al.: Single-atom catalysts: synthetic strategies and electrochemical applications. *Joule* **2**, 1242–1264 (2018). <https://doi.org/10.1016/j.joule.2018.06.019>
197. Vajda, S., White, M.G.: Catalysis applications of size-selected cluster deposition. *ACS Catal.* **5**, 7152–7176 (2015). <https://doi.org/10.1021/acscatal.5b01816>
198. Jin, Y.Y., Hao, P.P., Ren, J., et al.: Single atom catalysis: concept, method and application. *Prog. Chem.* **27**, 1689–1704 (2015)
199. Liu, J.Y.: Catalysis by supported single metal atoms. *ACS Catal.* **7**, 34–59 (2017). <https://doi.org/10.1021/acscatal.6b01534>
200. Dasgupta, N.P., Li, L., Sun, X.L.: Atomic layer deposition for energy and environmental applications. *Adv. Mater. Interfaces* **3**, 1600914 (2016). <https://doi.org/10.1002/admi.201600914>
201. O'Neill, B.J., Jackson, D.H.K., Lee, J., et al.: Catalyst design with atomic layer deposition. *ACS Catal.* **5**, 1804–1825 (2015). <https://doi.org/10.1021/cs501862h>
202. Wang, H.W., Lu, J.L.: Atomic layer deposition: a gas phase route to bottom-up precise synthesis of heterogeneous catalyst. *Acta Phys. Chim. Sin.* **34**, 1334–1357 (2018). <https://doi.org/10.3866/pku.whxb201804201>
203. Zhang, N.Q., Li, L.C., Huang, X., et al.: Research progress of single-atom catalysis. *J. Chin. Soc. Rare Earths* **36**, 513–532 (2018)
204. Cheng, N.C., Sun, X.L.: Single atom catalyst by atomic layer deposition technique. *Chin. J. Catal.* **38**, 1508–1514 (2017). [https://doi.org/10.1016/S1872-2067\(17\)62903-6](https://doi.org/10.1016/S1872-2067(17)62903-6)
205. Wang, C.L., Gu, X.-K., Yan, H., et al.: Water-mediated Mars–van Krevelen mechanism for CO oxidation on ceria supported single-atom Pt<sub>1</sub> catalyst. *ACS Catal.* **7**, 887–891 (2016). <https://doi.org/10.1021/acscatal.6b02685>
206. Yan, H., Lv, H.F., Yi, H., et al.: Understanding the underlying mechanism of improved selectivity in Pd<sub>1</sub> single-atom catalyzed hydrogenation reaction. *J. Catal.* **366**, 70–79 (2018). <https://doi.org/10.1016/j.jcat.2018.07.033>
207. Yan, H., Cheng, H., Yi, H., et al.: Single-atom Pd<sub>1</sub>/graphene catalyst achieved by atomic layer deposition: remarkable performance in selective hydrogenation of 1,3-butadiene. *J. Am. Chem. Soc.* **137**, 10484–10487 (2015). <https://doi.org/10.1021/jacs.5b06485>
208. Jiang, C.J., Shang, Z.Y., Liang, X.H.: Chemoselective transfer hydrogenation of nitroarenes catalyzed by highly dispersed, supported nickel nanoparticles. *ACS Catal.* **5**, 4814–4818 (2015). <https://doi.org/10.1021/acscatal.5b00969>
209. Sun, S.H., Zhang, G.X., Gauquelin, N., et al.: Single-atom catalysis using Pt/graphene achieved through atomic layer deposition. *Sci. Rep.* **3**, 1775 (2013). <https://doi.org/10.1038/srep01775>
210. Lang, R., Xi, W., Liu, J.C., et al.: Non defect-stabilized thermally stable single-atom catalyst. *Nat. Commun.* **10**, 234 (2019). <https://doi.org/10.1038/s41467-018-08136-3>
211. Jones, J., Xiong, H.F., DeLaRiva, A.T., et al.: Thermally stable single-atom platinum-on-ceria catalysts via atom trapping. *Science* **353**, 150–154 (2016). <https://doi.org/10.1126/science.aaf8800>
212. Cui, X.J., Dai, X.C., Surkus, A.E., et al.: Zinc single atoms on N-doped carbon: an efficient and stable catalyst for CO<sub>2</sub> fixation and conversion. *Chin. J. Catal.* **40**, 1679–1685 (2019). [https://doi.org/10.1016/S1872-2067\(19\)63316-4](https://doi.org/10.1016/S1872-2067(19)63316-4)
213. Zhao, S.Y., Cheng, Y., Veder, J.P., et al.: One-pot pyrolysis method to fabricate carbon nanotube supported Ni single-atom catalysts with ultrahigh loading. *ACS Appl. Energy Mater.* **1**, 5286–5297 (2018). <https://doi.org/10.1021/acsaem.8b00903>
214. Yang, H.B., Hung, S.F., Liu, S., et al.: Atomically dispersed Ni(I) as the active site for electrochemical CO<sub>2</sub> reduction. *Nat. Energy* **3**, 140–147 (2018). <https://doi.org/10.1038/s41560-017-0078-8>
215. Jiao, L., Yang, W.J., Wan, G., et al.: Single-atom electrocatalysts from multivariate metal–organic frameworks for highly selective reduction of CO<sub>2</sub> at low pressures. *Angew. Chem. Int. Ed.* **59**, 20589–20595 (2020). <https://doi.org/10.1002/anie.202008787>
216. Cheon, J.Y., Kim, T., Choi, Y., et al.: Ordered mesoporous porphyrinic carbons with very high electrocatalytic activity for the oxygen reduction reaction. *Sci. Rep.* **3**, 2715 (2013). <https://doi.org/10.1038/srep02715>
217. Yi, J.D., Xu, R., Wu, Q., et al.: Atomically dispersed iron-nitrogen active sites within porphyrinic triazine-based frameworks for oxygen reduction reaction in both alkaline and acidic media. *ACS Energy Lett.* **3**, 883–889 (2018). <https://doi.org/10.1021/acsenerylett.8b00245>
218. Sa, Y.J., Seo, D.J., Woo, J., et al.: A general approach to preferential formation of active Fe–N<sub>x</sub> sites in Fe–N/C electrocatalysts for efficient oxygen reduction reaction. *J. Am. Chem. Soc.* **138**, 15046–15056 (2016). <https://doi.org/10.1021/jacs.6b09470>
219. Cheng, Y., He, S., Lu, S.F., et al.: Iron single atoms on graphene as nonprecious metal catalysts for high-temperature polymer electrolyte membrane fuel cells. *Adv. Sci.* **6**, 1802066 (2019). <https://doi.org/10.1002/adv.201802066>
220. Derevyannikova, E.A., Kardash, T.Y., Stadnichenko, A.I., et al.: Structural insight into strong Pt–CeO<sub>2</sub> interaction: from single Pt

- atoms to  $\text{PtO}_x$  clusters. *J. Phys. Chem. C* **123**, 1320–1334 (2019). <https://doi.org/10.1021/acs.jpcc.8b11009>
221. Jan, A., Shin, J., Ahn, J., et al.: Promotion of Pt/CeO<sub>2</sub> catalyst by hydrogen treatment for low-temperature CO oxidation. *RSC Adv.* **9**, 27002–27012 (2019). <https://doi.org/10.1039/c9ra05965b>
222. Zhu, Y.F., Kong, X., Yin, J.Q., et al.: Covalent-bonding to irreducible SiO<sub>2</sub> leads to high-loading and atomically dispersed metal catalysts. *J. Catal.* **353**, 315–324 (2017). <https://doi.org/10.1016/j.jcat.2017.07.030>
223. Zheng, T.Q., Zhou, W., Gao, Y., et al.: Active impregnation method for copper foam as catalyst support for methanol steam reforming for hydrogen production. *Ind. Eng. Chem. Res.* **58**, 4387–4395 (2019). <https://doi.org/10.1021/acs.iecr.8b05241>
224. Feng, S.Q., Song, X.G., Ren, Z., et al.: La-stabilized, single-atom Ir/AC catalyst for heterogeneous methanol carbonylation to methyl acetate. *Ind. Eng. Chem. Res.* **58**, 4755–4763 (2019). <https://doi.org/10.1021/acs.iecr.8b05402>
225. Yang, H.L., Liu, Q.G., Li, Y., et al.: Isolated single-atom ruthenium anchored on beta zeolite as an efficient heterogeneous catalyst for styrene epoxidation. *ChemNanoMat* **6**, 1647–1651 (2020). <https://doi.org/10.1002/cnma.202000394>
226. Jiang, R.H., Liu, S.M., Li, L., et al.: Single Ir atoms anchored on ordered mesoporous WO<sub>3</sub> are highly efficient for the selective catalytic reduction of NO with CO under oxygen-rich conditions. *ChemCatChem* **13**, 1834–1846 (2021). <https://doi.org/10.1002/cctc.202001784>
227. Kwon, Y., Kim, T.Y., Kwon, G., et al.: Selective activation of methane on single-atom catalyst of rhodium dispersed on zirconia for direct conversion. *J. Am. Chem. Soc.* **139**, 17694–17699 (2017). <https://doi.org/10.1021/jacs.7b11010>
228. Hai, X., Xi, S., Mitchell, S., et al.: Scalable two-step annealing method for preparing ultra-high-density single-atom catalyst libraries. *Nat. Nanotechnol.* **17**, 174–181 (2022). <https://doi.org/10.1038/s41565-021-01022-y>
229. Kaiser, S.K., Fako, E., Manzocchi, G., et al.: Nanostructuring unlocks high performance of platinum single-atom catalysts for stable vinyl chloride production. *Nat. Catal.* **3**, 376–385 (2020). <https://doi.org/10.1038/s41929-020-0431-3>
230. Szilágyi, P.Á., Rogers, D.M., Zaiser, I., et al.: Functionalised metal–organic frameworks: a novel approach to stabilising single metal atoms. *J. Mater. Chem. A* **5**, 15559–15566 (2017). <https://doi.org/10.1039/C7TA03134C>
231. Liu, S.S., Tan, J.M., Gulec, A., et al.: Stabilizing single-atom and small-domain platinum via combining organometallic chemisorption and atomic layer deposition. *Organometallics* **36**, 818–828 (2017). <https://doi.org/10.1021/acs.organomet.6b00869>
232. Sun, Q.M., Wang, N., Zhang, T.J., et al.: Zeolite-encaged single-atom rhodium catalysts: highly-efficient hydrogen generation and shape-selective tandem hydrogenation of nitroarenes. *Angew. Chem. Int. Ed.* **58**, 18570–18576 (2019). <https://doi.org/10.1002/anie.201912367>
233. Yang, H.Z., Shang, L., Zhang, Q.H., et al.: A universal ligand mediated method for large scale synthesis of transition metal single atom catalysts. *Nat. Commun.* **10**, 4585 (2019). <https://doi.org/10.1038/s41467-019-12510-0>
234. Gao, C., Chen, S.M., Wang, Y., et al.: Heterogeneous single-atom catalyst for visible-light-driven high-turnover CO<sub>2</sub> reduction: the role of electron transfer. *Adv. Mater.* **30**, 1704624 (2018). <https://doi.org/10.1002/adma.201704624>
235. Abdel-Mageed, A.M., Rungtawevoranit, B., Parlinska-Wojtan, M., et al.: Highly active and stable single-atom Cu catalysts supported by a metal–organic framework. *J. Am. Chem. Soc.* **141**, 5201–5210 (2019). <https://doi.org/10.1021/jacs.8b11386>
236. Razmjooei, F., Yu, J.H., Lee, H.Y., et al.: Single-atom iron-based electrocatalysts for high-temperature polymer electrolyte membrane fuel cell: organometallic precursor and pore texture tailoring. *ACS Appl. Energy Mater.* **3**, 11164–11176 (2020). <https://doi.org/10.1021/acsaem.0c02111>
237. Zheng, Y., Qiao, S.Z.: Metal–organic framework assisted synthesis of single-atom catalysts for energy applications. *Natl. Sci. Rev.* **5**, 626–627 (2018). <https://doi.org/10.1093/nsr/nwy010>
238. Oisaki, K., Li, Q.W., Furukawa, H., et al.: A metal–organic framework with covalently bound organometallic complexes. *J. Am. Chem. Soc.* **132**, 9262–9264 (2010). <https://doi.org/10.1021/ja103016y>
239. Fan, Y., Liu, S.G., Yi, Y., et al.: Catalytic nanomaterials toward atomic levels for biomedical applications: from metal clusters to single-atom catalysts. *ACS Nano* **15**, 2005–2037 (2021). <https://doi.org/10.1021/acsnano.0c06962>
240. Rivera-Cárcamo, C., Serp, P.: Single atom catalysts on carbon-based materials. *ChemCatChem* **10**, 5058–5091 (2018). <https://doi.org/10.1002/cctc.201801174>
241. Kim, M.S., Park, H., Won, S.O., et al.: Copper-halide polymer nanowires as versatile supports for single-atom catalysts. *Small* **15**, 1903197 (2019). <https://doi.org/10.1002/smll.201903197>
242. Lin, R.H., Albani, D., Fako, E., et al.: Design of single gold atoms on nitrogen-doped carbon for molecular recognition in alkyne semi-hydrogenation. *Angew. Chem. Int. Ed.* **58**, 504–509 (2019). <https://doi.org/10.1002/anie.201805820>
243. Li, Q.H., Chen, W.X., Xiao, H., et al.: Fe isolated single atoms on S, N codoped carbon by copolymer pyrolysis strategy for highly efficient oxygen reduction reaction. *Adv. Mater.* **30**, 1800588 (2018). <https://doi.org/10.1002/adma.201800588>
244. Pan, Y., Chen, Y.J., Wu, K.L., et al.: Regulating the coordination structure of single-atom Fe–N<sub>x</sub>C<sub>y</sub> catalytic sites for benzene oxidation. *Nat. Commun.* **10**, 4290 (2019). <https://doi.org/10.1038/s41467-019-12362-8>
245. Li, X.N., Huang, X., Xi, S.B., et al.: Single cobalt atoms anchored on porous N-doped graphene with dual reaction sites for efficient Fenton-like catalysis. *J. Am. Chem. Soc.* **140**, 12469–12475 (2018). <https://doi.org/10.1021/jacs.8b05992>
246. Liu, J.H., Yang, L.M., Ganz, E.: Efficient and selective electroreduction of CO<sub>2</sub> by single-atom catalyst two-dimensional TM–Pc monolayers. *ACS Sustain. Chem. Eng.* **6**, 15494–15502 (2018). <https://doi.org/10.1021/acssuschemeng.8b03945>
247. Chen, X.F., Yan, J.M., Jiang, Q.: Single layer of polymeric metal-phthalocyanine: promising substrate to realize single Pt atom catalyst with uniform distribution. *J. Phys. Chem. C* **118**, 2122–2128 (2014). <https://doi.org/10.1021/jp411183h>
248. Abel, M., Clair, S., Ourdjini, O., et al.: Single layer of polymeric Fe-phthalocyanine: an organometallic sheet on metal and thin insulating film. *J. Am. Chem. Soc.* **133**, 1203–1205 (2011). <https://doi.org/10.1021/ja108628r>
249. He, X.H., He, Q., Deng, Y.C., et al.: A versatile route to fabricate single atom catalysts with high chemoselectivity and regioselectivity in hydrogenation. *Nat. Commun.* **10**, 3663 (2019). <https://doi.org/10.1038/s41467-019-11619-6>
250. Pan, Y., Liu, S.J., Sun, K.A., et al.: A bimetallic Zn/Fe polyphthalocyanine-derived single-atom Fe–N<sub>4</sub> catalytic site: a superior trifunctional catalyst for overall water splitting and Zn-air batteries. *Angew. Chem. Int. Ed.* **57**, 8614–8618 (2018). <https://doi.org/10.1002/anie.201804349>
251. Wu, H.H., Li, H.B., Zhao, X.F., et al.: Highly doped and exposed Cu(I)–N active sites within graphene towards efficient oxygen reduction for zinc–air batteries. *Energy Environ. Sci.* **9**, 3736–3745 (2016). <https://doi.org/10.1039/c6ee01867j>
252. Wu, K.L., Chen, X., Liu, S.J., et al.: Porphyrin-like Fe–N<sub>4</sub> sites with sulfur adjustment on hierarchical porous carbon for different rate-determining steps in oxygen reduction reaction. *Nano Res.* **11**, 6260–6269 (2018). <https://doi.org/10.1007/s12274-018-2149-y>

253. Yang, H.Z., Shi, R., Shang, L., et al.: Recent advancements of porphyrin-like single-atom catalysts: synthesis and applications. *Small Struct.* **2**, 2100007 (2021). <https://doi.org/10.1002/ssstr.202100007>
254. Zheng, Y., Jiao, Y., Zhu, Y.H., et al.: Molecule-level g-C<sub>3</sub>N<sub>4</sub> coordinated transition metals as a new class of electrocatalysts for oxygen electrode reactions. *J. Am. Chem. Soc.* **139**, 3336–3339 (2017). <https://doi.org/10.1021/jacs.6b13100>
255. Ren, C.J., Jiang, Q.Y., Lin, W., et al.: Density functional theory study of single-atom V, Nb, and Ta catalysts on graphene and carbon nitride for selective nitrogen reduction. *ACS Appl. Nano Mater.* **3**, 5149–5159 (2020). <https://doi.org/10.1021/acsnm.0c00512>
256. Chen, Y.J., Ji, S.F., Sun, W.M., et al.: Discovering partially charged single-atom Pt for enhanced anti-Markovnikov alkene hydrosilylation. *J. Am. Chem. Soc.* **140**, 7407–7410 (2018). <https://doi.org/10.1021/jacs.8b03121>
257. Liu, L.M., Wang, N., Zhu, C.Z., et al.: Direct imaging of atomically dispersed molybdenum that enables location of aluminum in the framework of zeolite ZSM-5. *Angew. Chem. Int. Ed.* **59**, 819–825 (2020). <https://doi.org/10.1002/anie.201909834>
258. Davis, M.E.: Ordered porous materials for emerging applications. *Nature* **417**, 813–821 (2002). <https://doi.org/10.1038/nature00785>
259. Masoumifard, N., Guillet-Nicolas, R., Kleitz, F.: Synthesis of engineered zeolitic materials: from classical zeolites to hierarchical core-shell materials. *Adv. Mater.* **30**, 1704439 (2018). <https://doi.org/10.1002/adma.201704439>
260. Guzman, J., Gates, B.C.: Supported molecular catalysts: metal complexes and clusters on oxides and zeolites. *Dalton Trans.* **17**, 3303–3318 (2003). <https://doi.org/10.1039/b303285j>
261. Zhang, W.J., Jiang, P.P., Wang, Y., et al.: Bottom-up approach to engineer a molybdenum-doped covalent-organic framework catalyst for selective oxidation reaction. *RSC Adv.* **4**, 51544–51547 (2014). <https://doi.org/10.1039/c4ra09304f>
262. Zhong, W.F., Sa, R.J., Li, L.Y., et al.: A covalent organic framework bearing single Ni sites as a synergistic photocatalyst for selective photoreduction of CO<sub>2</sub> to CO. *J. Am. Chem. Soc.* **141**, 7615–7621 (2019). <https://doi.org/10.1021/jacs.9b02997>
263. Huang, N., Wang, P., Jiang, D.L.: Covalent organic frameworks: a materials platform for structural and functional designs. *Nat. Rev. Mater.* **1**, 16068 (2016). <https://doi.org/10.1038/natrevmats.2016.68>
264. Ramalingam, V., Varadhan, P., Fu, H.C., et al.: Heteroatom-mediated interactions between ruthenium single atoms and an MXene support for efficient hydrogen evolution. *Adv. Mater.* **31**, 1903841 (2019). <https://doi.org/10.1002/adma.201903841>
265. Fu, Q., Li, W.X., Yao, Y.X., et al.: Interface-confined ferrous centers for catalytic oxidation. *Science* **328**, 1141–1144 (2010). <https://doi.org/10.1126/science.1188267>
266. Côté, A.P., Benin, A.I., Ockwig, N.W., et al.: Porous, crystalline, covalent organic frameworks. *Science* **310**, 1166–1170 (2005). <https://doi.org/10.1126/science.1120411>
267. Zhang, J.Q., Zhao, Y.F., Guo, X., et al.: Single platinum atoms immobilized on an MXene as an efficient catalyst for the hydrogen evolution reaction. *Nat. Catal.* **1**, 985–992 (2018). <https://doi.org/10.1038/s41929-018-0195-1>
268. Peng, Y., Lu, B.Z., Chen, S.W.: Carbon-supported single atom catalysts for electrochemical energy conversion and storage. *Adv. Mater.* **30**, 1801995 (2018). <https://doi.org/10.1002/adma.201801995>
269. Jiao, L., Jiang, H.L.: Metal-organic-framework-based single-atom catalysts for energy applications. *Chem* **5**, 786–804 (2019). <https://doi.org/10.1016/j.chempr.2018.12.011>
270. Liao, T., Kou, L.Z., Du, A.J., et al.: Simplest MOF units for effective photodriven hydrogen evolution reaction. *J. Am. Chem. Soc.* **140**, 9159–9166 (2018). <https://doi.org/10.1021/jacs.8b04599>
271. Sun, X.P., Sun, S.X., Gu, S.Q., et al.: High-performance single atom bifunctional oxygen catalysts derived from ZIF-67 superstructures. *Nano Energy* **61**, 245–250 (2019). <https://doi.org/10.1016/j.nanoen.2019.04.076>
272. Hou, C.C., Wang, H.F., Li, C.X., et al.: From metal-organic frameworks to single/dual-atom and cluster metal catalysts for energy applications. *Energy Environ. Sci.* **13**, 1658–1693 (2020). <https://doi.org/10.1039/c9ee04040d>
273. Yang, L.M., Zeng, Y.C., Tang, X.J., et al.: Self-sacrificial template synthesis of a nitrogen-doped microstructured carbon tube as electrocatalyst for oxygen reduction. *ChemElectroChem* **5**, 3731–3740 (2018). <https://doi.org/10.1002/celec.201801050>
274. Xiao, F., Xu, G.L., Sun, C.J., et al.: Nitrogen-coordinated single iron atom catalysts derived from metal organic frameworks for oxygen reduction reaction. *Nano Energy* **61**, 60–68 (2019). <https://doi.org/10.1016/j.nanoen.2019.04.033>
275. Ji, S.F., Chen, Y.J., Zhao, S., et al.: Atomically dispersed ruthenium species inside metal-organic frameworks: combining the high activity of atomic sites and the molecular sieving effect of MOFs. *Angew. Chem. Int. Ed.* **58**, 4271–4275 (2019). <https://doi.org/10.1002/anie.201814182>
276. Jiang, R., Li, L., Sheng, T., et al.: Edge-site engineering of atomically dispersed Fe-N<sub>4</sub> by selective C-N bond cleavage for enhanced oxygen reduction reaction activities. *J. Am. Chem. Soc.* **140**, 11594–11598 (2018). <https://doi.org/10.1021/jacs.8b07294>
277. Park, K.S., Ni, Z., Côté, A.P., et al.: Exceptional chemical and thermal stability of zeolitic imidazolate frameworks. *PNAS* **103**, 10186–10191 (2006). <https://doi.org/10.1073/pnas.0602439103>
278. Xiao, M.L., Zhu, J.B., Li, G.R., et al.: A single-atom iridium heterogeneous catalyst in oxygen reduction reaction. *Angew. Chem. Int. Ed.* **58**, 9640–9645 (2019). <https://doi.org/10.1002/anie.201905241>
279. Wang, X.J., Zhang, H.G., Lin, H.H., et al.: Directly converting Fe-doped metal-organic frameworks into highly active and stable Fe-N-C catalysts for oxygen reduction in acid. *Nano Energy* **25**, 110–119 (2016). <https://doi.org/10.1016/j.nanoen.2016.04.042>
280. Merzougui, B., Hachimi, A., Akinpelu, A., et al.: A Pt-free catalyst for oxygen reduction reaction based on Fe-N multiwalled carbon nanotube composites. *Electrochim. Acta* **107**, 126–132 (2013). <https://doi.org/10.1016/j.electacta.2013.06.016>
281. Zhang, H.G., Hwang, S., Wang, M.Y., et al.: Single atomic iron catalysts for oxygen reduction in acidic media: particle size control and thermal activation. *J. Am. Chem. Soc.* **139**, 14143–14149 (2017). <https://doi.org/10.1021/jacs.7b06514>
282. Han, A.J., Wang, B.Q., Kumar, A., et al.: Recent advances for MOF-derived carbon-supported single-atom catalysts. *Small Methods* **3**, 1800471 (2019). <https://doi.org/10.1002/smt.201800471>
283. Xuan, N.N., Chen, J.H., Shi, J.J., et al.: Single-atom electroplating on two dimensional materials. *Chem. Mater.* **31**, 429–435 (2019). <https://doi.org/10.1021/acs.chemmater.8b03796>
284. Su, X., Yang, X.F., Huang, Y.Q., et al.: Single-atom catalysis toward efficient CO<sub>2</sub> conversion to CO and formate products. *Acc. Chem. Res.* **52**, 656–664 (2019). <https://doi.org/10.1021/acs.accounts.8b00478>
285. Pan, Y., Lin, R., Chen, Y.J., et al.: Design of single-atom Co-N<sub>5</sub> catalytic site: a robust electrocatalyst for CO<sub>2</sub> reduction with nearly 100% CO selectivity and remarkable stability. *J. Am. Chem. Soc.* **140**, 4218–4221 (2018). <https://doi.org/10.1021/jacs.8b00814>

286. Chen, L.W., Wu, Z.Y., Nan, H., et al.: A metal-catalyzed thermal polymerization strategy toward atomically dispersed catalysts. *Chem. Commun.* **55**, 11579–11582 (2019). <https://doi.org/10.1039/c9cc05975j>
287. Zhang, M.L., Wang, Y.G., Chen, W.X., et al.: Metal (hydr) oxides@polymer core–shell strategy to metal single-atom materials. *J. Am. Chem. Soc.* **139**, 10976–10979 (2017). <https://doi.org/10.1021/jacs.7b05372>
288. Li, J., Liu, P., Tang, Y.Z., et al.: Single-atom Pt-N<sub>3</sub> sites on the stable covalent triazine framework nanosheets for photocatalytic N<sub>2</sub> fixation. *ACS Catal.* **10**, 2431–2442 (2020). <https://doi.org/10.1021/acscatal.9b04925>
289. Ren, Z., Liu, Y., Lyu, Y., et al.: Single-atom Rh based bipyridine framework porous organic polymer: a high active and superb stable catalyst for heterogeneous methanol carbonylation. *J. Catal.* **369**, 249–256 (2019). <https://doi.org/10.1016/j.jcat.2018.11.015>
290. Wang, D.H., Ao, C.C., Liu, X.K., et al.: Coordination-engineered Cu-N<sub>x</sub> single-site catalyst for enhancing oxygen reduction reaction. *ACS Appl. Energy Mater.* **2**, 6497–6504 (2019). <https://doi.org/10.1021/acsaem.9b01066>
291. Yang, H.P., Wu, Y., Li, G.D., et al.: Scalable production of efficient single-atom copper decorated carbon membranes for CO<sub>2</sub> electroreduction to methanol. *J. Am. Chem. Soc.* **141**, 12717–12723 (2019). <https://doi.org/10.1021/jacs.9b04907>
292. Qin, R.X., Liu, P.X., Fu, G., et al.: Strategies for stabilizing atomically dispersed metal catalysts. *Small Methods* **2**, 1700286 (2018). <https://doi.org/10.1002/smtd.201700286>
293. Chen, L.F., Yang, T., Cui, H., et al.: A porous metal–organic cage constructed from dirhodium paddle-wheels: synthesis, structure and catalysis. *J. Mater. Chem. A* **3**, 20201–20209 (2015). <https://doi.org/10.1039/c5ta05592j>
294. Kou, Z.K., Zang, W.J., Ma, Y.Y., et al.: Cage-confinement pyrolysis route to size-controlled molybdenum-based oxygen electrode catalysts: from isolated atoms to clusters and nanoparticles. *Nano Energy* **67**, 104288 (2020). <https://doi.org/10.1016/j.nanoen.2019.104288>
295. Zhang, H.J., Kawashima, K., Okumura, M., et al.: Colloidal Au single-atom catalysts embedded on Pd nanoclusters. *J. Mater. Chem. A* **2**, 13498–13508 (2014). <https://doi.org/10.1039/c4ta01696c>
296. Shi, Z.S., Yang, W.Q., Gu, Y.T., et al.: Metal-nitrogen-doped carbon materials as highly efficient catalysts: progress and rational design. *Adv. Sci.* **7**, 2001069 (2020). <https://doi.org/10.1002/advs.202001069>
297. Wang, J., Liao, T., Wei, Z.Z., et al.: Heteroatom-doping of non-noble metal-based catalysts for electrocatalytic hydrogen evolution: an electronic structure tuning strategy. *Small Methods* **5**, 2000988 (2021). <https://doi.org/10.1002/smtd.202000988>
298. Xi, J.B., Jung, H.S., Xu, Y., et al.: Single-atom catalysts: synthesis strategies, catalytic applications, and performance regulation of single-atom catalysts. *Adv. Funct. Mater.* **31**, 2170081 (2021). <https://doi.org/10.1002/adfm.202170081>
299. Zhao, H.Y., Zhang, C.X., Li, H., et al.: One-dimensional nano-material supported metal single-atom electrocatalysts: synthesis, characterization, and applications. *Nano Sel.* **2**, 2072–2111 (2021). <https://doi.org/10.1002/nano.202100083>
300. Calle-Vallejo, F., Koper, M.T.M.: Theoretical considerations on the electroreduction of CO to C<sub>2</sub> species on Cu(100) electrodes. *Angew. Chem. Int. Ed.* **52**, 7282–7285 (2013). <https://doi.org/10.1002/anie.201301470>
301. Schouten, K.J.P., Qin, Z.S., Pérez Gallent, E., et al.: Two pathways for the formation of ethylene in CO reduction on

single-crystal copper electrodes. *J. Am. Chem. Soc.* **134**, 9864–9867 (2012). <https://doi.org/10.1021/ja302668n>

302. Vijay, S., Ju, W., Brückner, S., et al.: Unified mechanistic understanding of CO<sub>2</sub> reduction to CO on transition metal and single atom catalysts. *Nat. Catal.* **4**, 1024–1031 (2021). <https://doi.org/10.1038/s41929-021-00705-y>

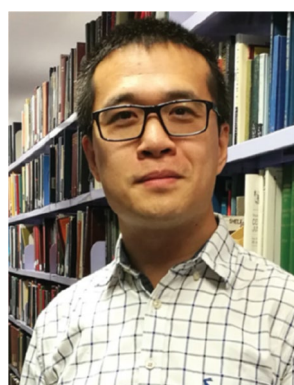


**Wenxian Li** is a professor at the School for Materials Science and Engineering, Shanghai University. Dr. Li received his Ph.D. degree from the University of Wollongong, Australia, in 2010. He received the Australian Postdoctoral Fellowship (Industrial) supported by the Australian Research Council in 2012 and then received financial support from the Australian Renewable Energy Agency as a Postdoctoral Fellowship. He joined the University of Western Sydney as a lecturer in the Solar Energy

Technologies Group in November 2012. His research focuses on the electron configuration modulation-induced performance optimization of functional materials for renewable energy utilization.



**Zehao Guo** is a Master student in the School of Materials Science and Engineering, Shanghai University, under the supervision of Prof. Wenxian Li. Currently, he is conducting research at the Ningbo Institute of Materials Technology and Engineering, Chinese Academy of Sciences, under the supervision of Prof. Haiyong He. His research interests include developing functional and stable separators for high-temperature lithium-ion batteries.



**Jack Yang** is currently a lecturer in the School of Materials Science and Engineering at The University of New South Wales (UNSW), Australia. He received his B.Sc. (2007) and Ph.D. (2011) degrees from the same institute. Before returning to UNSW in 2017, he was a postdoctoral fellow in Westfälische Wilhelms-Universität Münster, Germany, and the University of Southampton, UK. His current research focuses on theory and machine-learning-driven material studies on functional perovskites for electronic, photovoltaic, and energy conversion applications.

kites for electronic, photovoltaic, and energy conversion applications.



**Ying Li** is a professor at the School for Materials Science and Engineering, Shanghai University. She received her Ph.D. degree from the National Chungnam University in 2001. She was a postdoctoral fellow at the Research Materials Research Center of Chungnam National University, Republic of Korea, and National Chungnam University, Republic of Korea, from March 2001 to December 2002 and then joined Shanghai University as a professor. Her research activities include materials chemistry, such as conductive molecules, conductive materials, and energy materials.

materials chemistry, such as conductive molecules, conductive materials, and energy materials.



**Xueliang Sun** is a Canada Research Chair in Development of Nanomaterials for Clean Energy, Fellows of the Royal Society of Canada and Canadian Academy of Engineering, and Full Professor at the University of Western Ontario, Canada. Dr. Sun received his Ph.D. degree in materials chemistry in 1999 from the University of Manchester, UK, which he followed up by working as a postdoctoral fellow at the University of British Columbia, Canada, and as a Research Associate at L'Institut

National de la Recherche Scientifique (INRS), Canada. His current research interests are focused on advanced materials for electrochemical energy storage and conversion, including electrocatalysis in fuel cells and electrodes in lithium-ion batteries and metal–air batteries.



**Haiyong He** is a professor at the Ningbo Institute of Materials Technology and Engineering, Chinese Academy of Sciences. He obtained his Ph.D. degree from the National Center for Nanoscience and Technology, China. After graduating, he worked as a research fellow at Nanyang Technological University for three and a half years. In 2017, he became a professor at the Ningbo Institute of Materials Technology and Engineering, where he founded a laboratory at

the Institute of New Energy Technology. His group's research focuses on the synthesis and properties of functional carbonaceous materials and hybrid materials. There are several ongoing projects including graphite, hard/soft carbon, and silicon/carbon anodes. One objective is to understand the mechanisms and structural origin of the unique electrochemical properties of these materials.



**Sean Li** received his Ph.D. degree from The University of Auckland in 1998. He was subsequently appointed as an assistant professor at Nanyang Technological University, Singapore, and then joined The University of New South Wales in 2004. He is currently a director of the UNSW Materials and Manufacturing Futures Institute. His research interest focuses on advanced functional complex oxides and their heterostructures.



**Jiujun Zhang** is a professor in the College of Sciences/Institute for Sustainable Energy at Shanghai University and a former Principal Research Officer (Emeritus) at the National Research Council of Canada (NRC). Dr. Zhang is a Fellow of the Canadian Academy of Engineering (CAE), Fellow of The Academy of Science of The Royal Society of Canada (FRSCCA), Fellow of The Engineering Institute of Canada (EIC), Fellow of International Society of Electrochemistry (ISE), and Fellow of the

Royal Society of Chemistry (RSC-UK). Dr. Zhang received his B.S. and M.Sc. degrees in electrochemistry from Peking University in 1982 and 1985, respectively.